Non-conventional energy systems: Modeling, control and integration to power grids

Ahmad Hably

UNIVERSITÉ GRENOBLE ALPES

THÈSE

Pour obtenir le grade de

HABILITATION À DIRIGER DES RECHERCHES DE L'UNIVERSITÉ DE GRENOBLE ALPES

Spécialité : **Automatique et Productique**

Arrêté ministérial : 23 novembre 1988

Présentée par

Ahmad Hably

Non-conventional energy systems: Modeling, control and integration to power grids

Thèse soutenue publiquement le **03 mars 2017**,
devant le jury composé de :

Alexandre Trofino, Rapporteur
Pr
Mohamed Benbouzid, Rapporteur
Pr
Seddik Bacha, Rapporteur
Pr
Gildas Besancon, Examinateur
Pr
Lorenzo Fagiano, Examinateur
Dr-HDR
Alain Oustaloup, Examinateur
Pr

To the Memory of my mother Nazek and my father Khodor.

To Sirine, Nazek, Abed-Alrahamn, and Luna.

Contents

Chapter 1

Introduction

1 Some Personal History

From a young age, I wanted to become an electrical engineer. My dream was to find innovative solutions to the electricity shortage in Lebanon, my home country. Electricity cuts can reach more than 10 hours in some regions and I always remember studying under candle lights. In 2003, my last year at the faculty of engineering of the Lebanese University (UL), I get a scholarship to work on a final year project in France at "Heudyasic" laboratory of Compiègne. Although that I am English educated, I accepted without hesitation since I love to discover a new culture and because many of my best professors at the university have studied in France. In Compiègne, I discovered the interesting field of automatic control. I decided to continue my studies in this field. I joined a master degree at "Laboratoire d'automatique de Grenoble" (LAG) despite the refusal of my parents that wanted me to return to work in Lebanon as engineer. My first steps in the research started with a master thesis with Nicolas Marchand, a young fresh researcher, in the domain of bounded control for linear systems. The adventure continues with a PhD study on bounded control of unmanned aerial vehicles namely quadrotors. This PhD was supervised by the same Nicolas and officially by Mazen Alamir, an inspiring researcher. The scholarship was financed by the Lebanese scientific research center (CNRSL) in order, again, to return and work in Lebanon as a researcher. The destiny decided another "trajectory" after the war on Lebanon in 2006 where I was told that there are no available positions in CNRSL and that I can help my home country without being obliged to return physically to it. After one year as temporary researcher at LIRMM laboratory - Montpellier where I worked on the control of robotic manipulators, I returned to Grenoble, my second city, as an associate professor at ENSE3 of Grenoble-inp in the field of automatic control for energy systems!

2 My Research After the PhD

Between 2008 and 2010, my whole time was dedicated to prepare new courses and to organize the automatic control platform "AIDA". In 2010, I was thinking of a challenging system that combines automatic control and energy. After a discussion with Mazen Alamir, he reminded me of a presentation of Moritz Diehl[1] on the subject of Twin-kite and how it can

[1] This presentation was given at the First NMPC workshop organized at Grenoble in 2006!

be "controlled" to produce "energy". This unconventional idea of using high altitude wind energy attracted me. In this field, now called Airborne wind energy systems (AWE), I worked with more than 17 students at all the levels (PhD, master, final year project, engineering projects) with several papers published and several concepts designed. In 2015, AWE subject has been integrated in the Innovation and management course of ENSE3. 300 engineering students have worked more than 30 hours to propose innovative concepts related to AWE. The work of the inventor Rogelio Lozano Jr. and the hard worker Mariam Ahmed in their PhD gave Gipsa-lab and me a worldwide visibility in the AWE field. More details on my work in AWE field are given in Chapter 3.

Another turning point in my research was the meeting with professor Seddik Bacha of the electrical engineering lab of Grenoble (G2elab). This remarkable personality at all the levels proposed to cooperate with his PhD student Harun Turker working on the impact of the massive integration of plug-in electrical vehicles into the grid. This was a great opportunity to work on a challenging subject that again combines automatic control and energy. The PhD of Harun is considered the first french PhD study that addresses the impacts of integration electrical vehicles to the grid.
My contribution in this field of study continues with the "PARADISE" ANR project. In this project several partners work with the objective to study the optimal integration of renewable energy sources and electrical vehicles to the power grid. My work in this field with the exceptional Andres Ovalle and the hard learner Khaled Hajar and other students will be presented in Chapter 4.

In addition, I co-supervised Haiyang Ding in his PhD on theoretical development in the field of distributed cooperative control. The proposed control schemes are numerically applied on several energy systems. However these results will not be included in the present manuscript.

3 My Point View for the Scientific Research

The guidelines that I follow in my research can be summarized as follows:

- ◇ **Learn from others**: A bibliographic study will be the first step each time I start working on a new subject. This important phase will give me some insight of the work of other researchers in order to avoid their mistakes, to improve their results, or to propose new ideas and methods.

- ◇ **Simplicity**: In my opinion, complex problems can be solved with simple solutions. To overcome the complexity, an iterative approach can be applied with an increasing levels of complexity at each iteration.

- ◇ **Failure is a great teacher**: Any failure is an opportunity. At the same time, learning from failure is only effective if its origin is fully understood. The iterative approach facilitates the problem diagnosis and alternatives can be proposed.

- ◇ **Freedom and trust**: A researcher must have a free spirit and must trust people with whom he works. All the ideas are welcome. For this, my students have a lot of freedom to propose their ideas and to test them.

- **Team work**: Most of the results presented in this manuscript (theoretical and especially practical) are obtained in a team work. I work with my students as a team in order to find together solutions for the addressed problems. In addition,**gipsa**-labhas a skillful technical team in all the necessary practical domains. Without the effort of this team, many results will stay theoretical in papers without seeing the light in real life. Here I have to mention the efforts of Daniel Rey, the ex-head of the technical team, and Jonathan Dumon, the skillful research engineer.

4 A Classification of My Research

My research work includes several fields:

- Control theory including bounded control for linear systems, predictive control, and cooperative distributed control.
- Robotics and more precisely the control of drones such as quadrotors.
- Optimal integration and charging techniques for plug-in electrical electrical vehicles.
- Control of airborne wind energy systems.
- Control of energy systems in general.

5 The Organization of this Manuscript

This manuscript is composed of three chapters that can be read independently. These chapters details the application of control on "non-conventional" energy systems.

Chapter 2: In this chapter, my detailed Curriculum Vitae will be given.

Chapter 3: This chapter deals with a new wind energy concept called Airborne wind energy systems (AWE). AWE systems aim at replacing the blades of conventional wind by a controlled flying "wings" that captures the energy of the wind. This concept of producing more energy with less material (at least 90 % saving of used material) enters the current approach of Frugal innovation. Different aspects will be addressed in this chapter, from modeling, to control and practical indoor and outdoor validation. The integration of these systems to the grid is also presented.

Chapter 4 : This chapter deals with the integration of plug-in electrical vehicles (EV) to the grid. These systems represent several opportunities for modern electrical distribution systems. In fact, the presence of several chargers (power electronics converters) distributed throughout the electricity grid, represents technical challenges and opportunities for improving the quality and efficiency of future electricity grids. Besides, EVs energy storage capacities have a great potential in terms of benefits for electricity distribution systems: energy transportation, support for non-conventional energy sources, power quality services, etc. Nevertheless, in the most likely scenario, domestic EV load is expected to be drawn from the residential electrical distribution system infrastructure. Thus, without proper approaches for handling the charging of EVs, a high penetration rate supposes several negative impacts on stability, load balancing, voltage levels, etc. In

this chapter, optimal charging management schemes, taking into account EVs autonomy, and constraints of convenience from owners, are presented.

The manuscript ends with some conclusions and perspectives where a mid-term research project will be detailed.

Chapter 2

Detailed Curriculum Vitae

1 Curriculum Vitae

1.1 Civil Status

Name:	HABLY
First Name:	Ahmad
Date and place of Birth:	05 May 1980 at Sidon, Lebanon
Family situation:	Married, 2 children
Position:	Associate Professor at Grenoble-INP and **gipsa**-lab

1.2 Study/Professional Experience

2008 - .. : **Associate professor** at Grenoble-INP, Research at **gipsa**-lab(UMR 5216).

2007 - 2008: **ATER** at IUT Montpelier département Mesures Physiques, Research at LIRMM (UMR 5506).

2004 - 2007: **PhD:** Automatique-Productique, at Grenoble-INP,

Title : "Bounded Control of Unmanned Aerial Vehicles"

Defense :	05 December 2007
President :	D. Georges, Professor, LAG
Rapporteur :	Y. Chitour, Professor, L2S
	F. Mazenc, Chargé de recherche, INRIA
Examinator :	R. Lozano, Directeur de recherche, Heudiasyc
PhD supervisor :	M. Alamir, Directeur de recherche, LAG
PhD co-supervisor :	N. Marchand, Chargé de recherche, LAG

2003-2004 : **Master 2 Recherche:** Automatique, at Institut National Polytechnique de Grenoble (INPG).

1998-2003 : **Engineer:** Industrial Informatics at the Lebanese University (UL), Final year project at HEUDYASIC - France.

The PhD scholarship has been funded by the National Research Center of Lebanon (CNRSL).

2 Research Interests

During the last years, I have conducted several research studies on the control of aerial robotic systems. In parallel, I have proposed several control schemes for the control of energy systems, namely the integration of renewable energy systems and electric vehicles to the power grid. My research is related to the control of linear systems with bounded inputs, the control of interconnected systems, the modeling and control of airborne wind energy (AWE) systems, the control of different energy systems.

2.1 Bounded Control

Bounded control is inherent to practical stabilization problem: valves operate between closed and open, cars have limited steering angles, tanks have finite volumes, etc. Design of controllers for systems with bounds is an active area of research. For these systems, low gain control laws can be used [76, 111, 104, 85, etc.]. These consist of saturating a linear controller usually obtained by solving a Riccati equation. It is known that one can not achieve global stabilization by this mean for system of dimension $n \geq 3$ [110] and to disguise this drawback, it is proposed to tune the Riccati equation with some parameter that can be adapted online [55]. This enables global stability and better performances in terms of convergence.
From 2005 until 2010, I have worked on a generalization of the nonlinear control law proposed by [109]. The proposed extensions render nonlinear feedback very competitive compared to the other existing methods particularly for the simplicity of the feedback or the ability thanks to the Lyapunov theory to quantify the acceptable measurement or model errors. These results have been extended to the attitude stabilization of rigid bodies with an application on a quadrotor with some physical limits of its actuators. The bounded control of chained-form systems, first

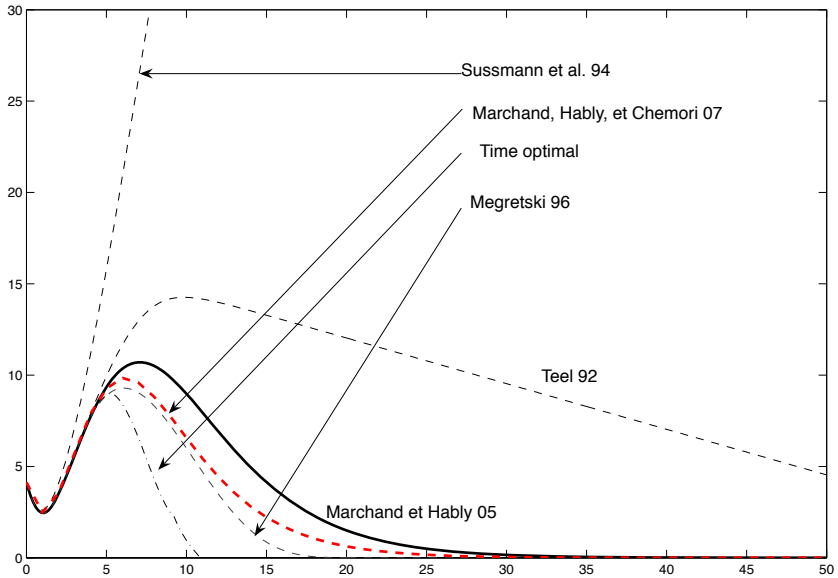

Figure 2.1: Control of a third order integrator with bounded control - Evolution of the norm of the state [84].

and second order, has been also studied. Controlling this type of system is not easy because it

does not meet the Brockett conditions [40]. These conditions are necessary for the existence of static state feedback control C^1. Second order chained system differs from first-order chained systems, initially proposed by [87] as it contains a drift component. Typical examples of this system include unicycle-type vehicles, car-like vehicles and planar underactuated manipulators. The V/STOL aircraft without gravity [68] can also be transformed into a system that is equivalent to the second-order chained form using coordinate and feedback transformation [31]. I have proposed state feedback controller based on model predictive control (MPC) and handles the singular situations without any special treatment. The proposed scheme, real-time implementable, also respects arbitrary saturation constraints on the control inputs.
Here are some papers published on the subject: [61, 62, 84, 60, 56, 83, 44].

2.2 Cooperative Distributed Control

There are several approaches to control interconnected systems: centralized, decentralized, and distributed control. Centralized frameworks are often very expensive in terms of communication if not impossible to be settled. On the other hand, when the interactions between subsystems are strong, the fully decentralized control schemes show bad performance. To overcome these limits, and during the PhD of H. Ding, I have worked on the design of distributed control framework for interconnected systems. The main idea is that each subsystem of the network has to cooperate with its neighbors by sharing partial information in order to contribute to the global objective of the network (or to manage its own objective) while avoiding destabilizing the whole network. We have proposed a modular design framework, for both linear and nonlinear interconnected systems, in which network-related issues and solutions are added as an additional layer that does not question the *old* existing widely assessed local controllers. The information exchanged between subsystems preserves the details of the local decisions and set-ups from being totally exchanged and only aggregated quantities are blindly transmitted as far as this transmission helps preserving the stability of the overall network. Since in many networks, some subsystems are more critical than others we have introduced the concept of relative priority where the stability constraints sent by critical subsystems are considered with higher weights. This approach has been applied to the problem of load frequency control and the control of a cryogenic plant. In the PhD of K. Hajar, we are studying the control of inter-connected micro-grids in presence of renewable energy systems.

Here are some papers published on the subject: [63, 64, 30, 48, 47].

2.3 Airborne Wind Energy (AWE) Systems

Airborne Wind Energy (AWE) systems generate renewable energy from wind by exploiting tethered aircrafts, whose motion is stabilized by active control systems. This emerging field has experienced an ever-increasing development in the last decade. On a large scale, this type of system aims at providing an alternative to conventional wind on the market of electric power. In can be used in many areas where production of the maximum power is not a goal in itself and where autonomy is the main concern. One can cite traveling science missions, ships, events, etc. Furthermore, the system can afford to carry a load in altitude for measurement, lighting, filming or communication, in addition to its main objective which is energy production.
During the PhD of R. Lozano, we have studied modeling, design, and control of several prototypes. Flexible and rigid wings have been used. These prototypes have been tested and

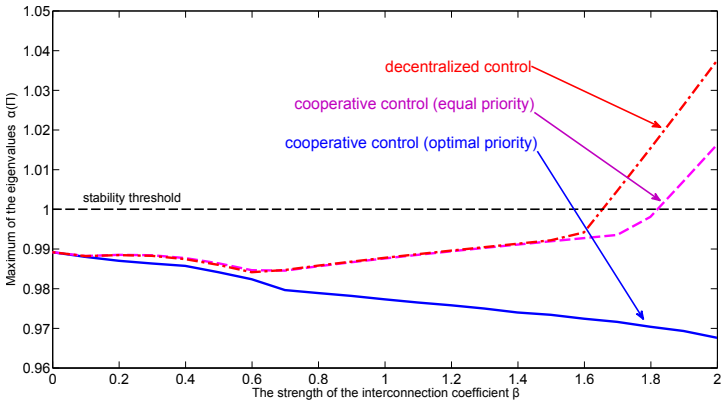

Figure 2.2: The evolution of the spectrum of a network under growing interconnection strength with the application of different control schemes.

validated in indoor and outdoor experiments in presence and in absence of wind.
In the PhD of M. Ahmed, we have studied the cycle optimization of these systems using MPC and virtual constraints. Grid integration of AWE systems has been also studied and validated in Hardware-In-the-Loop (HIL) simulator. Two cases have been considered: an infinite grid and an isolated microgrid. In the ongoing PhD of Y. Gupta, we are studying a Magnus-effect-

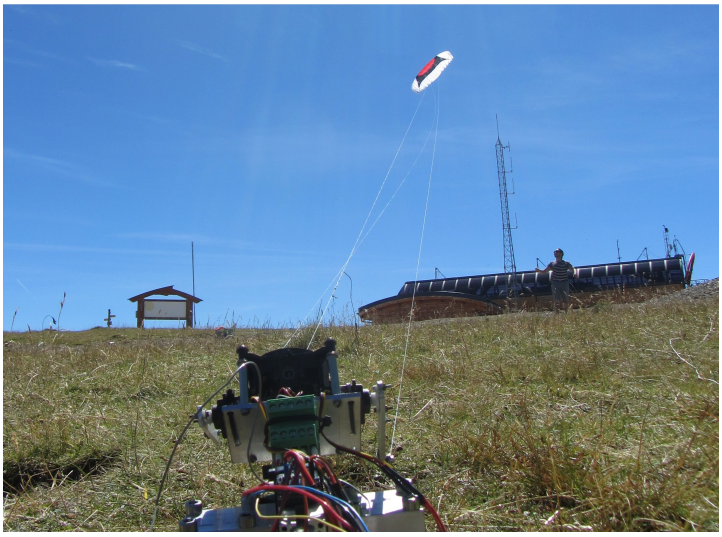

Figure 2.3: Test campaign in 2014 at Chamrousse.

based AWE system. Magnus cylinders are used instead of classical wings. Its symmetry axis gives the system the advantage, among others, to be insensitive to the apparent wind direction, and thus more robust with respect to wind gusts. On the other hand, it also has a lift coefficient which is much higher than that of conventional wings. This allows the system to fly at much slower speeds for a given power and thus be less sensitive to the drag of the whole system. This type of system has been used by Omnidea in two dimensional flights. We propose to exploit these cylinders in crosswind trajectories to extract the maximum of available energy [33]. Our first results on Magnus cylinders reinforce our belief that this type of wing offers

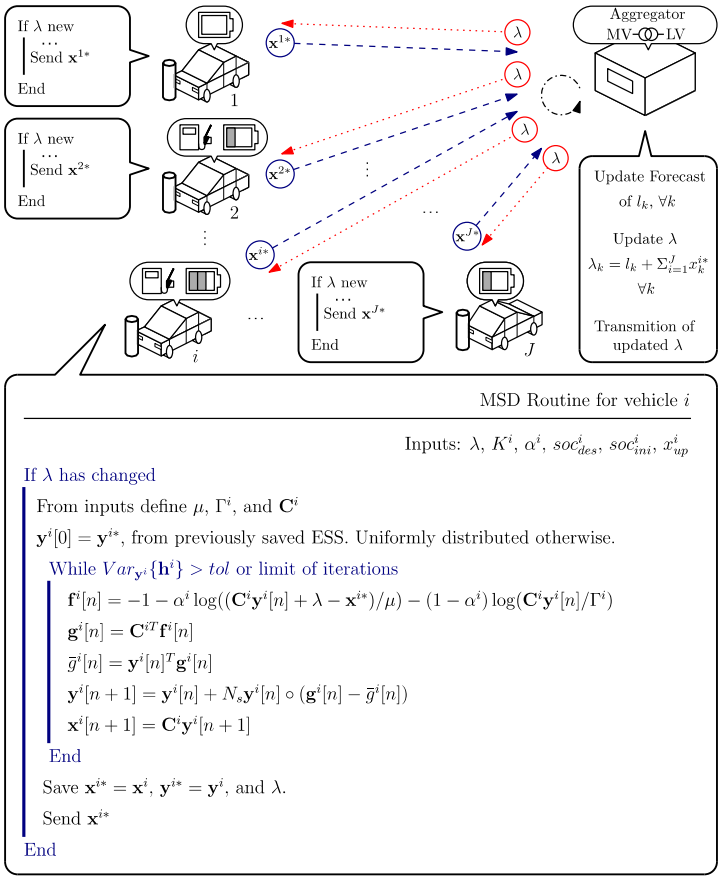

Figure 2.5: Mixed strategist dynamics (MSD) algorithm applied to the integration of electrical vehicles.

3 Teaching Activities

My teaching activities covers several fields of system theory, nonlinear control, and optimization for energy systems. I have developed complete courses. These courses will denoted by + in the following paragraphs. I have also participated in the development of several courses. These courses will be denoted by a ∗. Most of these courses are taught in English language.

From 2008 until 2012, I was the scientific administrator of the automatic control technical platform (AIDA). More than 450 students use this plateform (average 4 hours per week per student). This platform is considered for me as the first real contact between engineering students and the practical automatic control. My job was to organize the planning of this platform, to propose, buy and validate new labs and practical sessions, to train new professors, etc. From 2012, I am the coordinator of the collective engineering projects (2nd year ENSE3, 150 students/year) and the integrator projects (ASI program, 3rd year, 50 students/year). In addition, I am the correspondent of the international relation for the ASI program. I am the responsible of the first ENSE3 Innovation Challenge that concerns all the second year students of ENSE3. In the following, a detailed description of the courses will be presented.

- ◇ **Optimization and numerical analysis** *: Course (16 hours) and computer sessions (18 hours).

Figure 2.6: Teaching in a lab session.

This course covers the principal algorithms for linear, nonlinear, dynamic optimization and optimal control. Topics include the simplex method, optimality conditions for nonlinear optimization, Newton's method, heuristic methods, and dynamic programming and optimal control methods.

Public: Second year students of ENSE3 (50 students).

◇ **Modeling and control under state representation** $^{+}$: Course (14 hours), computer sessions (20 hours), and lab sessions (16 hours).

This course includes state-space methods of feedback control system design and design optimization for invariant continuous systems; pole positioning, observability, controllability, observer design, the linear quadratic optimal regulator problem, Lyapunov functions and stability theorems. Examples are be drawn from mechanical, electrical and hydraulic engineering applications. Matlab is used extensively during the course for the analysis, design and simulation.

Public: Second year students of ENSE3 and ENSIMAG (150 students). Master degree students of ENSE3 (20 students).

◇ **Linear systems** *: Course (8 hours), computer sessions (32 hours), and lab sessions (16 hours).

The course addresses dynamic systems, i.e., systems that evolve with time and how the input affects the output. In particular, we concentrate on systems that can be modeled by Ordinary Differential Equations (ODEs) or transfer functions, and that satisfy certain linearity and time-invariance conditions. The response of these systems to inputs and initial conditions is analyzed and in particular interest systems obtained as interconnections of two or more other systems. Design of control systems that ensure desirable properties (like stability and performance) is also addressed.

Public: First year students of ENSE3 (50 students) and students of IUT (150 students).

◇ **Embedded control**[*]: Computer sessions (10 hours) and lab sessions (12 hours).

This course aims to introduce the model development methodology of embedded control systems. The course contains a reminder of the basic knowledge of automatic control, design tools, embedded programming languages. As a research project, using a Lego Mindstorms NXT robot, students learn and practice all the steps of model development chain modeling, controller design, validation, simulation, and implementation of the controller in the Mindstorms robot.

Public: Second year students of ENSIMAG (40 students).

◇ **Predictive and nonlinear control** [*]: Computer sessions (14 hours). Numerical application of Predictive and nonlinear control on real industrial applications

Public: Third year students of ENSE3 (50 students).

◇ **Optimization for energy systems** [+]: Course (16 hours) and computer sessions (10 hours).

This course is devoted to industrial applications of optimization in the electricity production, transport and distribution. The tools for continuous optimization (linear programming and nonlinear) are applied to the problem of optimal power flow, while the unit commitment problem is submitted to the tools of combinatorial optimization (linear integer programming).

Public: Third year students of ENSE3 (about 40 students) and master degree students of ENSE3 (more than 20 students).

◇ **Innovation and management** [*]: Course (10 hours) and projects (20 hours).

In this course students work in a project mode on the generation of an innovative concept and its development, both technically and in its ability to generate value. They implement creativity techniques starting from a given issue to bring out an innovative concept that will be the object of study. They identify and formalize the innovative concept technically and learn the main market segmentation techniques to apply the concept to identify target markets. They formalize the broad outlines of a business model: possible scenarios, revenue models, risks and profit opportunities.

Public: Third year students of ENSE3 (300 students that worked on new design of airborne wind energy (AWE)).

◇ **Mechatronics** [*]: Course (10 hours) and computer sessions (18 hours).

This course gives an introduction on modeling mechatronic systems using Bond graph.

Public: Third year students of ENSE3 (30 students).

◇ **Robotics** [*]: Course (16 hours).

This course aims to give an initiation course on robotics using Mindstroms Lego robots. Algorithms and programming languages such as Scratch are also studied. This course is sponsored by Maison pour la science en Alpes Dauphiné.

Public: Professors of intermediate and high schools (16 students).

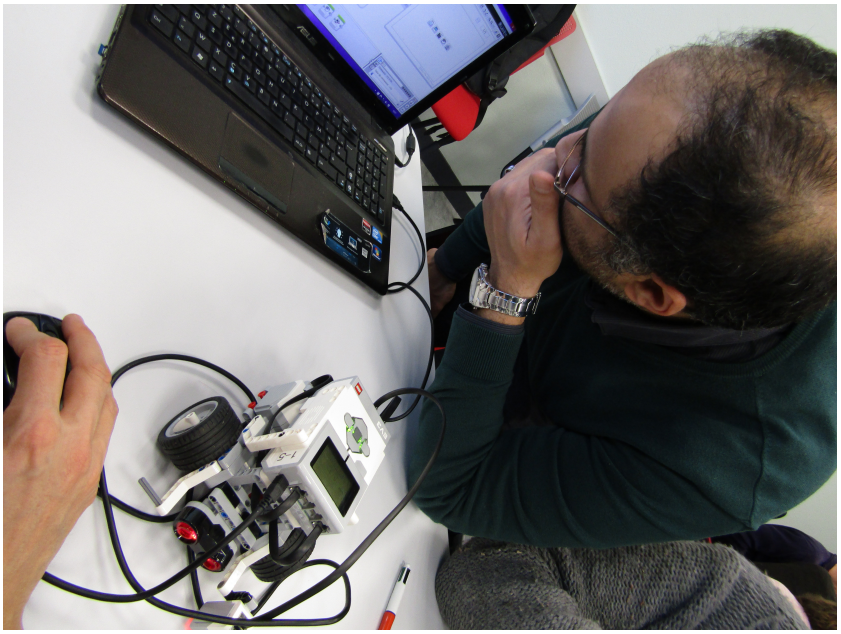

Figure 2.7: Teaching in the robotics course of Maison pour la Science en Alpes Dauphiné.

4 Contracts and Projects Responsibilities

I am involved in several academic and industrial contracts.

- ANR project "PARADISE" (2013-2017):

  Responsable of a workpackage and the **gipsa**-lab correspondent in this project.

  Budget for **gipsa**-lab is around 108 k€.

  Partners: G2ELAB, CEA/INES -L2S, LBMS, SOREA, SOCOMEC, AER, [15].

- Project "Smart Energy" (2012-2014):

  Coordinator of the "system" axis of a project financed by Grenoble-INP: 4 post-doc in the field of **SMART Grids**.

  Four postdoctoral positions for one year.

  Partners: G2Elab, G- SCOP and LIG.

- ARC Energies Rhone-Alpes (2013-2017):

  Project coordinator on the subject "Gestion coopérative de flotte de véhicules électriques en vue de son intégration optimale au réseau électrique SMARTGRID" financed by the Rhone-Alpes region.

  A doctoral position for 3 years.

  Partner: G2Elab.

- Project "WindFisher" (2015-2016):

  Scientific collaborator on an industrial study with Cosmica spacelines and Airstar-light company [confidential].

  A contract of 15k €.

- Project "VM2C" (2015-2016) :

  Scientific collaborator on an industrial study on a small airborne wind energy system with VM2C startup [confidential].

- Project "Persycup" (2013-2015):

  Co-coordinator with D. Pellier (LIG) on an educational project financed by PERSYVAL-Lab.

  Budget for **gipsa**-lab is around 8 k€.

- Project "Hydraulic valley" (2014-2016):

  Co-coordinator with N. Meslem (Gipsa-lab) on an educational project financed by PERSYVAL-Lab.

  Budget for **gipsa**-lab is around 15 k€.

- Project "Drone Captif" (2016-2017):

  A research study on tethered drones financed by Coopera project of Région Auvergne-Rhône-Alpes.

  Budget for **gipsa**-lab is 4 k€.

5 Research Supervision Activities

5.1 Master Students

I have supervised or co-supervised 10 master degree students: PHAN Han-Huu (2009, LCIS), Jamil Haddad (2010, Lebanese University), Miguel Martin (2010, UPM Spain), Rogelio Lozano (2010), Sergio Murillo (2011, G2Elab), Waleed Nwesaty (2012, **gipsa**-lab), Olivier Goudard (2013, CNAM), Azzam Alwan (2015, Polytech Grenoble), Radhika Chatterjee (2015, ENSE3), Bassima Atrachan (2016, Lebanese University). The subjects concern mainly the control of drones, airborne wind energy systems and microgrids.

5.2 PhD Students

During the last 8 years, I have participated in the supervision of 7 PhD students. One of them has abandoned her study due to health problems. Four PhD students have defended their thesis after a work duration less than 39 months.

Past PhD Students

◇ Stefana, Andreea:

Title : Intégration des véhicules électriques: aspects techniques et économiques

Major : Automatic control and Electrical engineering | Financing : Bourse Erasmus

Start : Oct. 2013 | Contract annulation : 01-02-2015 due to health problems.

Supervising percentage : 50% | co-supervisor : S. Bacha (G2Elab, 50%)

Present position : Assistant lecturer at the university of Bucharest.

◇ Lozano Jr., Rogelio:

Title : Étude du vol d'un générateur cerf-volant

Major : Automatic control | Financing : Bourse Fléchée EEATS

Start : 01-10-2010 | PhD Defense : 30-04-2014

Supervising percentage : 50% | co-supervisor: M. Alamir (**gipsa**-lab, 50%)

Present position: Postdoc at **gipsa**-lab(2016) and CEO of BlateTips Energy

Publications : 4 international conference papers [80, 57, 79, 81].

◇ Ahmed, Mariam,

Title : Optimisation du contrôle commande de systèmes de génération d'électricité à cycle de relaxation

Major : Automatic control and Electrical engineering | Financing : Bourse Syrienne

Start : 15-09-2010 | PhD Defense : 28-02-2014

Supervising percentage : 50% | co-supervisor : S. Bacha (G2Elab, 50%)

Present position : Research engineer at Valeo

Publications : 1 international journal [26] and 6 international conference papers [25, 28, 24, 23, 27].

◇ Ding, Hiayang,

Title : Commande prédictive distribuée pour un réseau de systèmes partiellement coopératifs

Major : Automatic control | Financing : Bourse Chinoise

Start : 30-03-2010 | PhD Defense : 10-07-2013

Supervising percentage : 50% | co-supervisor : M. Alamir (**gipsa**-lab, 50%)

Present position : Research engineer at Huawei

Publications : 3 international conference papers [30, 48, 47].

◇ Ovalle, Andres

Title : Gestion coopérative de flotte de véhicules électriques en vue de son intégration optimale au réseau électrique

Major : Electrical Engineering | Financing : Projet Arc energies

Start : 01-09-2013 | PhD Defense : 14-12-2016

Supervising percentage : 50% | co-supervisor : S. Bacha (G2Elab, 50%)

Present position : Postdoc at G2elab

Publications : 2 international journals [97, 91] and 6 international conference papers [94, 37, 93, 95, 96, 39].

Present PhD Students

◇ Gupta, Yashank,

Title : Airborne wind energy system: Control and experimentation

Major : Automatic control Financing : Bourse Fléchée EEATS

Start : 16-11-2015

Supervising percentage : 50% co-supervisor : J. Dumon (**gipsa**-lab, 50%)

◇ Hajar, Khaled,

Title : Coopérative énergétique intelligente

Major : Automatic control Financing : Bourse AUF, thèse cotutelle entre le Liban et Université de Grenoble.

Start : 01-11-2013

Supervising percentage : 50% co-supervisor : S. Bacha (G2Elab, 50%)

Present position : Assistant lecturer at UFL.

Publications : 4 international conference papers [65, 64, 39, 63].

5.3 Post-doctoral Students

I was the scientific supervisor with Anotneta Bratcu (**gipsa**-lab) of Julian Fernandez (2014, six months) who is now in a postdoctoral position in Université de Victoria. I have published with him one journal paper [54] and two international conference papers [53, 52]. I have supervised Salam Hajjar (2014, six months). After a postdoctoral position at Universidade Federal do Rio de Janeiro, she is now and associate professor in Marshall University of West Virginia. I published with her one international conference paper [66]. I have also worked with Kaustav Basu in his postdoc position at **gipsa**-lab(2016, three months). We published two international conference papers [37, 39]. He is now data scientist at Quby, Netherlands.

5.4 Participation in PhD Defense

I participated as an examinator in the PhD defense of Harun Turker (G2Elab 20/12/2012).

6 Scientific production

6.1 International journals

1. Ovalle, Andres; Fernandez, Julian; Bacha, Seddik; Hably, Ahmad, **"*Mixed strategist dynamics and Entropy maximization: Electric vehicle distributed load scheduling*"**, *IEEE Transactions on Industrial Electronics* (2016) **63**, **5**, 3060-3071.

2. Fernandez, Julian; Riu, Delphine; Bacha, Seddik; Hably, Ahmad, **"*Real-time plug-in electric vehicle charging strategies for current unbalance minimization and voltage unbalance reduction*"**, *Journal Européen des Systèmes Automatisés* (2016) **49**, **3**, 271-298.

3. Hossain, Jahangir; Mahmud, Apel; Milano, Federico; Bacha, Seddik; Hably, Ahmad, **"*Design of robust distributed control for interconnected microgrids*"**, *IEEE Transactions on Smart Grid* (2015) **99** 1-12.

4. Turker, Harun; Bacha, Seddik; Hably, Ahmad, **"*Rule-Based charging of plug-in electric vehicles (PEVs): Impacts on the aging rate of low-voltage transformer*"**, *IEEE Transactions on Power Delivery* (2014) **29**, **3**, 1012-1019.

5. Ovalle, Andres; Ramos, Gustavo; Bacha, Seddik; Hably, Ahmad; Rumeau, Axel, **"*Decentralized control of voltage source converters in microgrids based on the application of instantaneous power theory*"**, IEEE Transactions on Industrial Electronics. (2014) **62**, **2**, 1152-1162.

6. Ahmed, Mariam; Hably, Ahmad; Bacha, Seddik, **"*Kite generator system modeling and grid integration*"**, *IEEE Transactions on Sustainable Energy* (2013) **4**, **4**, 968-976.

7. Turker, Harun; Bacha, Seddik; Chatroux, Daniel; Hably, Ahmad, **"*Low voltage transformer loss of life assessments for a high penetration of plug-in hybrid electric vehicles (PHEVs)*"**, *IEEE Transactions on Power Delivery* (2012) **27**, **3**, 1323-1331.

8. Guerrero-Castellanos, Fermi; Marchand, Nicolas; Hably, Ahmad; Lesecq, Suzanne; Delamare, Jérôme, **"*Bounded attitude control of rigid bodies: Real-time experimentation to a quadrotor mini-helicopter*"**, *Control Engineering Practice* (2011) **19**, **8**, 790-797.
In the list of the most cited articles in Control Engineering Practice Journal (Elsevier) since 2011.

During my PhD:

9. Marchand, Nicolas; Hably, Ahmad; Chemori, Ahmed, **"*Global stabilization with low computational cost of the discrete-time chain of integrators by means of bounded controls*"**, *IEEE Transactions on Automatic Control* (2007) **52**, **5**, 948-952.

10. Marchand, Nicolas; Hably, Ahmad, **"*Nonlinear stabilization of multiple integrators with bounded controls*"**, *Automatica* (2005) **41**, **12**, 2147-2152.

6.2 Chapters

1. Hably, Ahmad; Dumon, Jonathan; Smith, Garrett; Bellemain, Pascal, **"*Control of a Magnus effect-based airborne wind energy system*"**, *Airborne Wind Energy Systems* (2016) **To appear**,

During my PhD:

2. Hably, Ahmad; Marchand, Nicolas, **"*Further results on global stabilization of the PVTOL aircraft*"**, Positive Systems. Proceedings of the Second Multidisciplinary International Symposium on Positive Systems: Theory and Applications, POSTA'06.

6.3 International conferences

1. Hably, Ahmad; Dumon, Jonathan; Smith, Garrett, **"*Control of an airborne wind energy system with a Magnus effect*"**, ACC 2016 - USA.

2. Ovalle, Andres; Bacha, Seddik; Hably, Ahmad; Basu, Kaustav, **"*On the most convenient Mixed Strategies in a mixed strategist dynamics approach for load management of Electric vehicle Fleets*"**, IECON'2016 - Italy.

3. Basu, Kaustav; Hably, Ahmad; Debusschere, Vincent; Bacha, Seddik; Dirven, Geert Jan; Ovalle, Andres, **"*A comparative study of low sampling non intrusive load dis-aggregation*"**, IECON'2016 - Italy.

4. Hajar, Khaled; Hably, Ahmad; Bacha, Seddik; Rafhi, Ahmad; Obeid, Ziad, **"*An application of a centralized model predictive control on microgrids*"**, IEEE Electrical Power and Energy Conference, EPEC 2016 - Canada.

5. Basu, Kaustav; Ovalle, Andres; Guo, Baoling; Hably, Ahmad; Bacha, Seddik; Hajar, Khaled, **"*Online forecasting of electrical load for distributed management of plug-in electric vehicles*"**, International Conference on Renewable Energies for Developing countries, REDEC 2016 - Lebanon.

6. Hajar, Khaled; Hably, Ahmad; Bacha, Seddik; Rafhi, Ahmad; Obeid, Ziad, **"*Optimal centralized control application on microgrids*"**, International Conference on Renewable Energies for Developing countries, REDEC 2016- Lebanon.

7. Ovalle, Andres; Hably, Ahmad; Bacha, Seddik, **"*Mixed strategist dynamics: Electrical vehicle distributed load scheduling*"**, IECON'2015 - Japan.

8. Hajjar, Salam; Bratcu, Antoneta Iuliana; Hably, Ahmad, **"*A Day-ahead centralized unit commitment algorithm for a multi-agent smart grid*"**, The Federated Conference on Computer Science and Information Systems, FedCSIS 2015 - Poland.

9. Hajar, Khaled; Hably, Ahmad, Elrafhi, Ahmad; Obeid, Ziad; Bacha, Seddik, **"*Optimization of a microgrid with renewable energy and distributed generation: a case study*"**, The 9th International Conference on System Theory, Control and Computing, ICSTCC 2015 - Romania.

10. Fernandez, Julian; Hably, Ahmad, Bratcu, Antoneta Iuliana, **"*Assessing the economic profit of a vehicle-to-grid strategy for current unbalance minimization*"**, IEEE International Conference on Industrial Technology, ICIT 2015 - Spain.

11. Ovalle, Andres; Hably, Ahmad; Bacha, Seddik, **"*Optimal management and integration of electric vehicles to the grid: Dynamic programming and game theory approach*"**, IEEE International Conference on Industrial Technology, ICIT 2015 - Spain.

12. Fernandez, Julian; Bacha, Seddik; Riu, Delphine; Hably, Ahmad, **"*Plug-in electric vehicle collaborative charging for current unbalance minimization: Ant system optimization application*"**, IEEE International Conference on Industrial Technology, ICIT 2015 - Spain.

13. Ding, Haiyang; Alamir, Mazen; Bonne, Francois; Hably, Ahmad; Bonnay, Patrick, **"*Distributed cooperative control framework of a cryogenic system*"**, IEEE International Conference on Industrial Technology, ICIT 2015 - Spain.

14. Hably, Ahmad; Marchand, Nicolas, **"*Bounded control of a general extended chained form systems*"**, 53rd IEEE Conference on Decision and Control, CDC 2014 - USA.

15. Ahmed, Mariam; Hably, Ahmad; Bacha, Seddik; Ovalle, Andres, **"*Kite generator system: Grid integration and validation*"**, IECON'2014 - USA.

16. Ovalle, Andres; Bacha, Seddik; Hably, Ahmad, **"*Voltage support by optimal integration of plug-in hybrid electric vehicles to a residential grid*"**, IECON'2014 - USA.

17. Ding, Haiyang; Alamir, Mazen; Hably, Ahmad, **"*A distributed cooperative control scheme with optimal priority assignment and stability assessment*"**, IFAC world congress 2014 - South Africa.

18. Harun, Turker; Bacha, Seddik; Hably, Ahmad, **"*Application of housing peak shaving (HPS) algorithms with plug-in hybrid electric vehicles (PHEVs): Impacts on the aging rate of low voltage transformer*"**, Saudi Arabia Smart Grid 2013.

19. Ahmed, M.; Hably, Ahmad; Bacha, Seddik, **"*Kite generator system periodic motion planning via virtual constraints*"**, IECON'2013 - Austria.

20. Lozano, Rogelio Jr; Dumon, Jonathan; Hably, Ahmad; Alamir, Mazen, **"*Energy production control of an experimental kite system in presence of wind gusts*"**, Proceedings of the IEEE/RSJ IROS 2013 - Japan.

21. Lozano, Rogelio Jr; Dumon, Jonathan; Hably, Ahmad, **"*Reverse pumping: theory and experimental validation on a multi-kites system*"**, Proceedings of the 17th International Conference on System Theory, Control and Computing Joint Conference 2013 - Romania.

22. Nwesaty, Waleed; Bratcu, Antoneta Iuliana; Hably, Ahmad, **"*Extremum seeking control techniques applied to photovoltaic systems with multimodal power curves*"**, ICRERA 2013 - Spain.

23. Harun, Turker; Hably, Ahmad; Bacha, Seddik, **"*Housing peak shaving algorithm (HPSA) with plug-in hybrid electric vehicles (PHEVs): Vehicle-to-Home (V2H) and Vehicle-to-Grid (V2G) concepts*"**, POWERENG 2013.

24. Hably, Ahmad; Lozano, Rogelio Jr; Alamir, Mazen; Dumon, Jonathan, **"*Observer-based control of a tethered wing wind power system: indoor real-time experiment*"**, ACC 2013 - USA.

25. Turker, Harun; Hably, Ahmad; Bacha, Seddik, **"*Smart Charging of plug-in hybrid electric vehicles (PHEVs) on the residential electric grid regarding the voltage plan*"**, IEEE International IEVC 2013 - Turkey.

26. Harun, Turker; Hauck, Matthieu; Hably, Ahmad; Bacha, Seddik, **"*A tool of Vehicle-to-Grid (V2G) concept for voltage plan control of residential electric grid areas with plug-in hybrid electric vehicles (PHEVs)*"**, IECON'2012 - Canada.

27. Turker, Harun; Hably, Ahmad; Bacha, Seddik, **"*Dynamic programming for optimal integration of plug-in hybrid electric vehicles (PHEVs) in residential electric grid areas*"**, IECON'2012 - Canada.

28. Ahmed, Mariam; Hably, Ahmad; Bacha, Seddik, **"*High altitude wind power systems: A survey on flexible power kites*"**, ICEM 2012 - France.

29. Hauck, Matthieu; Rumeau, Axel; Munteanu, Iulian; Bratcu, Antoneta Iuliana; Bacha, Seddik; Roye, Daniel; Hably, Ahmad, **"*A 1:1 prototype of power generation system based upon cross-flow water turbines*"**, ISIE 2012 - China.

30. Ahmed, Mariam; Murillo-Cruz, Sergio-Camilo; Hably, Ahmad; Bacha, Seddik, **"*A comparative study on a pumping wave energy conversion system*"**, ISIE 2012 - China.

31. Turker, Harun; Bacha, Seddik; Chatroux, Daniel; Hably, Ahmad, **"*Modeling of system components for Vehicle-to-Grid (V2G) and Vehicle-to-Home (V2H) applications with plug-in hybrid electric vehicles (PHEVs)*"**, IEEE PES ISGT 2012 - USA.

32. Turker, Harun; Hably, Ahmad; Bacha, Seddik; Chatroux, Daniel, **"*Rule-based algorithm for plug-in hybrid electric vehicles (PHEVs) integration in residential electric grid areas*"**, IEEE PES ISGT 2012 - USA.

33. Turker, Harun; Bacha, Seddik; Chatroux, Daniel; Hably, Ahmad, **"*Aging rate of low voltage transformer for a high penetration of plug-in hybrid electric vehicles (PHEVs)*"**, IEEE PES ISGT 2012 - USA.

34. Turker, Harun; Hauck, Matthieu; Hably, Ahmad; Bacha, Seddik, **"*A tool of Vehicle-to-Grid (V2G) concept for voltage plan control of residential electric grid areas with Plug-in Hybrid Electric Vehicles (PHEVs)*"**, IECON'2012 - Canada.

35. Lozano Jr, Rogelio; Alamir, Mazen; Dumon, Jonathan; Hably, Ahmad, **"*Control of a wind power system based on a tethered wing*"**, EGNCA 2012 - India.

36. Ahmed, Mariam; Hably, Ahmad; Bacha, Seddik, **"*Grid-connected kite generator system: electrical variables control with MPPT*"**, IECON'2011 - Australia.

37. Hably, Ahmad; Dumon, Jonathan, **"*Observation et commande par retour d'état d'un procédé de bacs communicants*"**, CETSIS 2011 - Canada.

38. Alamir, Mazen; Hably, Ahmad; Ding, Haiyang, **"*A Novel distributed NMPC control structure for partially cooperative systems under limited information sharing*"**, IFAC World Congress 2011 - Italy.

39. Ahmed, Mariam; Hably, Ahmad; Bacha, Seddik, **"*Power maximization of a closed-orbit kite generator system*"**, CDC-ECC 2011 - USA.

During my PhD:

40. Guerrero Castellanos, Fermi; Hably, Ahmad; Marchand, Nicolas, **"*Bounded attitude stabilization: Application on four-rotor helicopter*"**, Proceedings of the 2007 IEEE International Conference on Robotics and Automation, ICRA'07 - Italy.

41. Hably, Ahmad; Marchand, Nicolas, **"*Global stabilization of a four rotor helicopter with bounded inputs*"**, Proceedings of the 2007 IEEE International Conference on Intelligent Robots and Systems, IROS'07 - USA.

42. Marchand, Nicolas; Hably, Ahmad; Alamir, Mazen, **"*Constrained minimum time oriented stabilization of extended chained form systems*"**, Proceedings of the 2005 joint Conference on Control and Decision and European Control Conference.

43. Marchand, Nicolas; Hably, Ahmad, **"*Improving the performance of nonlinear stabilization of multiple integrators with bounded controls*"**, IFAC World congress 2005- Czech Republic.

6.4 Oral Presentations

1. Hably, Ahmad, **"*Airborne wind energy systems: Gipsa-lab activites*"**, AWEC 2015 at Delft [58].

2. Oral presentations at: CDC/ECC 2005, POSTA'06, ISIE 2012, IECON 2013, AWEC 2013 (poster), IFAC WC 2014, CDC 2014 (chairman of a session in place of Nicolas Marchand), ICIT 2015, REDEC 2016, ACC 2016, EPEC 2016, IECON 2016.

3. **Two seminars** at Beirut Arab University - Lebanon (2011 and 2012) and **one seminar** at UFL - Lebanon (2014).

6.5 Distinctions for My Students

1. Ahmed, Mariam: Jorma Luomi Student Forum Presentation Award of the international conference ICEM 2012. Best poster award in the EEATS Day 2012.

2. Lozano, Rogelio: Best Paper award for PhD Student in the international conference ICSTCC 2013. Best poster award in the EEATS Day 2011.

3. Ovale, Andres: ICIT 2015 IEEE Student Travel Scholarship.

Figure 2.8: Mariam Ahmed: Presentation Award of the international conference ICEM 2012.

4. Hajar, Khaled: Best project award at Order of Engineers of Lebanon (Tripoli - 2015).

   His work has been mentioned in "How Smart Microgrids Could Ease Lebanon's Electricity Woes" of the MIT Technology review [7].

6.6 Scientific Animation and Implication

◇ Member of the national organization committee of **CIFA 2012** and *chair* of one session. Chair of a session in EPEC 2016.

◇ Co-organizer of an "invited track" on AWE systems at IFAC WC 2017.

◇ Member of the international program committee of **AWEC 2015**.

◇ Responsible of a scientific program with the Université de Technologie et de Sciences Appliquées Libano-Française. Automatic control course at the same university (28 hours in 2015 and 2016).

◇ Member of the organization committee of Persycup challenge, a robotic competition funded by Persyval.

◇ **gipsa**-lab correspondent in the HNW500 network.

◇ **IEEE member**.

◇ Reviewer (more than 80 reviews): International Journal of Robust and Nonlinear Control, IEE Proceedings Control Theory & Applications, IEEE transactions on Sustainable Energy, IEEE Robotics and Automation Magazine, Automatica, IEEE transactions on

Chapter 3

Airborne Wind Energy Systems

1 Introduction

Conventional wind turbine converts the kinetic energy of wind into electrical energy using a rotor with three or several blades coupled with an electric generator. The turbine is connected to the network via an electrical power electronic interface. The turbine power is controlled by its rotational speed via the resistant torque and the pitch control of the blades. For these wind turbine, the conversion chain and the control units are placed in the nacelle on the top of the mast of the turbine. In 2010, ENERCON presented its E-126 wind turbine with rotor diameter reaches 126m, a mast height 135m, and a total mass of 6000 tons. The rated power of this turbine is 7.5 MW. The objective behind the increase of the turbines size is to reach higher

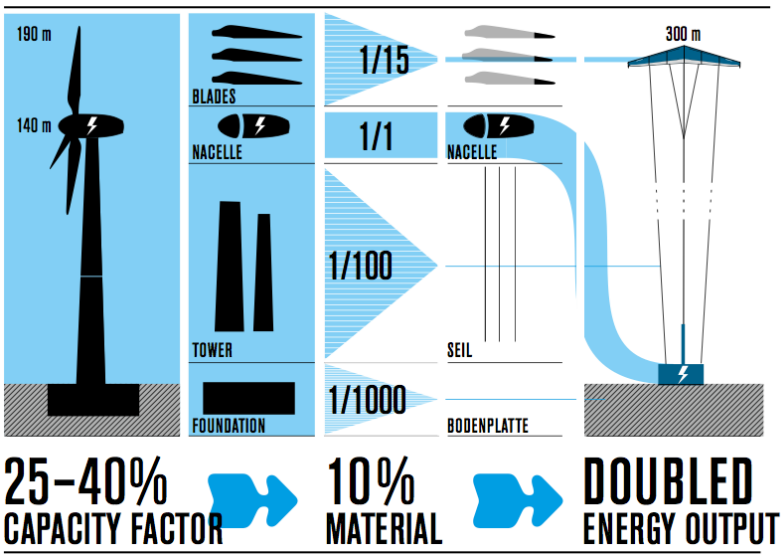

Figure 3.1: The use of a airborne wind energy system would double the power generated with a saving in materials over 90 %[14].

altitudes where the wind is known to be stronger and more stable [32]. Indeed, the amount of wind energy available increases with the cube of the wind speed. The other objective is to

increase the area swept by the blades with which the wind power available increases linearly. Nevertheless, the size of the wind turbines will not grow as quickly as in the past [112]. Indeed, its manufacturing cost, which includes the construction of its foundations, grows as fast as its rated power [50].
To overcome the limitations of conventional wind turbines, the concept of airborne wind energy (in French **eoliennes volantes**) has emerged and is currently studied by many research groups and start-up (see Sect. 2 for an overview of the international landscape).

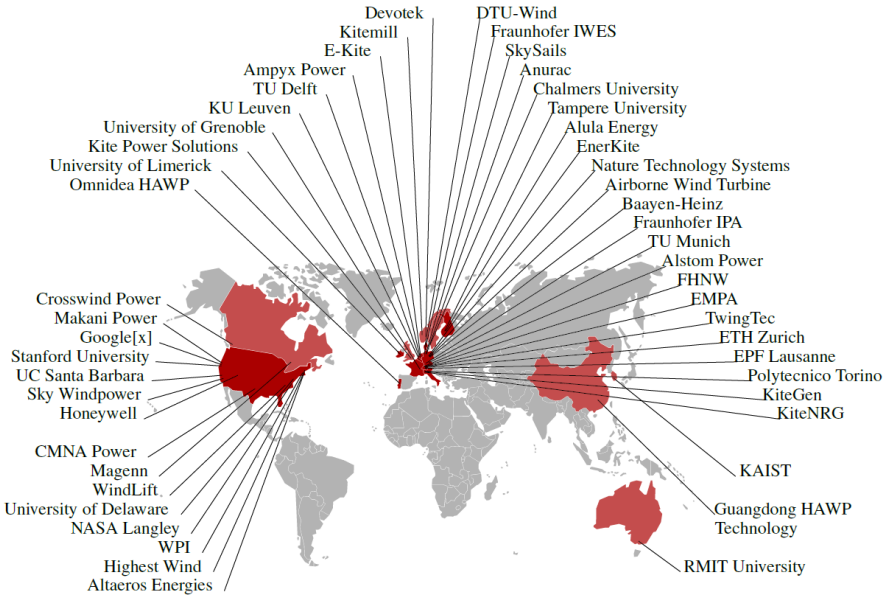

Figure 3.2: The airborne wind energy community (from [22]).

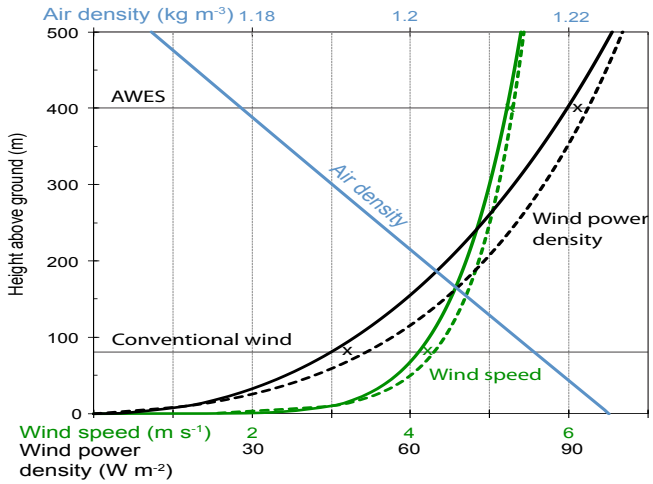

Figure 3.3: Changes in wind speed and air density as a function of altitude [32].

Airborne wind energy systems are therefore designed to replace the blades of conventional

wind by controlled flying system that captures the energy of the wind. This considerably simplifies the construction for removing the mast and its foundations, and one can reduce by 90 % the material requirements (Fig.3.1). This allows to use offshore floating platforms, opening access to deeper areas such as the Mediterranean coasts currently inaccessible to the actual systems (Fig.3.4). Finally, airborne wind energy systems can reach much higher altitudes, where the wind is stronger and more regular (Fig.3.3). The expected ultimate cost for such systems would be of the order of 4c€/kWh [14], half of the conventional wind and below the nuclear evaluated in 2012 around 5c€/kWh [12].

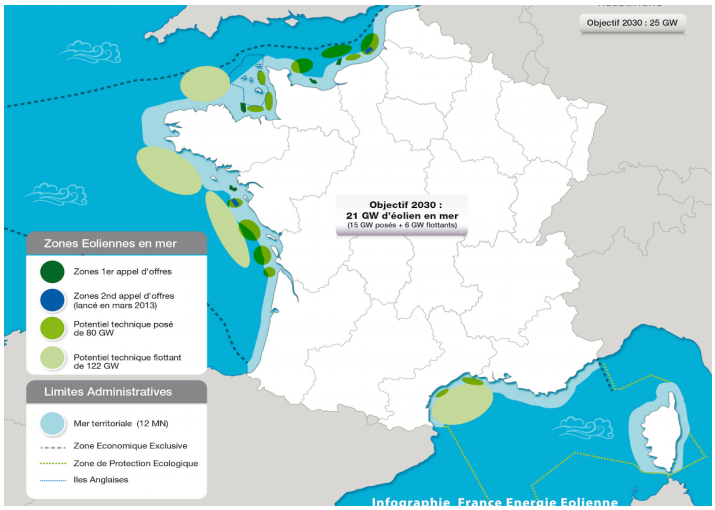

Figure 3.4: Technical potential for floating and installed wind turbines [4].

1.1 Organization of the Chapter

Airborne wind energy is a challenging domain that needs several skills in different fields. For this, I co-supervised several internships (second year projects and final year projects), student collective projects, in addition of two PhD thesis. The first PhD is of Rogelio Lozano Jr. a motivated and skillful person who proposed a lot of solutions to several complicated technical and theoretical problems. The second PhD thesis is of Mariam Ahmed, a very serious hard worker with a lot of ideas and results despite the bad conditions that she had during her PhD [1]. In addition, I have participated in the last two Airborne wind energy conferences, AWEC 2013 at Berlin and AWEC 2015 at Delft. I am member of the program committee of AWEC 2015 conference [11]). I also participated in the review of the airborne wind energy book [22]. My work in the field of airborne wind energy has focused on the following points:

- ◇ Modeling (Sect.3) and control (Sect.4).
- ◇ Prototypes and experiments (Sect.5)
- ◇ Grid integration (Sect.6).

[1] Problems in her country Syria.

- ◇ The tether is inelastic and almost straight. This hypothesis is correct when the tether's length is less than $1000m$ and its inclination is less than 80 degrees.
- ◇ Wind is uniform with a non-varying direction, because the wind speed at high altitudes is regular.
- ◇ The geometry of the tether allows neglecting its lift force, and considering only the drag C_{dt}.
- ◇ A high effective aerodynamic efficiency G_e of the kite/wing and the tether. In this case, this factor is introduced in [71] by:

$$G_e = \frac{C_L}{C_D + \frac{A_c}{4A} C_{dt}} \tag{3.1}$$

with A is the kite's surface and A_c is the crosswind area of the tether.

- ◇ Kite position and velocity as well as the traction force are known throughout the system functioning using observers or sensors.
- ◇ The orientation mechanism is used to control the kite/wing by either controlling the roll angle and the traction force T.

3.1.1 System Dynamics

The kite dynamical model was originally introduced in [46] and developed in [41]. As illustrated in Fig. 3.12, forces acting on the kite include the gravity force $\mathbf{F}_{grav}$, the aerodynamic force $\mathbf{F}^{aer}$ and the tether traction force T. The dynamics can be expressed in the spherical coordinates $\mathbf{e}_r, \mathbf{e}_\theta, \mathbf{e}_\phi$ as follows:

$$M\gamma = \mathbf{F}_{grav} + \mathbf{F}^{aer} + T \tag{3.2}$$

where M is the kite mass, and γ is the kite acceleration expressed in Eq.3.3.

$$\gamma = \begin{bmatrix} r\ddot{\theta} + 2\dot{r}\dot{\theta} - r\dot{\phi}^2 \sin\theta\cos\theta \\ r\sin\theta\ddot{\phi} + 2\dot{\phi}(\dot{r}\sin\theta + r\dot{\theta}\cos\theta) \\ \ddot{r} - r(\dot{\theta}^2 + \dot{\phi}^2\sin^2\theta) \end{bmatrix} \tag{3.3}$$

The gravity force is expressed in Eq.3.4.

$$\mathbf{F}_{grav} = Mg \begin{bmatrix} \sin\theta \\ 0 \\ -\cos\theta \end{bmatrix} \tag{3.4}$$

The aerodynamic force F_{aer} is related directly to the effective wind and v_a, that is the difference between the wind speed and the Kite's velocity. Assuming the wind speed v_w is in the direction of x-axis, v_a is given by Eq.3.5.

$$\mathbf{v}_a = \begin{bmatrix} v_{a\theta} \\ v_{a\phi} \\ v_{ar} \end{bmatrix} = \begin{bmatrix} v_w\cos\theta\cos\phi - \dot{\theta}r \\ -v_w\sin\phi - \dot{\phi}r\sin\theta \\ v_w\sin\theta\cos\phi - \dot{r} \end{bmatrix} \tag{3.5}$$

The aerodynamic force has two components, a drag and a lift force. In order to express both, a kite related coordinates $(\mathbf{x}_w, \mathbf{y}_w, \mathbf{z}_w)$ is defined as follows:

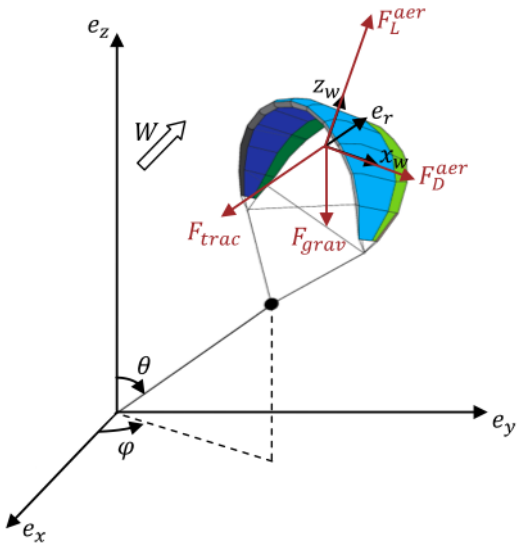

Figure 3.12: Kite's main forces.

- $\mathbf{x}_w = -\frac{\mathbf{v_a}}{|v_a|}$ is carried on the longitudinal axis of the kite.
- $\mathbf{y}_w$ is carried on the line connecting the kite end tips.
- $\mathbf{z}_w = \mathbf{x}_w \times \mathbf{y}_w$ is perpendicular on the kite surface and directed upwards.

With these definitions, the drag and the lift components of F_{aer} are:

$$\begin{array}{rcl} \mathbf{F}_D^{aer} & = & -\frac{1}{2}\rho S C_D |v_a|^2 \mathbf{x}_w \\ \mathbf{F}_L^{aer} & = & -\frac{1}{2}\rho S C_L |v_a|^2 \mathbf{z}_w \end{array} \tag{3.6}$$

The coefficients C_L, C_D are functions of the angle of attack α to be controlled. The kite-related coordinates $(\mathbf{x}_w, \mathbf{y}_w, \mathbf{z}_w)$ can be expressed in the spherical coordinates $\mathbf{e}_r, \mathbf{e}_\theta, \mathbf{e}_\phi$, the drag and lift are written in Eq.3.7 and Eq.3.8,

$$F_D = \frac{1}{2}\rho S C_D |v_a| \mathbf{v_a} \tag{3.7}$$

$$F_L = \frac{1}{2}\rho S C_L |v_a| \sin\psi \begin{bmatrix} v_{a\phi} \\ -v_{a\theta} \\ 0 \end{bmatrix} + \frac{1}{2}\rho S C_L |v_a| \cos\psi \begin{bmatrix} \frac{v_{ar}}{L}[v_{a\phi}\sin\eta - v_{a\theta}\cos\eta] \\ \frac{-v_{ar}}{L}[v_{a\theta}\sin\eta + v_{a\phi}\cos\eta] \\ L\cos\eta \end{bmatrix} \tag{3.8}$$

with ρ is the air density.

3.2 A Two Dimensional Model

The model developed in this section is used to describe both the dynamics of an AWE system with a tethered rigid wing and the dynamics of AWE system with a light-weight rotating Magnus cylinder. The forces acting on flying part of the system, as shown in the Fig.3.15, are lift force L, drag force D, weight of the wing P, buoyant force B in the case of Magnus

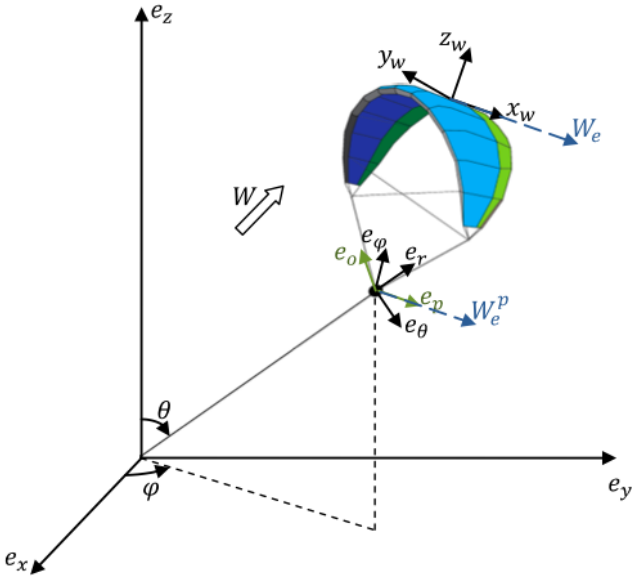

Figure 3.13: Kite's attached coordinates.

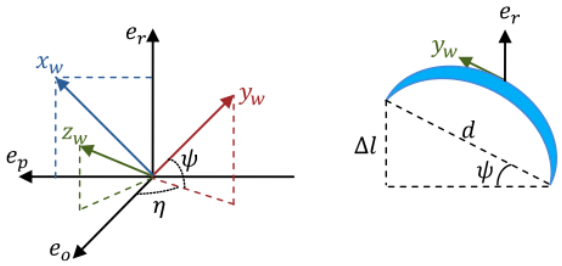

Figure 3.14: Definition of ψ and η angles.

effect-based AWE system, and traction force T in the tether. Lift and drag forces can be expressed by:

$$L = \frac{1}{2}\rho S v_a^2 C_L, \quad D = \frac{1}{2}\rho S v_a^2 C_D \tag{3.9}$$

where ρ is the air density, S is the wing projected surface area, v_a is the norm of the apparent wind velocity vector, C_L and C_D are respectively lift and drag coefficients. In the case of Magnus effect-based AWE system, the buoyancy force can be calculated from Archimedes' principle:

$$B = (\rho - \rho_\mathrm{g}) V_0 g \tag{3.10}$$

where V_0 is the volume of the Magnus cylinder, ρ_g is the gas density, and g is the gravitational acceleration. The Magnus cylinder mass is:

$$M_\mathrm{Mag} = M + V_o \rho_\mathrm{g} + M_l r \tag{3.11}$$

where M is the mass of the airborne structure and M_l denotes the mass per tether length. The wind velocity v_w is assumed exactly horizontal (i.e. parallel to ground plane). The apparent

wind velocity v_a is defined by:

$$\mathbf{v}_a = \mathbf{v}_w - \mathbf{v}_k \tag{3.12}$$

where $\mathbf{v}_k$ is the Magnus-effect-based system. The apparent wind velocity forms an angle α_w with the horizontal. In this study, the movement of the Magnus cylinder is assumed to be in the vertical plane. It is also assumed that tether of length r is always in tension and a straight line. It has an elevation angle β with respect to the horizon. F_r and F_τ are respectively the radial and tangential force components according to the 2D polar coordinate as shown in Fig.3.15. These forces can be expressed as follows:

$$F_r = -T + L\sin(\beta - \alpha_w) + D\cos(\beta - \alpha_w) - P\sin\beta + B\sin\beta \tag{3.13}$$

$$F_\tau = L\cos(\beta - \alpha_w) - D\sin(\beta - \alpha_w) - P\cos\beta + B\cos\beta \tag{3.14}$$

where α_w is the angle that the apparent wind velocity forms with the horizontal. For Magnus-

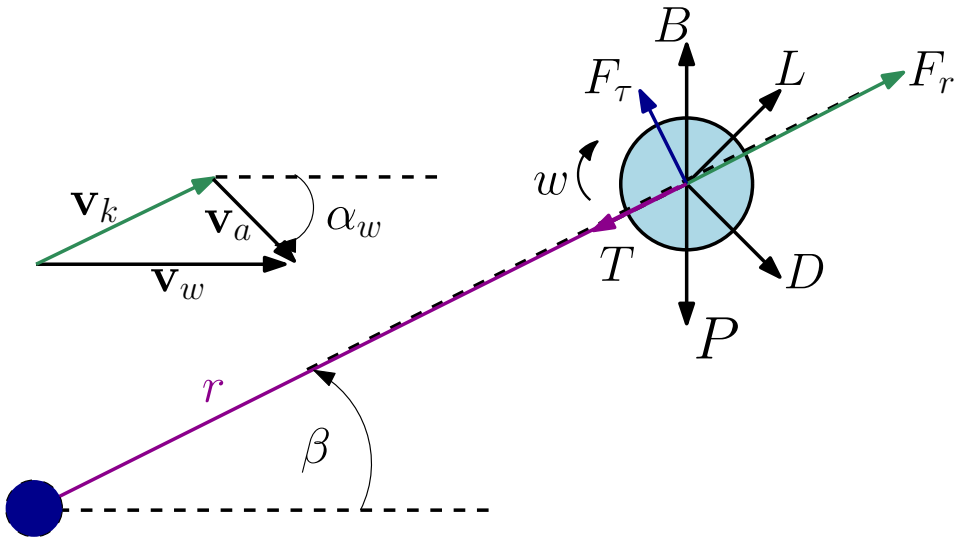

Figure 3.15: The forces acting on the Magnus cylinder airborne wind energy system. v_k is the vector velocity of the Magnus cylinder. ω is the Magnus cylinder rotational velocity. v_w is the airspeed with respect to the ground. α_w in the figure is of negative sign.

effect-based systems, aerodynamic lift coefficient C_L and drag coefficient C_D are functions of the spin ratio X and not of the angle of attack as specified for airfoils. The Magnus cylinder spin ratio is given by the following equation [107]:

$$X = \frac{\omega R}{v_a} \tag{3.15}$$

where ω is the Magnus cylinder rotational velocity and R is its radius. The system dynamic model can be derived by imposing the mechanical equilibrium of a point mass model in 2D polar coordinates:

$$\ddot{\beta} = \frac{1}{r}\left[-2\dot{\beta}\dot{r} + \frac{F_\tau}{M_{Mag}}\right] \tag{3.16}$$

$$\ddot{r} = \frac{1}{M_{Mag} + M_D}\left[r\dot{\beta}^2 M_{Mag} + F_r\right] \tag{3.17}$$

where $M_D = \frac{I}{R_d^2}$ with moment of inertia of the ground-based motor I and its radius R_d. The traction force is measured by a torque sensor divided by the radius of the drum. One has:

$$\dot{T} = \beta_T\Big(u_T - T\Big) \tag{3.18}$$

Eq.(3.18) represents the first order dynamic response of actuators used in the experimental platform to control the traction force in the tether.

4 Control of AWE Systems

Several control schemes have been proposed for the control of AWE systems. In the following sections, several results will be presented.

4.1 Nonlinear Model Predicitive Control Design [28]

A nonlinear model predictive control have been designed for the three dimensional model proposed in Sect.3.1. The objective is to maximize the produced average power during one cycle. In order to do so, both the produced power and the closed orbit conditions are expressed as functions of a dimensionless variable τ.

4.1.1 Orbit Optimization

The system average mechanical power over one period σ is:

$$\bar{P}_M = \frac{1}{\sigma}\int_0^{\sigma} TV_L(t)dt \tag{3.19}$$

where V_L is the tether radial velocity. According to [35], by changing the integral time variable $t \in [0, \sigma]$ to the dimensionless parameter $\tau \in [0, 2\pi]$, and making use of the substitution $V_L(t) = Vv(\tau)$, Eq.3.19 can be expressed as follows:

$$\bar{P}_M(v) = \frac{1}{2}\rho S C_L G_e^2 V^3 J_0(v) \tag{3.20}$$

where V is the wind speed amplitude and

$$J_0(v) = \frac{\int_0^{2\pi}(w_{||} - v)vh(\tau)d\tau}{\int_0^{2\pi}\frac{h(\tau)}{w_{||}-v}d\tau} \tag{3.21}$$

with $h(\tau) = \sqrt{d\theta^2 + d\phi^2\sin^2(\theta)}$ and $w_{||} = \sin(\theta)\cos(\phi)$. When the attack angle α is constant, the effective glide ratio G_e, C_L are constant and J_0 represents the normalized average power $\bar{P}_M$ [34], where the normalizing coefficient is : $\rho A C_L G_e^2 V^3$.

Orbit optimization aims at having a high crosswind speed, which develops high traction force and thus higher power production. The crosswind speed is expressed by:

$$|v_a^p| = G_e V(w_{||} - v) \tag{3.22}$$

The velocity $\hat{v}(\tau)$ that maximizes the power produced presented earlier by the Eq.3.21, and satisfies the closed loop orbit condition $\int_0^T V_L(t)dt = 0$, which is expressed, by making the variable change $V_L = Vv$, by [34]:

$$\int_0^{2\pi} \frac{vh(\tau)}{w_{||} - v} d\tau = 0 \tag{3.23}$$

Once found, $\hat{v}(\tau)$ is used to derive the traction force [35] by:

$$T = \frac{1}{2}\rho S C_L G_e^2 v_w^2 (w_{||} - \hat{v})^2 - (M + M_l) g \cos\theta \tag{3.24}$$

4.1.2 Orbit Period

Previous calculations and variables are functions of the dimensionless parameter τ and have a period of 2π. The orbit time period σ and the relation between the time variable $t \in [0, \sigma]$ and τ need to be defined. The period equals the orbit length devised by the kite speed:

$$\sigma = \oint \frac{dl}{|\dot{r}|} \tag{3.25}$$

With dl is a differential length along the orbit:

$$\mathbf{dl} = dr\mathbf{e}_r + rd\theta\mathbf{e}_\theta + r\sin\theta d\phi\mathbf{e}_\phi = (r'\mathbf{e}_r + r\theta'\mathbf{e}_\theta + r\sin\theta\phi'\mathbf{e}_\phi)d\tau = \dot{\mathbf{r}}d\tau$$

The velocity vector $\dot{\mathbf{r}}$ at a certain point of the orbit is carried on its tangent:

$$\mathbf{t}(\tau) = \frac{\mathbf{dl}}{\|dl\|} = \frac{r'\mathbf{e}_r + r\theta'\mathbf{e}_\theta + r\sin\theta\phi'\mathbf{e}_\phi}{\sqrt{r'^2 + r^2\left(\theta'^2 + \phi'^2\sin^2\theta\right)}}$$

Due to the crosswind motion law $|v_a^p| = G_e(V_{||} - \dot{r})$ one gets [35]:

$$T = \oint \frac{r\sqrt{\theta'^2 + \sin\theta\phi'^2}}{|\dot{\mathbf{r}}_\perp|} d\tau \tag{3.26}$$

The quantity Ge has a high value. Therefore, the mathematical model of wind energy generation can be further simplified as follows:

$$\frac{|\dot{\mathbf{r}}_\perp|}{V} = \omega_\perp + \sqrt{\omega_\perp^2 + G_e^2(w_{||} - v)^2 - |\mathbf{w}_\perp|^2} = G_e(w_{||} - v)$$

Hence the period can be finally expressed in the equation Eq.3.27.

$$\sigma = \int_0^{2\pi} \frac{r(\tau)h(\tau)}{G_e(w_{||}(\tau) - v(\tau))} d\tau \tag{3.27}$$

and:

$$t = \int_0^{\tau} \frac{r(\sigma)h(\sigma)}{G_e(w_{||}(\sigma) - v(\sigma))} d\sigma \tag{3.28}$$

Now that the optimal tether radial velocity and the period corresponding to a given eight-figured orbit are found, a nonlinear model predictive control (NMPC) is applied to achieve tracking the generated orbit while respecting the system constraints. This is done via control of the kite roll angle and the tether's traction force, in addition to the attack angle if the aerodynamic efficiency is optimized as well.

The resulted kite orbit is a three-dimensional orbit described in the spherical coordinates by $r(t), \theta(t), \phi(t)$. Tracking this orbit is divided into orienting the kite hence controlling its roll angle to follow the reference $(x, \dot{x})$ with $x = (\theta, \phi)$, and controlling the radial velocity by control of the on-ground electric machine rotation velocity ($V_L = \Omega_s / K$). At each time step, $\ddot{x}$ that minimizes the cost function of Eq.3.29, that reflects the distance from the reference orbit, is calculated and controlled by the roll angle ψ.

$$\|(\ddot{x}_{ref} - \ddot{x}) + \lambda_1(x_{ref} - x) + \lambda_2(\dot{x}_{ref} - \dot{x})\|^2 \tag{3.29}$$

where λ_1, λ_2 determine how fast the state converges to the reference orbit.
Figure 3.16 summarizes the AWE proposed control strategy. It starts from the parametric initial orbit and generates a time-dependent orbit with an optimal radial velocity. The control is applied to find the roll angle that achieves tracking of $(\theta(t), \phi(t))$, while the radial velocity is controlled by controlling the ground machine rotation velocity.

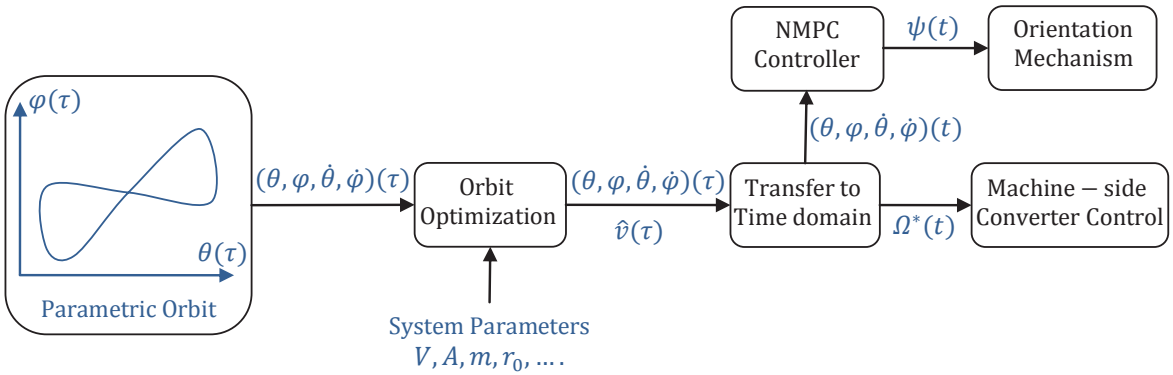

Figure 3.16: The Nonlinear Model predictive control strategy.

Numerical Application As mention above, choosing the primary orbit to be optimized is an essential step in determining the maximum possible extracted average power, and the ratio between the average and the maximum power, or what we choose to call "Performance". Table.3.1 shows the AWE parameters and the wind velocity is assumed to be constant and regular with a speed $V = 4m/s$. Figure 3.17 shows the test orbits. Test orbits 2 and 3 results from amplifying the reference test orbit 1, while orbits 4 and 5 results form rotating the reference orbit 30 and 90 degrees respectively.

Table 3.2 shows the characteristics of the five chosen test orbits with $\theta_0 = 55^o$ and $\phi_0 = 0^o$, as well as, the estimated corresponding mean power, performance, and the orbits period. In [36], it is demonstrated that a larger trajectory correspond to greater average power, further more, a bigger rotation of the orbit leads to more average power which agrees with the results obtained and displayed in Table.3.2. As noticed, the mean generated power increases as the orbit size increases. The performance gets better as well, because a larger orbit allows the kite

Table 3.1: AWE system parameters

Symbol	Name	Value
R	$Rotor Diameter$	0.3 m
Ω_{max}	Maximum rotor rotation velocity	25 rd/sec
Γ_{max}	Motor maximum torque	22 $N.m$
M	Kite mass	2.5 kg
S	Kite area	5 m^2
ρ	Air density	1.2 kg/m^3
C_L	Lift coefficient	1.5
C_D	Drag coefficient	0.15
T_s	Sampling time	0.1 sec

recovery phase to occur further from the center of the power region, hence consumes less energy. The size, however, is a parameter to be optimized according to the system location. The orbits

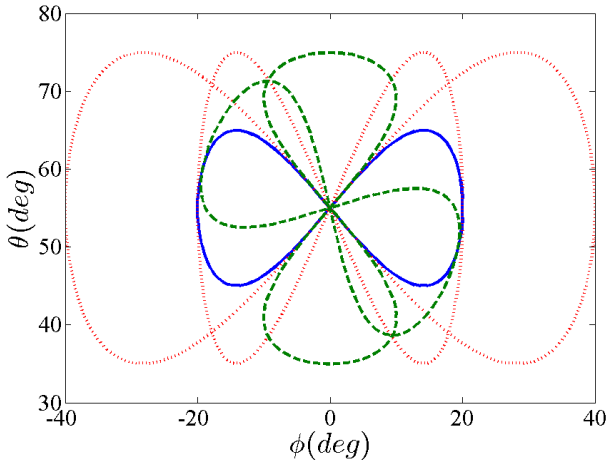

Figure 3.17: Test orbits: Reference orbit (1) in continuous line, amplified orbits (2,3) in dotted line, and rotated orbits (4,5) in dashed line.

optimization results in the normalized parametric radial velocity $\hat{v}$ which depends only on the wind direction and the parametric orbit. The time dependent radial velocity profile is found after calculating the orbit period and time vector (Eq.3.27-Eq.3.28). The resulted profiles in the case of orbits $1, 2$ and 3 are shown in Fig. 3.18. Notice that the optimal velocity has double the calculated period hence during one orbit two traction and two recovery phases. This means doubling the resulted power profile and decreases its continuity. The top figure of Fig.3.20 shows the AWE energy profile for the orbits $1, 2$ and 3.

Figure 3.19 shows the radial velocity profiles for orbits 4 and 5 compared to the reference 1. Rotating the orbit results in more average generated power and increases the performance without the need to increase the orbit size or the system parameters. On the contrary with respect to the case of 0^o rotation, a 90^o rotated orbit preserve the orbit period which means only one traction and one recovery phase during the orbit. This can be also observed by the

Table 3.2: Testing orbits parameters and optimized orbits' period, mean mechanical power and performance

Orbit	1	2	3	4	5
$\Delta\theta$	10^o	20^o	20^o	10^o	10^o
$\Delta\phi$	20^o	20^o	40^o	20^o	20^o
Rot	0^o	0^o	0^o	30^o	90^o
Period (sec)	35.4	59.0	78.4	35.4	35.0
Mean power (W)	240	732	844	398	840
Performance	0.058	0.094	0.108	0.058	0.100

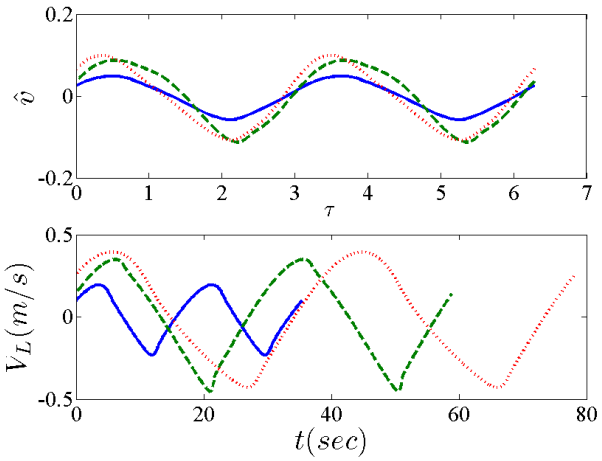

Figure 3.18: Normalized and time dependent radial velocity in top and bottom figure respectively. Reference orbit (1): continuous, orbit (2): dotted, orbit (3): dashed.

energy profiles shown on the lower plot of Fig.3.20. As noticed, the AWE system will offer a very high adaptability, as its rated power can be modified by changing the kite orbit size and/or rotation. It can also be modified by changing the orbit inclination θ_0, or the altitude at which the kite is flying for example. Figure 3.21 shows how the AWE system generated average power changes as a function of the kite surface S, the orbit rotation angle; and the orbit inclination θ_0. Figure 3.22 shows the orbit tracking by applying the predictive control in the case of the first orbit. Here the radial velocity, hence the tether length, is assumed to be controlled by the ground machine.

4.2 Virtual Constraint-based Controller (VC) [24]

In this section, the AWE system periodic target motion is ensured by a state feedback control law based on virtual constraints approach. The proposed motion planning strategy is a fast in-loop control method that is robust against disturbances, and it guarantees an exponential orbital stabilization. The application of the VC-based control method can be summarized by the following steps (see Fig.3.23)

- ◇ Finding the model of the system.

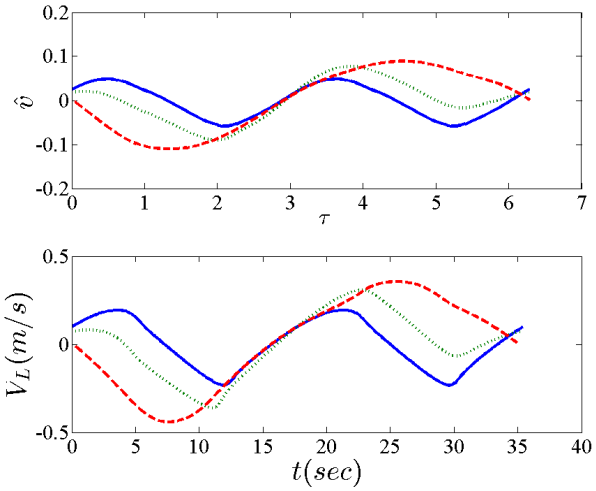

Figure 3.19: Normalized and time dependent radial velocity in top and bottom figure respectively. Reference orbit (1): continuous, orbit (4): dotted, orbit (5): dashed.

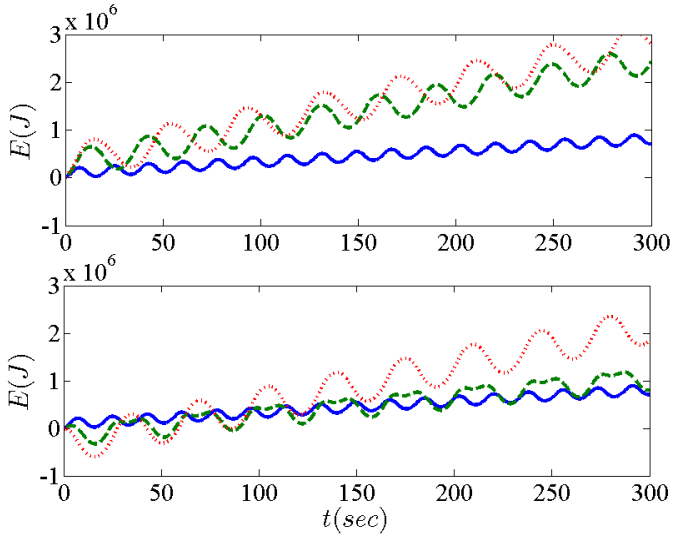

Figure 3.20: AWE energy generation. Reference orbit (1): continuous. Top figure plot: orbit (2) energy profile in dotted line, orbit (3): dashed. Bottom figure: orbit (4) energy profile in dotted line, orbit (5): dashed.

- ◇ Choice of a suitable virtual constraint.
- ◇ Application of a partial feedback linearization, where the remaining nonlinear part is integrable.
- ◇ Construction of an auxiliary linear periodic control system of reduced order.
- ◇ Control design for the auxiliary system.
- ◇ A modification of the control developed in the previous item to be applied to the original nonlinear system.

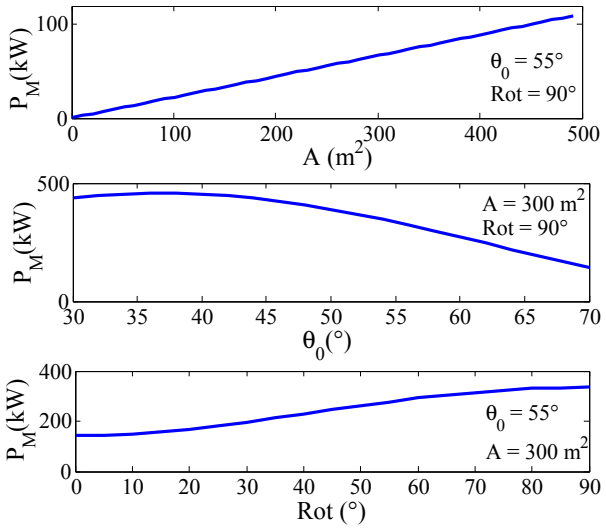

Figure 3.21: Starting from top figure: The average mechanic power as a function of the kite surface S, the inclination angle θ_0; and the orbit rotation Rot.

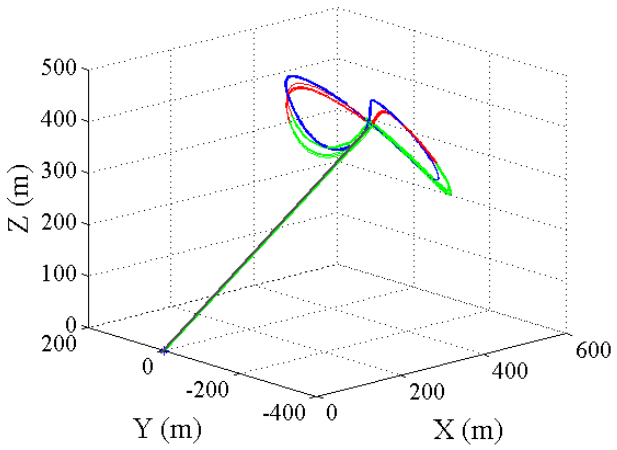

Figure 3.22: Tracking orbit 1 using optimal predictive control

Starting from an arbitrary point $(\theta, r, \dot{\theta}, \dot{r})$ within the power region of the kite, the application of proposed virtual constraints-based control developed here gives the closed loop behavior of Fig.3.24. One can clearly see the effectiveness of the proposed feedback control. Several initial conditions have been tested and for all of them, the trajectories have stabilized on a periodic orbit in a short time. The speed of convergence depends on the gain of the feedback control v.

4.3 Observer-based Control

An observer-based control strategy has been proposed. The observer is used to estimate badly known aerodynamic parameters that need to be reconstructed. This control strategy allows us

the same manner. Note that the equation (3.16) can be rewritten in the following condensed form:

$$\ddot{\beta} = \chi + Qu_\beta \tag{3.30}$$

where Q is given by

$$Q = -\frac{\rho S v_r^2 \gamma_\beta}{2Mr}\sin(\beta - \alpha_w)$$

and χ represents the *relatively badly known* term

$$\chi = -\frac{2\dot{r}\dot{\beta}}{r} + \frac{L\cos(\beta-\alpha_w) - P\cos\theta}{rM} - \frac{\rho S v_r^2(\frac{C_L^2}{\pi e\lambda} + C_{D_0})\sin(\beta-\alpha_w)}{2rM}$$

This suggests that χ can be estimated using the following Luenberger estimator based on the sole measurement of β:

$$\hat{\chi} = \begin{pmatrix}0 & 0 & 1\end{pmatrix}\hat{X}_1 \tag{3.31}$$

$$\dot{\hat{X}}_1 = (A_1 - L_1C_1)\hat{X}_1 + B_1u_\beta + L_1\beta \tag{3.32}$$

where the observer's state is $X_1 = [\beta\ \dot{\beta}\ \chi]$ and

$$A_1 := \begin{pmatrix}0 & 1 & 0\\ 0 & 0 & 1\\ 0 & 0 & 0\end{pmatrix};\ B_1 := \begin{pmatrix}0\\ Q\\ 0\end{pmatrix};\ C_1 := \begin{pmatrix}1 & 0 & 0\end{pmatrix} \tag{3.33}$$

while L_1 is the observer gain obtained for instance using LQE design. Q is a slow time-varying parameter. This gives the control law given by (3.31)-(3.32) together with:

$$u_\beta = -\frac{1}{Q}\Big[\hat{\chi} + \lambda_{1_\beta}(\dot{\beta} - \omega_{ref}) + \lambda_{2_\beta}(\beta - \beta_{ref})\Big] \tag{3.34}$$

where β_{ref} and ω_{ref} are respectively some desired angle and angular velocity while λ_{1_β} and λ_{2_β} are some design parameters. Note that feedback law (3.34) only needs the estimation of β, $\dot{\beta}$ and χ and does not need any particular knowledge on the drag force expression. The complete system (observers, feedback control, and the tethered wing power system) is shown on figure 3.25.

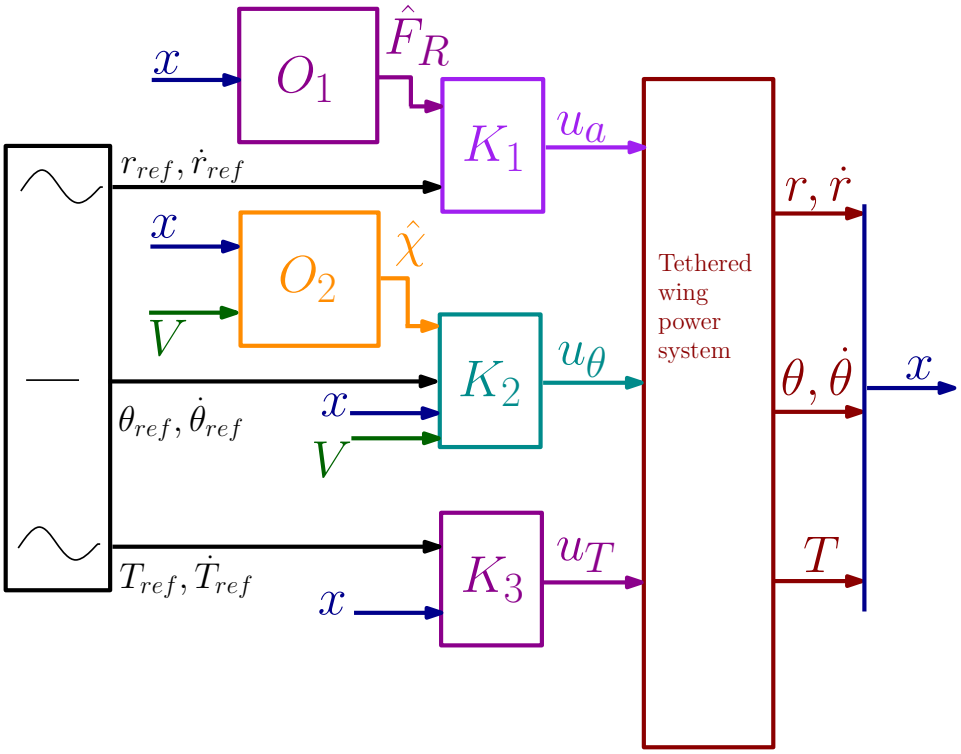

Figure 3.25: The complete system: O_1 and O_2 are respectively the observers of F_R and χ. K_1, K_2, and K_3 are respectively the state feedback control of u_a , u_θ, and u_T.

4.4 Energy Control Strategy

In this section, the control strategy to be applied to the AWE system aims at stabilizing the mean output power produced during a given cycle (recovery phase then production phase). The tether traction force T and its speed $\dot{r}$ are forced to track some reference signals related to a desired reference power P_{ref} to be produced. For simplicity, P_{ref} is assumed to be constant, however the control strategy can be adapted to varying P_{ref} as shown later.

During the cycle, the AWE system moves from a minimum radial position r_{min} to a maximum radial position r_{max} at a reel-out speed $\dot{r}_{prod}$ during production phase and from r_{max} to r_{min} at a negative reel-in speed $\dot{r}_{rec}$ during the recovery phase. Since $\dot{r}_{prod}$ and $\dot{r}_{rec}$ are assumed to be constant, the proposed algorithm tracks P_{ref} by controlling the traction force T. A given cycle is defined by the time period from the beginning of the recovery phase to the end of the production phase. The recovery phase starts at time t_0 and ends at time t_1. Then the production phase starts at time t_1 and ends at time t_2 (see Fig. 3.26). Time t_1 can be calculated by

$$t_1 = t_0 + \frac{(r_{max} - r_{min})}{-\dot{r}_{rec}} \tag{3.35}$$

Time t_2 can be calculated by

$$t_2 = t_1 + \frac{(r_{max} - r_{min})}{\dot{r}_{prod}} \tag{3.36}$$

In order to produce a net output power equals to P_{ref}, the output energy to be produced

during a cycle E_{ref} is given by $P_{ref}(t_2 - t_0)$. During the cycle, the output energy produced

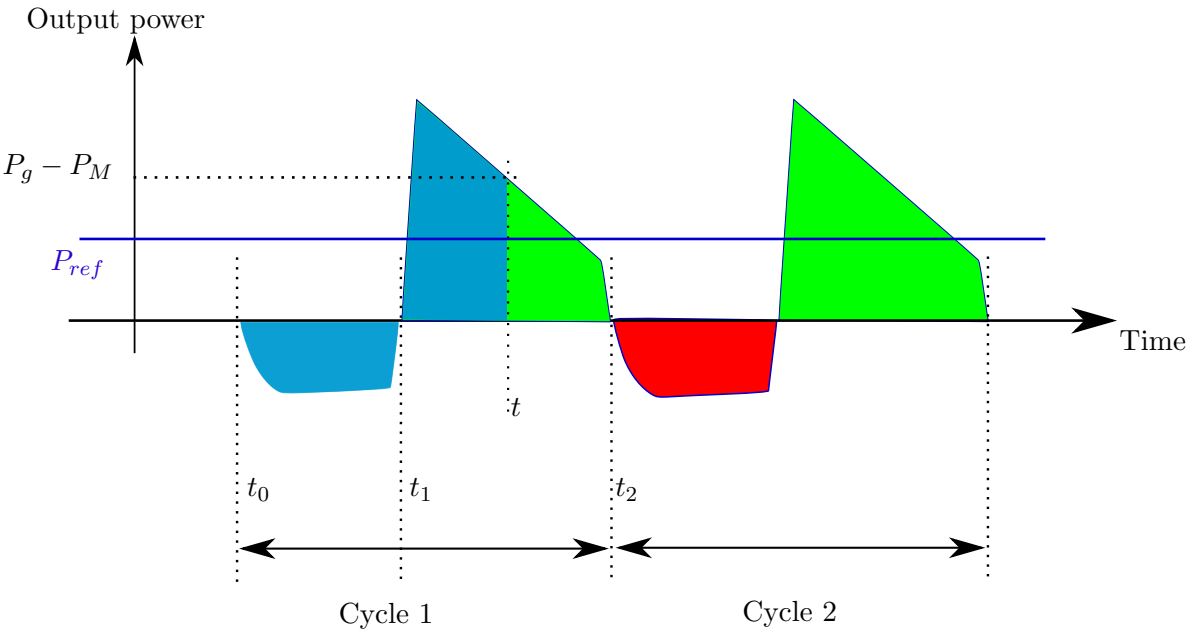

Figure 3.26: A sketch of the instantaneous output power as a function of time covering several pumping cycles. For a cycle, the red area E_{rec} represents the energy consumed during the recovery phase between time t_0 and time t_1 and the green area E_{prod} represents the energy produced during the production phase between time t_1 and time t_2. The blue area represents the output energy at time t for the beginning of the cycle. Desired reference power P_{ref} is assumed to be constant.

from time t_0 to time t is calculated by

$$E = \int_{t_0}^{t} (P_g - P_M) dt \tag{3.37}$$

where P_g is the produced output power of the on-ground generator and P_M is the power consumed by the Magnus motor. In order to satisfy $E = E_{ref}$ at the end of the cycle, the remaining energy to be produced E_{prod} from time t to time t_2 has to satisfy:

$$E_{prod} = E_{ref} - E \tag{3.38}$$

Subsequently, the reference traction force has to satisfy for $t \in [t_0, t_2]$

$$T_{ref} = \frac{1}{\dot{r}} \frac{E_{prod}}{(t_2 - t)} \tag{3.39}$$

As T cannot be negative, T_{ref} is set to zero for $t \in [t_0, t_1]$.

In order to implement the proposed control strategy, two other controllers K_1 and K_2 are used as shown in Fig. 3.27. The tether length is controlled by K_1 through the desired traction force u_T of the on-ground generator. In order to track T_{ref} obtained from controller K_3, K_2 controls spin ratio X of the Magnus rotor. Controller K_3 is given in Eq. (3.39). Controllers K_1

and K_2 are classical PID controllers in parallel form whose parameters are tuned empirically with the following constraints:

- K_2 is set to have a fast response time to get $T_{ref} = T$.
- K_1 is set to have a faster response time than K_2 in order to have a decoupled control between the tether length r and the traction force T.

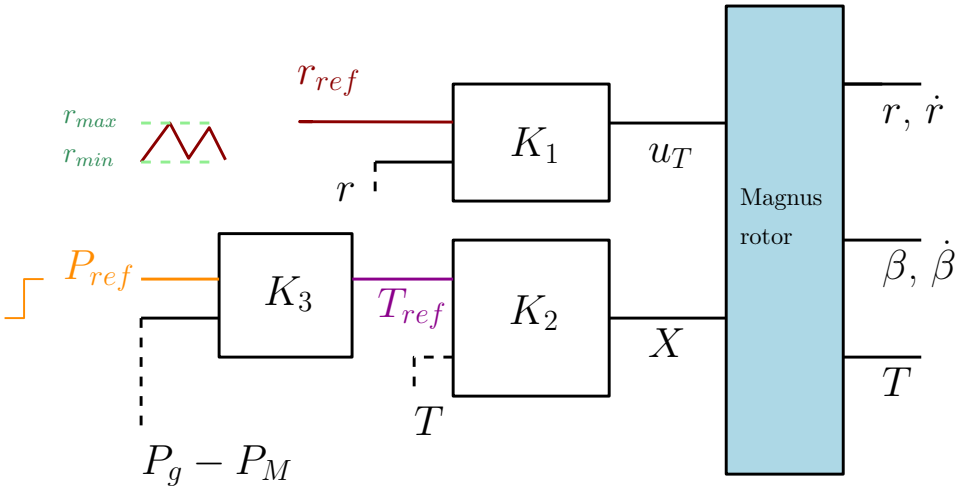

Figure 3.27: An overview of the proposed control system. Three controllers K_1, K_2, and K_3 are used. The Magnus rotor moves from minimum radial position r_{min} to a maximum radial position r_{max}. T_{ref} is obtained by Eq.(3.39). X is the spin ratio and u_T is the desired traction force.

5 Experimental Apporoach

In order to validate the theoretical studies on modeling and control of our airborne wind energy systems, a practical approach has been followed. The main directions have been followed will be listed.

5.1 Indoor Experiments

Several indoor prototypes have been build and tested in the context of the Rogelio Lozano PhD and several engineering final year projects. In total, more than thirteen prototypes (flexible and rigid) has been constructed and tested.

5.1.1 Wind Tunnel

A wind tunnel has been built. Its fan section is composed of nine brushless electrical motors equipped with two-blade fans of 0.355 m diameter, see Fig. 3.28 (top left). These motors, 800 W each, are distributed on a tunnel cross section area of 1.85 m^2. The air flow first passes through a honeycomb then in a tunnel of 1.8 m length in order to stabilize it. A hot wire wind

5.1.5 Reverse Pumping Prototypes

Several prototypes have been tested by R. Lozano in order to validate the reverse pumping principle. Following the guidelines presented in the paper [79] and inspired from the twin kite system, R. Lozano has built a system that can only fly by turning symmetrically around a vertical axis (Fig. 3.32).

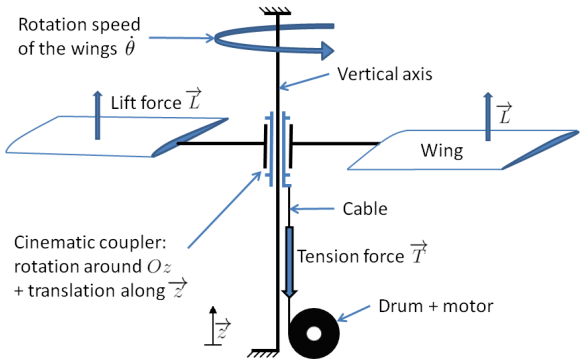

Figure 3.32: A scheme of the reverse pumping setup.

5.2 Outdoor Experiments

An outdoor experimental setup has been also built. It is composed of a ground station (Fig. 3.33) connected by tethers to either an OXY kite of 0.5 m^2 or UNO kitesurf of 2.5 m^2 (Fig. 3.34). This setup has been used in several outdoor tests mainly performed by Jonathan Dumon, Rogelio Lozano, and many engineering students during their projects and internships. Several videos are posted online in the setup website [1].

6 Grid Integration

The kinetic energy, captured by the airborne wind energy systems, needs to be transformed into an electric power that can be injected in the electric grid or used to supply a certain load. Among the proposed power transformation systems associated to renewable energy grid integration, the one shown in Fig.3.35 offers a suitable solution for the studied system.

6.1 Hardware In the Loop (HIL)

The traction force of the AWE system is transformed into a torque applied to an on-ground permanent magnet synchronous machine (PMSM). This produces an alternative electrical energy with variable frequency. The machine is coupled with the grid, or with a certain load, via a power electronics interface that consists of two bidirectional AC/DC converters. An energy storage should be added in the case of a load or an isolated grid connection, in order to provide the necessary energy during the system recovery phase. It is installed on the DC-bus level relating both converters.

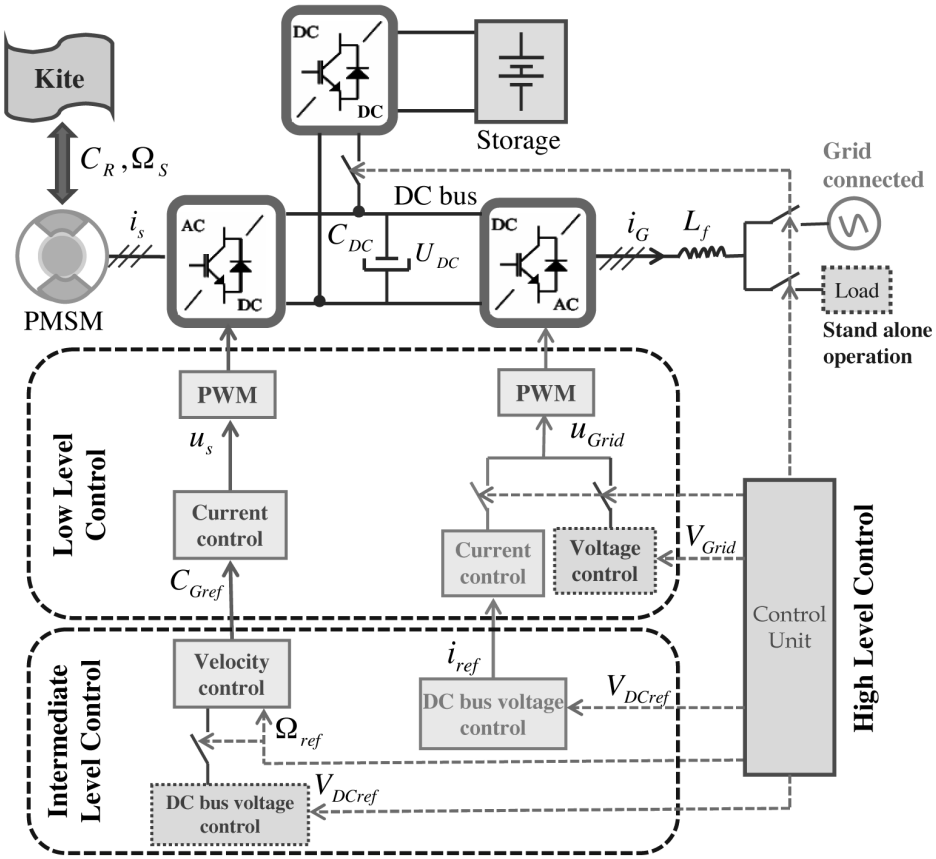

Figure 3.36: General control scheme of the AWE power transformation system. Two control tracks applied depending whether the system is grid connected or in a stand-alone operation.

formation system. As shown, the control scheme is divided into three levels: Low, intermediate and high. Each level operates in accordance with the system operation status: Grid-connected or stand-alone operation.

6.1.1 Validation

To validate the control scheme presented previously, a Power-Hardware-In-the-Loop (PHIL) of G2Elab is used. It is a real-time hybrid simulator that consists of three main parts: A direct current machine (DCM) coupled to a permanent magnets synchronous machine (PMSM), two converters (DC/AC, AC/DC), and a grid emulator. These hardware elements are interconnected and are supported and driven by real-time digital simulators: RT-lab and dSPACE. In this simulator, the tethered AWE system behavior and its associated drum and gearbox are emulated by a direct current machine (DCM), while the rest of the system is physically present. The hardware is interfaced with the real-time simulator on which the optimization and the control strategy in addition to the AWE model are implemented.
Employing the PHIL-simulator instead of building a prototype is justified because the tests carried on here, focuses on the grid integration aspect, and the produced power maximization via control of the power conversion chain, and not on the AWE orientation control. Furthermore, PHIL simulator requires less material and human investments, it can be modified

in the kite torque, which shows how generated power is optimized from the machine point of view. Torque and velocity variations are represented by the machine currents whose frequency, amplitude and phase change accordingly. The frequency is related directly to the rotation speed $f = \frac{\omega}{2\pi} = \frac{p\Omega}{2\pi}$, meanwhile the current amplitude expresses the torque variations, and the phase is inverted when the rotation velocity direction changes. Notice as well that the DC-bus voltage keeps a constant value despite the variations in the rotation velocity. For the grid-side converter electrical variables, Figure 3.41 shows the variations of the output current and the grid voltage following those of the rotation velocity. The current becomes zero before the rotation velocity reaches zero that is due to losses in the converters elements. This explains also why the current amplitude is higher when the velocity is negative (recovery phase) than when it is positive (generation phase).

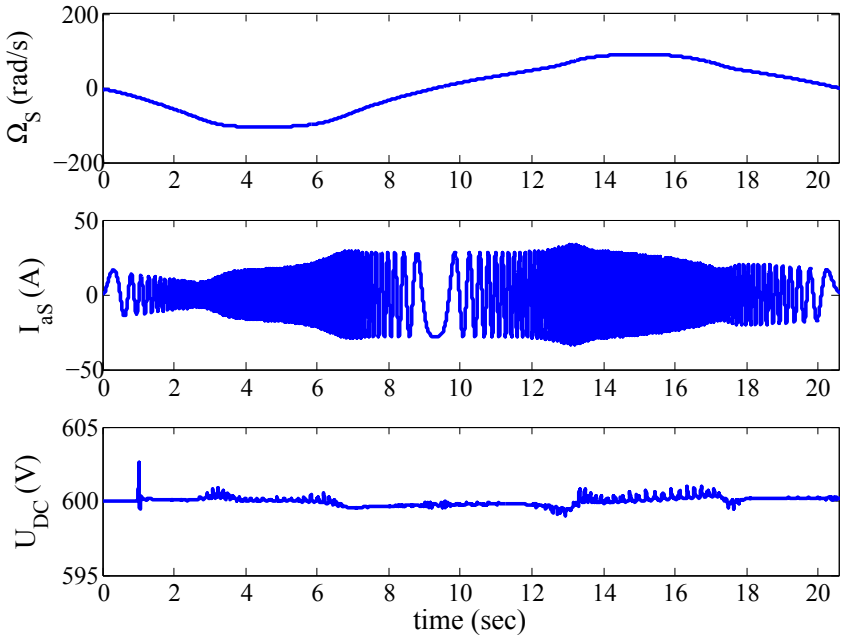

Figure 3.38: Starting from above: The PMSM rotation velocity (Ω_S), PMSM phase current (I_{aS}), DC bus voltage (U_{DC}).

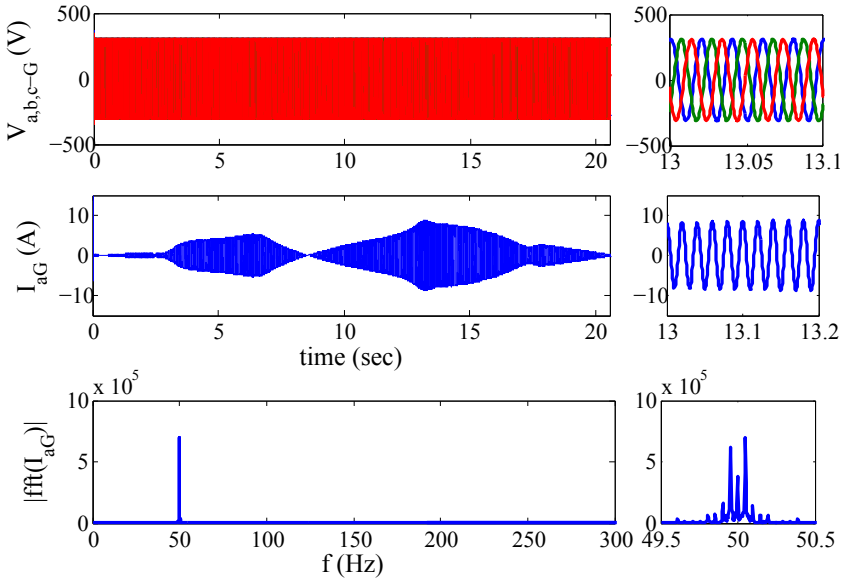

Figure 3.39: Starting from above: Grid voltages, grid current (I_{aG}), its frequency analysis.

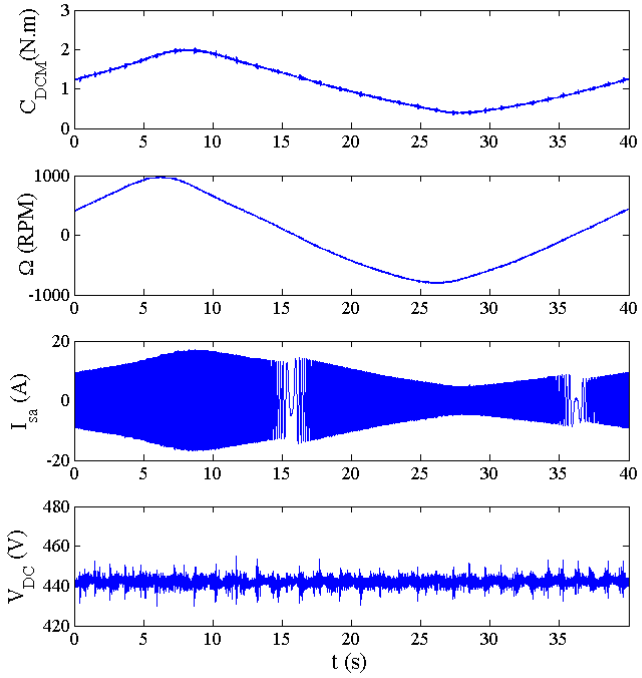

Figure 3.40: Starting from above: DCM torque (C_{DCM}), PMSM rotation velocity (Ω_s), PMSM phase current (I_{sa}), and DC bus voltage (U_{DC}).

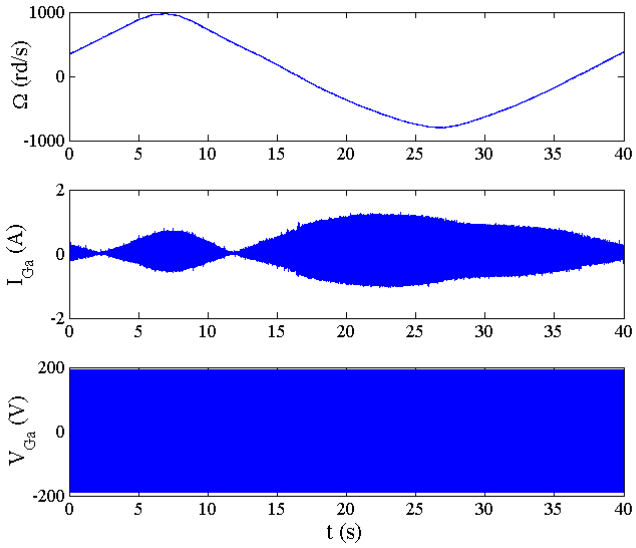

Figure 3.41: Starting from above: PMSM rotation velocity (Ω_s), grid phase current (I_{sa}), and grid phase voltage (V_{Ga}).

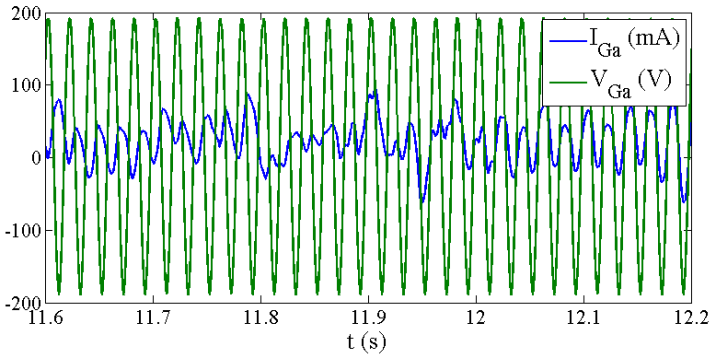

Figure 3.42: Zoom into the grid voltage and current changes when the PMSM changes its rotation direction. It shows how the current is in phase with the voltage during the generation phase, and $\frac{\pi}{2}$ shifted during the recovery phase.

7 Results on the Energy Control of a Magnus Rotor

In this section, the proposed control strategy in Sect.4.4 is applied on Magnus rotor described in Sect.5.1.3. Our objective is to test the control strategy and to have a cycle with a positive net energy output.

7.1 Numerical Application to a Medium Scale System

The complete control strategy has been numerically applied to Omnidea's system. This Magnus rotor is filled with Helium. Its parameters are listed in Table 3.5. Note that for a wind speed $v_w = 10$ m/s, Reynolds number is $\mathrm{Re} = 1.7 \times 10^6$. In order to implement the proposed

Table 3.5: Parameters of the medium scale Magnus rotor.

Symbol	Name	Value
M_M	Mass of airborne subsystem	91.22 kg
R	Magnus rotor radius	1.25 m
L_m	Magnus rotor length	16 m
ρ_{He}	Helium density	0.1427 kg/m^3
ρ_{air}	Air density	1.225 kg/m^3
M_l	Mass per tether length	0.2 kg/m
M_D	Ground station rotor mass	2000 kg
$u_{T_{max}}$	Saturation on traction actuator	65 kN
v_w	Wind speed	10 m/s
Re	Reynolds number	1.7×10^6

control strategy, a vertical trajectory is chosen. The feasibility regions for $r_{min} = 200$ m and $r_{max} = 300$ m have been determined. For a wind speed $v_w = 10$ m/s, the tether speed during the production phase $\dot{r}_{prod}$ and during the recovery one $\dot{r}_{rec}$ are found numerically offline. One gets $\dot{r}_{rec} = -0.52 v_w$ and $\dot{r}_{prod} = 0.33 v_w$ which is not the optimal value given by the main theory of simple kite [78]. This is because the colinearity condition of v_k and T is not satisfied in vertical trajectories. By simulating this system at a wind speed $v_w = 10$ m/s , we get the net output power produced during a full cycle as a function of X during the production phase (Fig. 3.43). X is then set to 0 during the recovery phase. The maximum net output power equals 59.23 kW for $X = 4.3$. The proposed control strategy will therefore use this nominal production cycle and vary the spin ratio X between 0 and 4.3 in order to stabilize the desired power produced.

For this nominal production cycle, the energetic performance is 1.48 kW/m^2 which is consistent with 1.25 kW/m^2 found in [86] where a similar sized system is used.

Note that we do not consider here the motor consumption that actuates the Magnus rotor. An estimation of this consumption can be computed as follows: Based on the C_{M_z} Magnus parameter of [99] for Re $= 10^6$, the torque exerted on the Magnus rotor is:

$$M_z = 0.5 \rho \pi R^2 L_m v_a^2 C_{M_z} \tag{3.40}$$

and the motor power consumption can be calculated by:

$$P_M = \omega M_z = v_w \frac{X}{R} M_z = 0.5 X \rho \frac{\pi}{2} S v_w^3 C_{M_z} \tag{3.41}$$

If one considers a spin ratio of $X = 4.3$ and $v_w = 10$ m/s, one can estimate $C_{M_z} = 0.0055$, and $P_M = 910$ W for the production phase (61.2% of the time). The consumption of the motor is 556.7 W for the whole cycle which is 0.9% of the 59.23 kW produced.

7.1.1 Nominal Production Cycle

In this section, the results of the nominal production cycle are presented. In order to have a smooth movement of the Magnus rotor, the reference tether length r_{ref} is filtered by $1/(\tau_R s+1)^2$ with $\tau_R = 2$s.

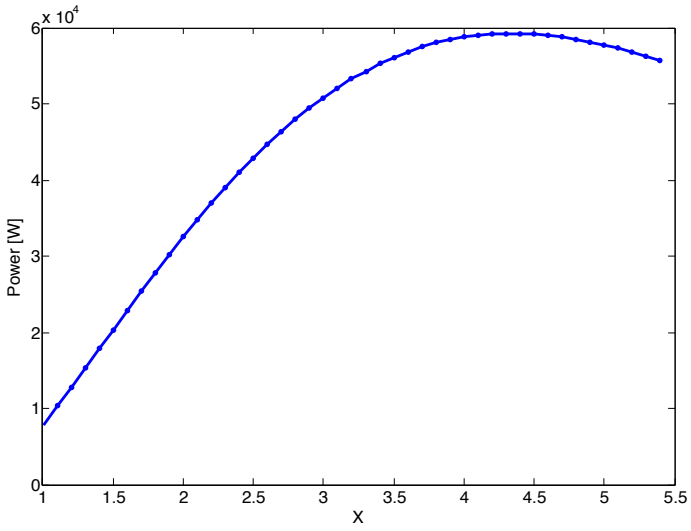

Figure 3.43: The variation of the net output power as a function of the spin ratio X during the production phase for the medium scale system. During the recovery phase, X is set to zero. Wind speed $v_w = 10$ m/s.

The PID controller K_1 parameters are $K_p = 8250$ N/m, $K_i = 1.32$ N/(ms), $K_d = 45 \times 10^3$ Ns/m. We find that the apparent wind speed increases thanks to the temporal evolution of elevation angle β (Fig. 3.44) which produces the cycle of Fig. 3.45 with a maximum of $v_a = 14.26$ m/s in the production phase and $v_a = 14.79$ m/s in the recovery phase. Following the simple kite theory, one can get an elevation angle $\beta = 0$ for the recovery phase and $\beta = 52.6$ deg for the production phase. This type of cycle is composed of the succession of transition phases between these two values of β. In Fig. 3.46, we show the temporal evolution of the tether length, tether tension and angular speed of the Magnus rotor. One can find the maximum tension on the tether is $T_{max} = 42.4$ kN, the maximum angular speed $\omega_{max} = 49.02$ rad/s. The production phase reel-out speed is 3.3 m/s with an overshoot measured at 8 m/s, the recovery phase speed is set to -5.2 m/s, without any observed overshoot.

7.1.2 Energy Control

In this section, the complete control strategy has been applied. To find the control parameters of the controller K_2 (PD controller), we have chosen the increasing line slope of Fig. 3.43 between $X = 1$ and $X = 4.3$. The control parameters are then $K_p = 6.4 \times 10^{-3}$ N^{-1} and $K_d = 6.4 \times 10^{-3}$ s/N. One can clearly see the performance of the proposed control strategy (Fig. 3.47). The produced power will follow the desired one even in the presence of noise on the wind speed. It is worth noting that if the output of PD is saturated, one can simply apply a very large reference to achieve the nominal production cycle, with $X = 4.3$ throughout the production phase.

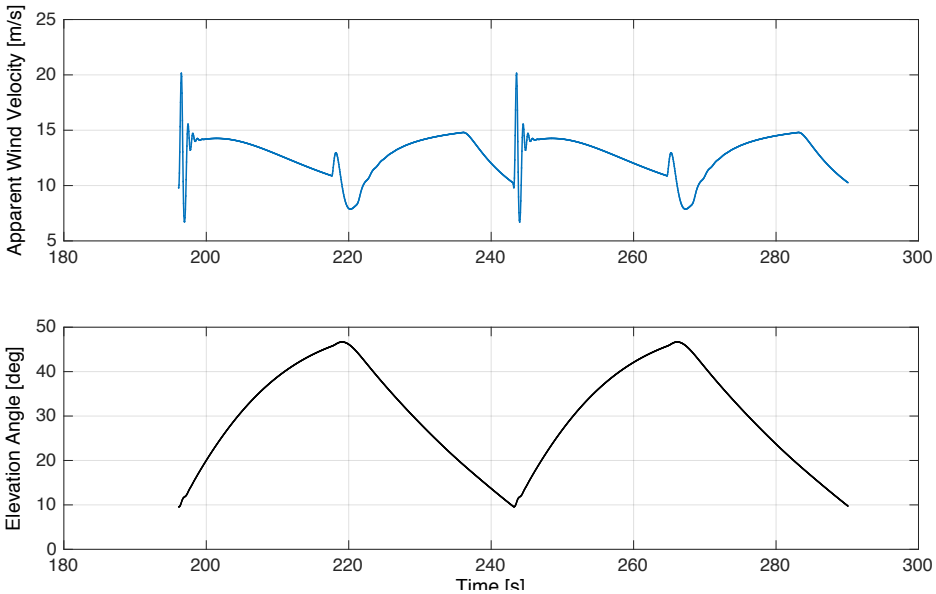

Figure 3.44: Apparent wind speed in [m/s] (top) and elevation angle β in [deg] (bottom) as function of time for the medium scale system. Wind speed $v_w = 10$ m/s.

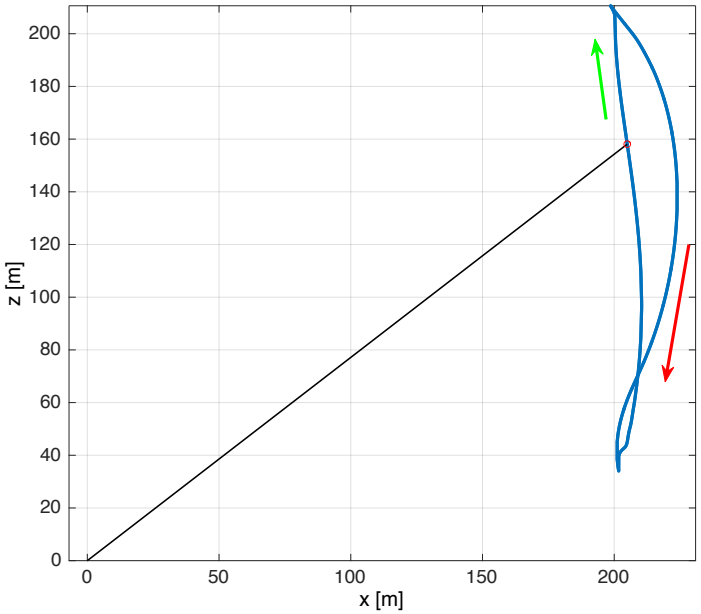

Figure 3.45: The production cycles of the medium scale system. Wind speed $v_w = 10$ m/s. The direction of the arrows indicates the movement of the Magnus rotor: Green for the production phase and red for the recovery phase.

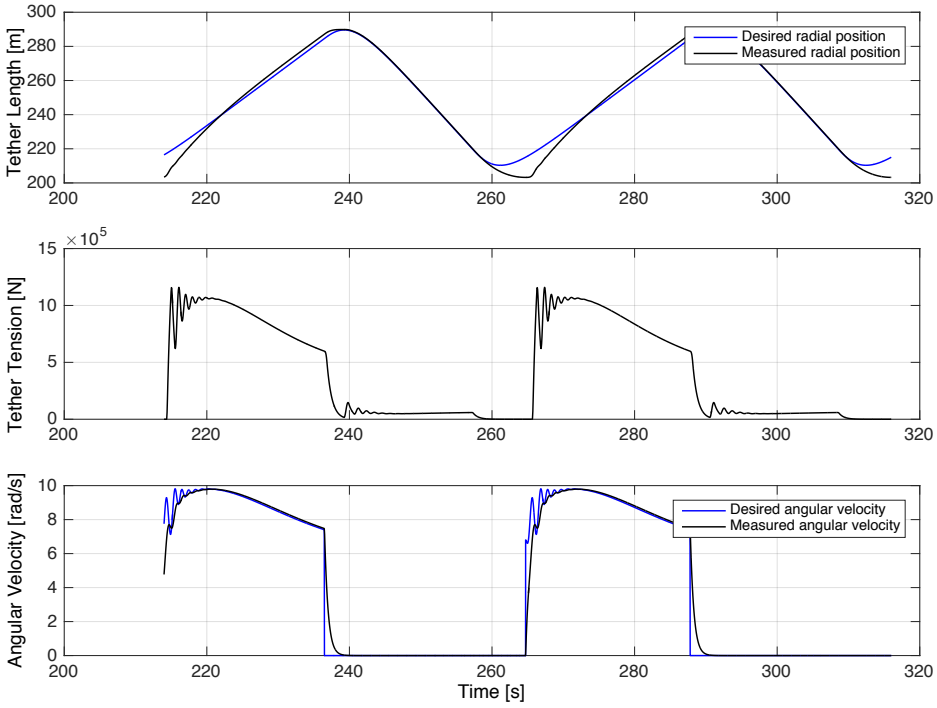

Figure 3.46: Tether length, tether tension and the angular speed of the Magnus rotor as function of time for the medium scale system. Wind speed $v_w = 10$ m/s.

7.1.3 Energy Control with Real Wind Data

The energy control algorithm is also applied using real wind data taken on October 2015 at the Bard station of the Loire region in France[3]. Only the wind magnitude is considered given that we are studying the movement in the vertical plane. The wind speed varies from 7 m/s to 20 m/s. Three power reference levels are considered (Fig. 3.49):

- ◇ $P_{ref} = 20$ kW: In this case, the system succeeds to track the desired power reference by limiting the energy produced even in the presence of wind turbulence. These variations in the wind speed generate a traction force that exceeds the on-ground generator saturation which causes an error on the control of r but does not affect the power produced.

- ◇ $P_{ref} = 50$ kW: The system succeeds to track the desired power reference when the available wind speed is enough. A short-term storage system can be used to ensure that the system catches up with the remaining energy of the previous cycle and thus obtains the desired average power in the presence of such fast changes in the wind.

- ◇ $P_{ref} = 90$ kW: In this case, the wind speed is not high enough and the desired power reference is never attained.

[3]The measurement sampling period is five seconds.

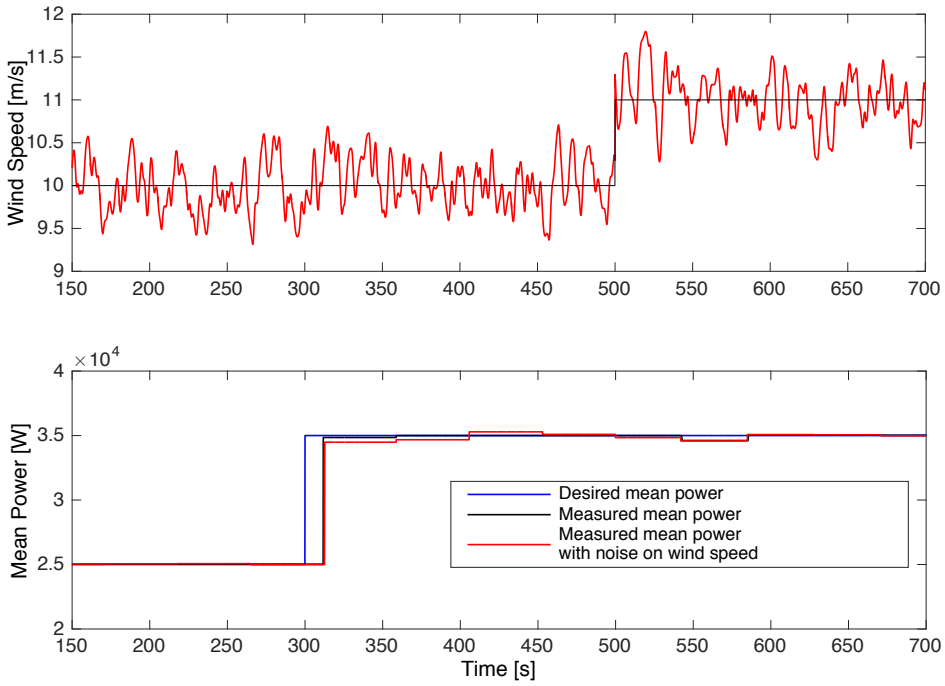

Figure 3.47: A noise is added to the wind speed to test the performance of the control strategy (top). The net output power produced as a function of the desired level of power reference with a change in wind speed (from 10 m/s to 11 m/s) for the medium scale system (bottom).

7.2 Numerical Application to a Future MW Scale System

In order to evaluate the feasibility and scaling behavior of this kind of system, numerical simulations for a MW scale system have been performed. Its parameters are listed in Table 3.6 and correspond to a factor 25 from the medium scale system of the previous section. For $v_w = 10$ m/s, Reynolds number reaches $\mathrm{Re} = 8.6 \times 10^6$. By scaling up, the volume of the Magnus rotor increases with the cube of the rotor dimension while the mass increases with the square, because it is related to the Magnus rotor surface. The gas used to fill the Magnus rotor can be more dense, keeping the whole system lighter-than-air without using pure Helium. As in the previous section, the cycle parameters are set in order to get a nominal production cycle with vertical trajectories. We have determined the feasibility regions for $r_{min} = 200$ m and $r_{max} = 300$ m. For a wind speed $v_w = 10$ m/s, the tether speed in the production phase $\dot{r}_{prod}$ and in the recovery phase $\dot{r}_{rec}$ are found numerically offline. One gets $\dot{r}_{prod} = 0.31 v_w$ and $\dot{r}_{rec} = -0.46 v_w$ which are slightly different form those found for the medium scale system.

By simulating this system at a wind speed $v_w = 10$ m/s, with the same method of the previous section, the net output power is found to be 1.37 MW for $X = 4.3$, which corresponds to an energetic performance of 1.37 kW/m^2. This is consistent with the results of the medium scale system 1.48 kW/m^2 and 1.25 kW/m^2 found in [86].

PID controller K_1 parameters are $K_p = 5.16 \times 10^5$ N/m, $K_i = 82.5$ N/ms, $K_d = 2.81 \times 10^6$ Ns/m. These control parameters are chosen empirically.

In Fig. 3.50, tether length, tether tension and the angular speed of the Magnus rotor as function of time are shown. One can find the maximum tension in the tether $T_{max} = 1.16 \times 10^6$

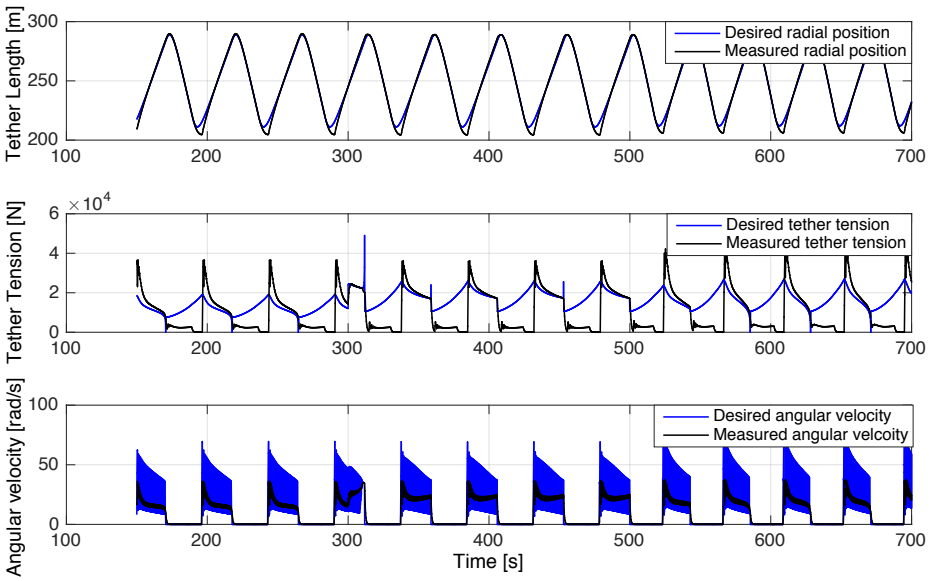

Figure 3.48: Tether length, tether tension and the angular speed of the Magnus rotor as function of time in absence of noise for the medium scale system. The oscillations in the rotation speed are due to the choice of the control parameters. Wind speed $v_w = 10$ m/s.

N and the maximum angular speed $\omega_{max} = 9.8$ rad/s. The production phase reel-out speed is 3.1 m/s with an overshoot measured at 7.4 m/s, the recovery phase reel-in speed is set to -4.6 m/s, without any observed overshoot.

In Fig. 3.51, one can see the vertical trajectory of the MW scale system. We also present a comparison with an equivalent conventional wind turbine. Even though the Magnus effect-based system is less efficient to capture mechanical energy from wind, it produces the same amount of power as an 80 m diameter wind turbine (around 1.4 MW for 10 m/s wind speed) since it works on a larger area. In other words, an 80 m diameter wind turbine works on 5000 m^2 with a power coefficient $c_p = 0.45$ where the Magnus effect-based system works on 13940 m^2 with a power coefficient $c_p = 0.157$. With the same method used in Sect. 7.1, the Magnus motor consumption can be estimated by $P_M = 22.7$ kW for $C_M = 0.0055$, $X = 4.3$ and $v_w = 10$ m/s. Knowing that production phase is 59% of the time, the net output power of the Magnus motor over the whole cycle is 13.56 kW which is about 1% of the power produced.

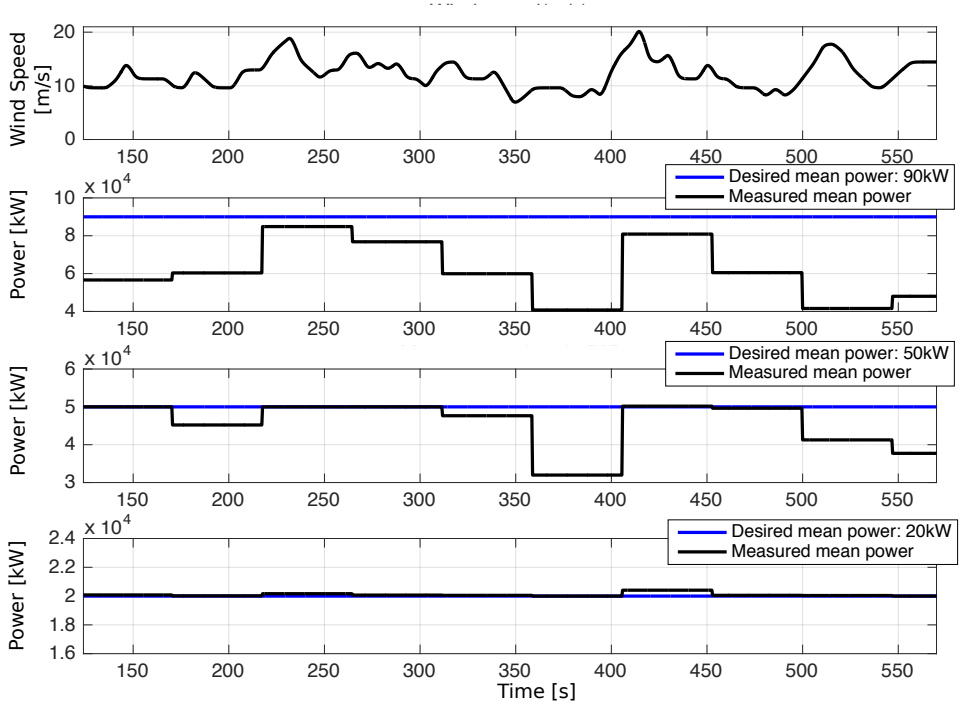

Figure 3.49: Energy control of the medium scale system. Real wind speed data is used (top). Three levels of power reference are considered: 20 kW, 50 kW, and 90 kW. The wind speed varies from 7 m/s to 20 m/s.

8 What if There is No Wind?

Most airborne wind energy systems have a great drawback that classical wind turbines do not have: they cannot stay in the air if the wind is not strong enough. As a consequence, most of the AWE systems need to land when there is no wind, and to take-off once the wind is strong enough. These maneuvers are quite risky because generally the wind gets weak and turbulent close to the ground's surface. Moreover, as the wind can be strong enough at high altitude and weak close to the ground, it might lead to losses in energy production. From a material point of view, classical landings and takeoffs need a landing zone, ground handling or infrastructure (such as pylons) that reduces the advantages of AWE systems. Some ideas, such as embedded motors or Magnus rotors, might solve this problem, but they have their own drawbacks such as the weight of the motor, the autonomy of the embedded battery, the necessity of a conductive cable or the need to refill the balloons and finally the total price of the system. I have investigated, in the PhD study of R. Lozano Jr., the "Reverse Pumping" solution. It basically consists of providing kinetic energy to the kite by pulling the kite with a rope. This kinetic energy is then transformed into potential energy by gaining altitude. This technique allows to keep the kite airborne in total absence of wind. This solution of reverse pumping principle has been explored theoretically and experimentally (Fig.3.52).

Table 3.6: Parameters of the MW scale Magnus rotor

Symbol	Name	Value
M_M	Mass of airborne subsystem	1.133×10^4 kg
R	Magnus rotor radius	6.25 m
L_m	Magnus rotor length	80 m
ρ_g	Buoyant gas density	0.95 kg/m^3
ρ_{air}	Air density	1.225 kg/m^3
M_l	Mass per tether length	5 kg/m
M_D	Magnus rotor mass	50000 kg
$u_{T_{max}}$	Saturation on traction actuator	2×10^6 N
v_w	Wind speed	10 m/s
Re	Reynolds number	8.6×10^6

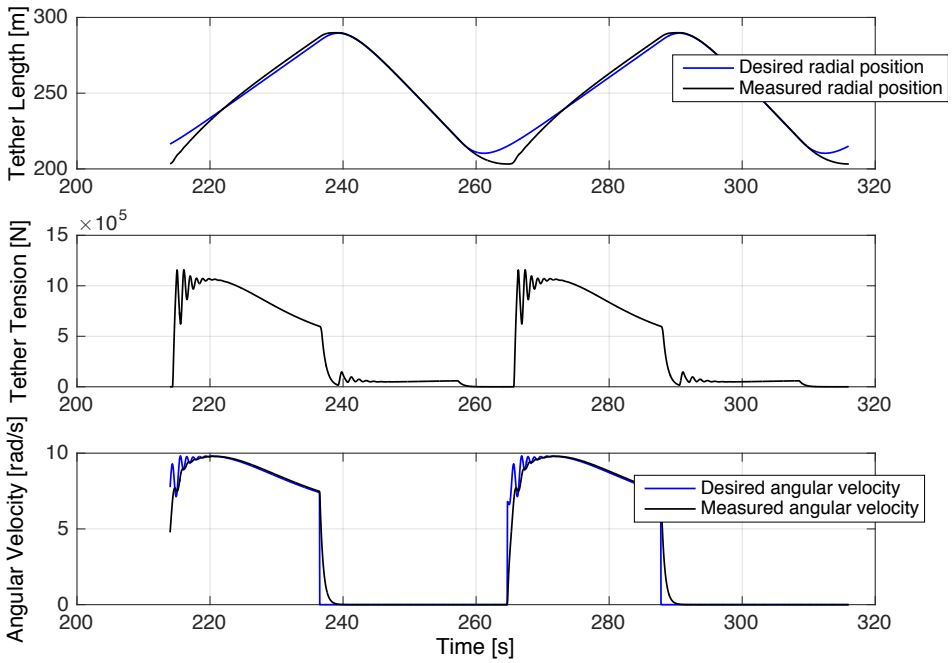

Figure 3.50: Tether length, tether tension and the angular speed of the Magnus rotor as function of time for the MW scale system. Wind speed $v_w = 10$ m/s.

9 Conclusions

In this chapter, different research actions have been presented in the field of airborne wind energy starting from modeling and design, proposing several control schemes, passing by experiments indoor and outdoor, and ending by validation using Hardware-in-the-loop setups.

Chapter 4

Electrical Vehicles Integration to the Grid

1 Introduction

As reported in the Global EV Outlook 2016 report of the International Energy Agency [Age16], 2015 was the year where the threshold of 1 million Electric cars on the roads was exceeded (1.26 million including plug-in electrics vehicles (PEVs), plug-in electrics hybrid vehicles (PHEVs), and Fuel cell electric vehicles). This is a curious fact since by 2013 most of the reports suggested this threshold was not going to be exceeded before 2020 [EUR14]; [Avi14]; [(EP15]. Most of these electrical vehicles (EV) are localized in the United States, China, Japan, and European countries like Netherlands, Norway, France, and Germany, all of them members of the Electric Vehicle Initiative (EVI) group.

This increase of penetration of EVs into the electric power system is a major challenge [108]. It requires to look for ways of managing the spatio-temporal demand inherent to these vehicles in order to adapt them to the technical and economic constraints of the grid.

Uncontrolled or uncoordinated charging of these EVs generates increased losses, consumption peaks, overloads, excessive voltage drops, congestion, stability and unbalanced problems, decreased life duration of transformers etc. The literature on this subject can be classified into two categories. The first category studies the impact of integration these vehicles on the grid [126]. The second category represents the different load management methodologies aiming to reduce these impacts while providing multiple benefits to electricity distribution systems including energy transportation, support for non-conventional energy sources, power quality services, etc. [29].

Based on several studies, the majority of EV charging systems are conceived to be undertaken at home. EV batteries can be used to support the power grid and can serve as a reserve against unexpected outages. This concept is denoted by vehicle-to-grid (V2G) [77]. At home these batteries can be used to supply a portion of the domestic load. This concept is denoted by vehicle-to-home (V2H).

My work in this field is classified into two classes:

- ◇ Modeling of different elements in the residential power grid namely the electrical vehicles.
- ◇ Load management methodologies that minimize the impacts of integration of these vehicles into the residential power grid.

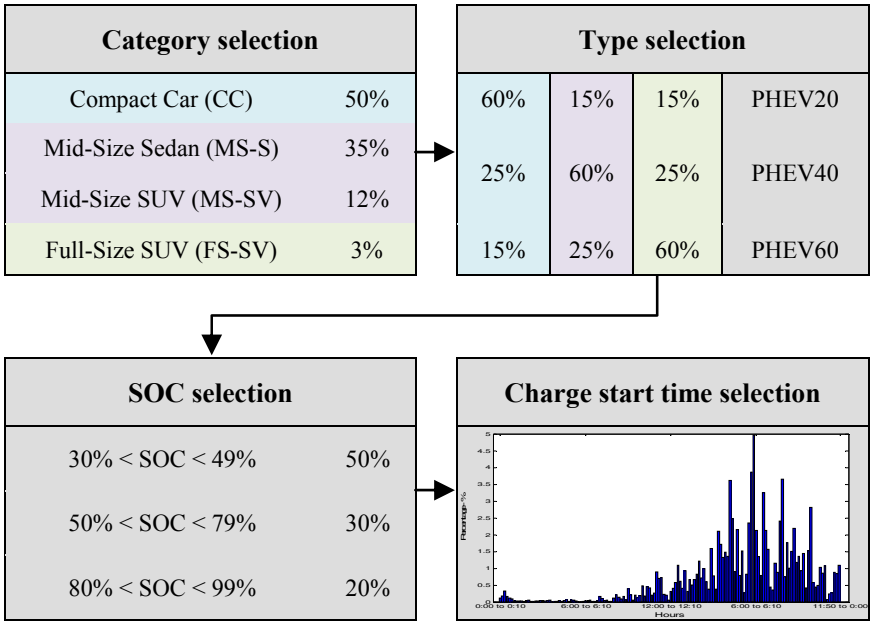

Figure 4.3: Synoptic of probabilistic algorithm for the PHEHs connection.

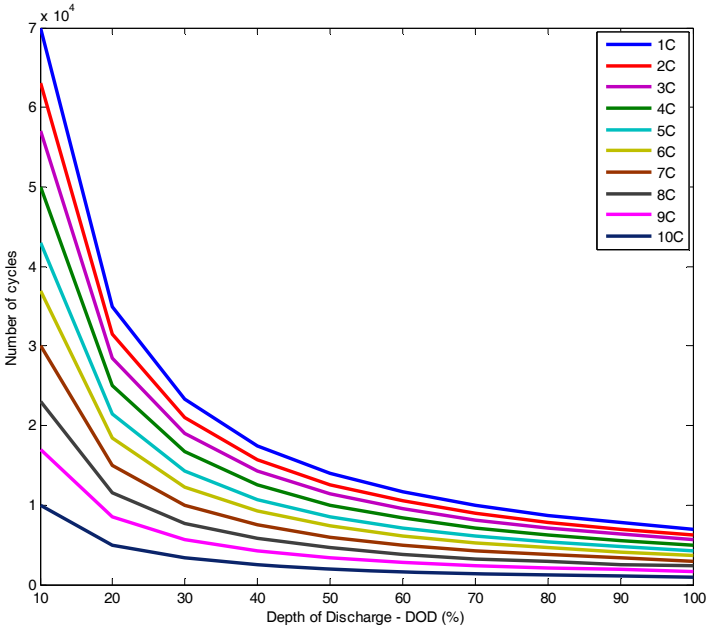

Figure 4.4: Cycle life depending on the depth of discharge (DOD).

a. LV transformer DLPs

An algorithm that generates LV transformers DLPs is proposed taking into account costumers number, disparity between houses and apartments number, and disparity in the their size

(Fig.4.5).

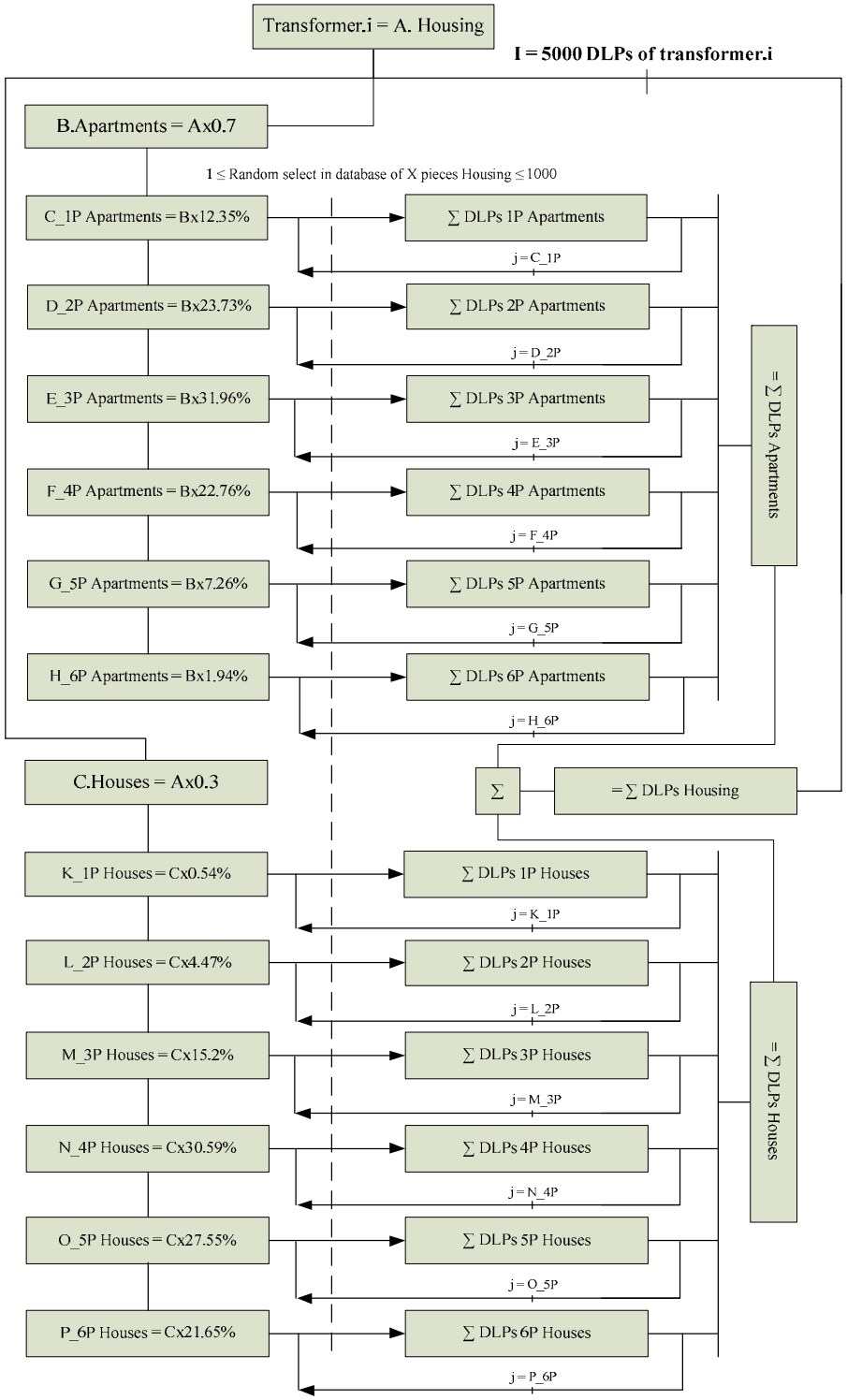

Figure 4.5: Synoptic of transformer DLPs generator.

2.2 Mathematical Modeling approach

In this approach, the modeling of voltage levels of the components of residential electrical distribution system has been given using single-line radial topology model of Fig. 4.6. In order to have a simplified model, the resistive portion of lines impedance is assumed much larger than the reactive portion ($R >> X$), so the second one can be neglected. In addition, only unitary power factor loads has been considered, eliminating the reactive portion of loads as well. This assumption can be justified since low power factors are usually penalized with higher bill costs for electricity service customers.
For a grid node labeled with index n, with active power consumption l_k^n at time k, the load is approximately represented with a resistance R_k^n given by,

$$R_k^n := \frac{V_{nom}^2}{l_k^n}, \tag{2.1}$$

where V_{nom} is the nominal voltage value of the grid. On the other hand, in order to model the behavior of EVs modulating their charge/discharge rates, batteries are represented as current sources with variable currents. Given a power consumption/injection reference x_k^n for an EV connected to node n, the corresponding current value h_k^n for the model, at time k, is approximated as,

$$h_k^n := \frac{x_k^n}{V_{nom}}. \tag{2.2}$$

Finally, the transformer node is modeled as an ideal voltage source. The original single-line radial topology model becomes a linear circuit, as on Fig. 4.6 The radial circuit topology is

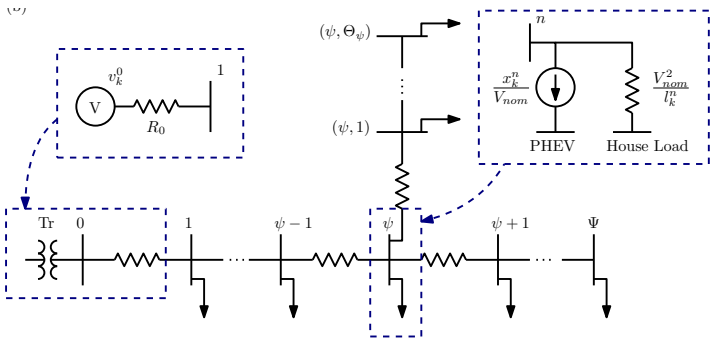

Figure 4.6: Linear approximation of transformer, line and load elements of a single-line low voltage grid wiht radial topology.

then decomposed, on several cells defined by nodes. Fig. 4.7 shows a cell corresponding to the node n in the basic feeder. By Kirchhoff's circuit laws, the currents on the node n define,

$$\begin{aligned} h_k^n = v_k^{in}\left(\frac{1}{R_{in}^n}\right) - v_k^n\left(\frac{1}{R_{in}^n} + \frac{1}{R_k^n} + \frac{1}{R_{o_1}^n} + \frac{1}{R_{o_2}^n} + \cdots + \frac{1}{R_{o_M}^n}\right) \\ + v_k^{o_1}\left(\frac{1}{R_{o_1}^n}\right) + v_k^{o_2}\left(\frac{1}{R_{o_2}^n}\right) + \cdots + v_k^{o_M}\left(\frac{1}{R_{o_M}^n}\right). \end{aligned} \tag{2.3}$$

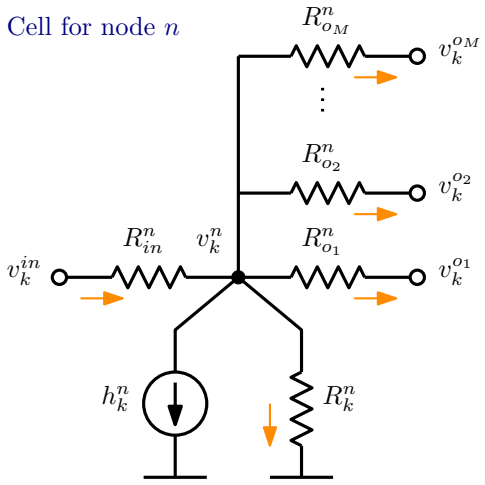

Figure 4.7: Cell representing the currents flowing through a node in the approximated model of the grid.

Organizing all the expressions for each node, as it was mentioned before, an expression with the following structure,

$$\dot{\mathbf{A}}_k \mathbf{v}_k = \mathbf{h}_k + \left(\frac{1}{R_0}\right) \mathbf{v}_k^0 \tag{2.4}$$

can be constructed. Here, matrix $\dot{\mathbf{A}}_k$ collects all the conductance coefficients multiplying voltage unknowns in linear eqs. (2.3), for each node at time k. Vector $\mathbf{v}_k$ is the vector of unknown voltages organized as it was mentioned before,

$$\mathbf{v}_k = \left[v_k^1, v_k^2, \cdots, v_k^n, \cdots, v_k^N\right]^{\mathrm{T}}. \tag{2.5}$$

On the other hand, vector $\mathbf{h}_k$ gathers the current references of EVs at each node at time step k,

$$\mathbf{h}_k = \left[h_k^1, h_k^2, \cdots, h_k^n, \cdots, h_k^N\right]^{\mathrm{T}}. \tag{2.6}$$

If there is no connected EV on the node n, its current entry is $h_k^n = 0$. Finally, vector $\mathbf{v}_k^0$ is a vector with the same dimensions of $\mathbf{h}_k$, whose first element is the transformer voltage at time k, and all the other elements are zero, i.e.,

$$\mathbf{v}_k^0 = \left[-v_k^0, 0, \cdots, 0\right]^{\mathrm{T}}. \tag{2.7}$$

The unknown voltage values can be found given information of forecasted residential load (on $\mathbf{A}_k$), and reference voltage and power values from the transformer and EVs (on $\mathbf{v}_k^0$, and $\mathbf{x}_k$):

$$\mathbf{v}_k = \left(\frac{1}{V_{nom}}\right) \mathbf{A}_k \mathbf{x}_k + \left(\frac{1}{R_0}\right) \mathbf{A}_k \mathbf{v}_k^0, \tag{2.8}$$

for all times $k = \{1, 2, \cdots, K\}$. It is important to notice that the base voltage on each node, without including EVs, is given by the second term $\left((1/R_0)\, \mathbf{A}_k \mathbf{v}_k^0\right)$, while the first term $\left((1/V_{nom})\, \mathbf{A}_k \mathbf{x}_k\right)$ provides information on the voltage variations introduced by EVs consumption/injection of power.

2.2.1 Modeling both EV and residential load as a current sources

Instead of modeling residential loads by resistances R_k^n approximated by (2.1), they can be modeled as current sources as it was chosen for EV load. Similar to Eq. (2.2), for the residential load the current value is approximated by,

$$g_k^n := \frac{l_k^n}{V_{nom}}., \tag{2.9}$$

where l_k^n is the active power consumption at the node n at time k. Then, the individual cell of a node becomes the one shown on Fig. 4.7, and the expression of the node becomes,

$$\begin{aligned} h_k^n + g_k^n = v_k^{in}\left(\frac{1}{R_{in}^n}\right) - v_k^n\left(\frac{1}{R_{in}^n} + \frac{1}{R_{o_1}^n} + \frac{1}{R_{o_2}^n} + \cdots + \frac{1}{R_{o_M}^n}\right) \\ + v_k^{o_1}\left(\frac{1}{R_{o_1}^n}\right) + v_k^{o_2}\left(\frac{1}{R_{o_2}^n}\right) + \cdots + v_k^{o_M}\left(\frac{1}{R_{o_M}^n}\right), \end{aligned} \tag{2.10}$$

where all the possible variations on the topology can be considered as well. The unknown voltage values can then be found using the following equation:

$$\mathbf{v}_k = \left(\frac{1}{V_{nom}}\right)\mathbf{A}\mathbf{x}_k + \left(\frac{1}{V_{nom}}\right)\mathbf{A}\mathbf{l}_k + \left(\frac{1}{R_0}\right)\mathbf{A}\mathbf{v}_k^0, \tag{2.11}$$

provides the values of voltage unknowns for all times $k = \{1, 2, \cdots, K\}$, given information of forecasted residential load (on $\mathbf{l}_k$), and reference voltage and power values from the transformer and EVs (on $\mathbf{v}_k^0$, and $\mathbf{x}_k$). It is important to notice that now, the base voltage on each node without including EVs, is given by the terms $\left((1/R_0)\,\mathbf{A}\mathbf{l}_k + (1/R_0)\,\mathbf{A}\mathbf{v}_k^0\right)$, while the first term $((1/V_{nom})\,\mathbf{A}\mathbf{x}_k)$ provides information on the voltage variations introduced by EVs consumption/injection of power. This alternative approximation is more flexible than the first one, especially when the amount of nodes and lines is large.

3 Load Management Strategies

Several load management strategies have been developed during my cooperation with H. Turker (in his PhD and his postdoctoral position at G2elab), my work with J. Fernandez (in his postdoctoral position at **gipsa**-lab), and A. Ovalle (in his PhD). These strategies can be classified into:

- ◇ Centralized approaches in the sense the decisions are taken at a global level.
- ◇ Decentralized approaches where decisions are taken at a local level.

3.1 Centralized Approach

In centralized schemes, decision making and data are managed by electric vehicle aggregators. In the literature, several approaches have been proposed. Authors of [45] propose a centralized method where the objective is to minimize a linear function representing the cost of the energy consumed for charging the EVs. All the constraints concerning states of charge, power boundaries and voltages are formulated as linear constraints so linear programming techniques

can be applied. In [73], a centralized approach where the EV load scheduling problem is solved under static and dynamic conditions. Static conditions refer to deterministic scenarios where all the information from EVs (arrival and departure times, required energy, charger's power constraints, etc.) is known in advance. Under dynamic conditions, the information is unknown in advance. In this case, author consider that each time a EV arrives, its schedule is computed knowing that schedules from previously connected EVs have already been calculated. A centralized unidirectional EV load scheduling is presented in. The approach recognizes, in addition to EV, three instances for the load scheduling: charging service provider (CSP), distribution system operator (DSO), and retailer which participates in the electricity market. Based on historical information, CSP estimates the total amount of energy that will be consumed in order to charge EVs during the day. With this estimation, the retailer optimizes its participation in the market by defining a preferred EV load curve during the day. After receiving this preferred EV load curve from the retailer, CSP computes individual optimal power consumption profiles for each EV such that the final total EV load curve is as close as possible to the preferred load curve provided by the retailer. Authors of [90] propose a centralized EV load management approach where the objective is to minimize the cost of energy for charging EVs connected to a parking/charging station with photo-voltaic modules. Authors propose a binary integer programming and a linear programming approach in order to compute the consumption schedules of the connected EVs. Authors of [105] propose a centralized strategy with a charging station. This approach considers bidirectional chargers assuming charge, discharge, and idle, as the states of the control variables. Under these conditions, authors propose an optimization model where first the controller optimizes the subscribed power of the charging station over a year given accurate past information and estimations. On a second step, authors optimize for each day a reference ideal load profile minimizing a cost function. With this reference load profile, authors apply a sequential optimization approach where each EV is attended in a queue. Schedules of each of the EVs are obtained by minimizing the distance between daily reference load profile and the actual load profile with EVs.

As it can be seen from the above discussion, different have been proposed in the literature. In the following sections, my contribution and results for the centralized approach are presented.

3.1.1 Rule-based Strategy [117]

Using the database developed in Sect.2.1, a rule-based algorithm applied to one house equipped with a single plug-in electrical vehicle is proposed (Fig.4.8). It is assumed that the electrical vehicle leaves and arrives at home only one time per day. The objective is to have minimal constant-charging power level while allowing recharging EVs at any time and strictly prohibiting charging during peak hours. In this way, the vehicle battery can reach a desired state of charge at the departure time. To respect the values of houses subscription contracts, the charging grid-side current of the EV charger is determined as a function of the houses consumption at each time step. To prevent EVs from accentuating the households peak electricity consumption, a SOC_{SOFT} criterion is introduced to prohibit EVs charging from 6 A.M. to 3 P.M. and from 5 P.M. to 10 P.M. which corresponds to peak hours for most regions in France. As a result, the minimal charging power levels which ensures statistically for the 10 000 cases that 99% of the EVs batteries have a final full SOC with the charging levels of 2460 W and 3400 W, respectively (Fig.4.9).
Another rule-based strategy called house peak shaving algorithm (HPSA) has been developed

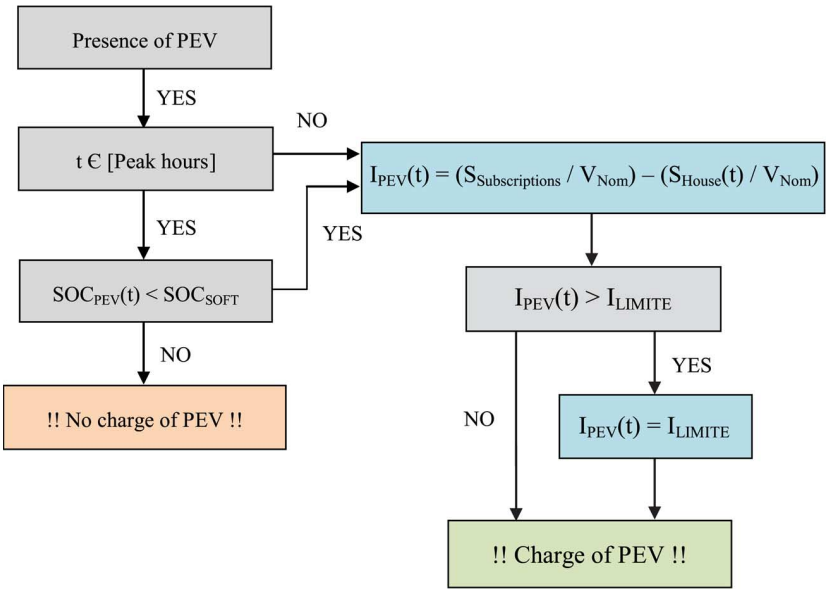

Figure 4.8: Synoptic of the rule-based algorithm. Explain the different steps

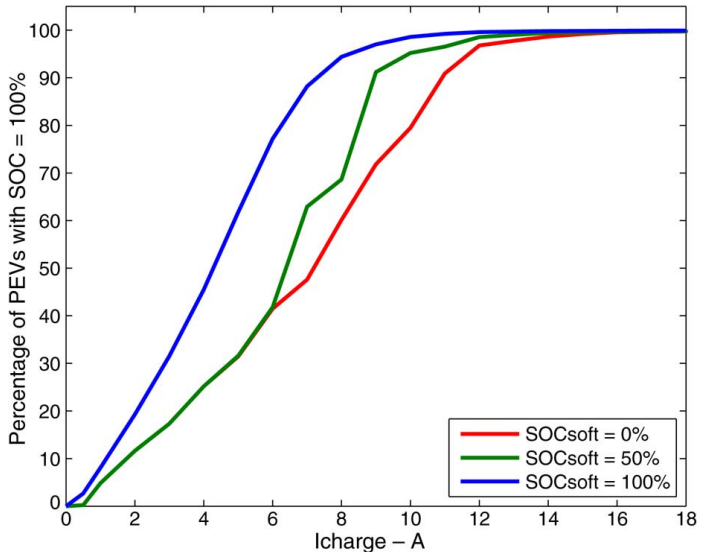

Figure 4.9: Percentage of EVs with final SOC =100%.

[67]. Initially, a constant minimum charge power (S_{PHEV}) throughout the period during which the vehicle is available for charging is set. At this step, the user arrival and departure time, EV state of charge on arrival, the desired state of charge at departure, and the capacity of the battery pack are known. Secondly, knowing house DLP, average power (S_{AVR}) is calculated. Finally, at each time step, EV charging and discharging will take place in function of the difference between S_{AVR} and the house DLP. Fig.4.10 shows a result of the application of the

HPSA algorithm.

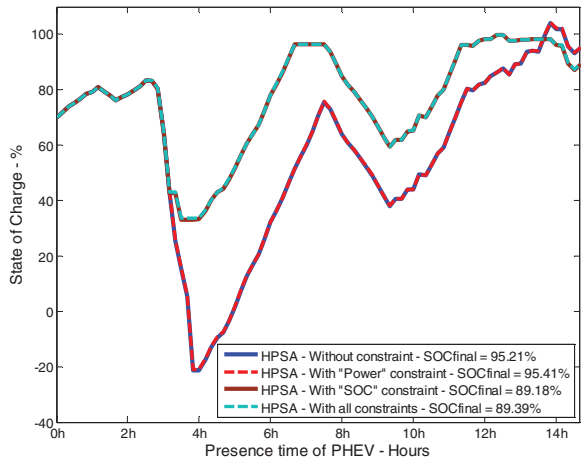

Figure 4.10: Application of a house peak shaving algorithm (HPSA): State of charge subject to different constraints.

a. Impact on the Voltage Plan

I have studied the impacts of the application of rule-based algorithm on the voltage plan of a low voltage residential electric grid consisting of 96 houses and powered by a transformer MV/LV 400kVA. An index ηV that assesses compliance with the standard NF-EN-50160 (voltage quality supplied to housing) is introduced:

$$\eta V(\%) = \left[1 - \frac{\sum_{i=1}^{N}(\sum_{j=1}^{M} K_{ij})}{N.M}\right] \times 100 \tag{3.12}$$

where $K_{ij} = 0$ if $T_{ij} < T$ and $K_{ij} = 1$ if $T_{ij} > T$. T_{ij} is the time when the instantaneous voltage $V_{ij} < V_{NF}$, M is number of houses, N is the simulation number, and $V_{NF} = 0.9$ (Standard NF-EN-50160). The evolution of ηV is plotted in Fig.4.11. This result infers that it is better to allow charging EV at any time instead of prohibiting charging during peak hours. It recommends as it is found to create a standard that limits charging power to 800W for home-charged EVs which ensures statistically that all EVs will have a full charged battery (SOC= 100%) for the next use.

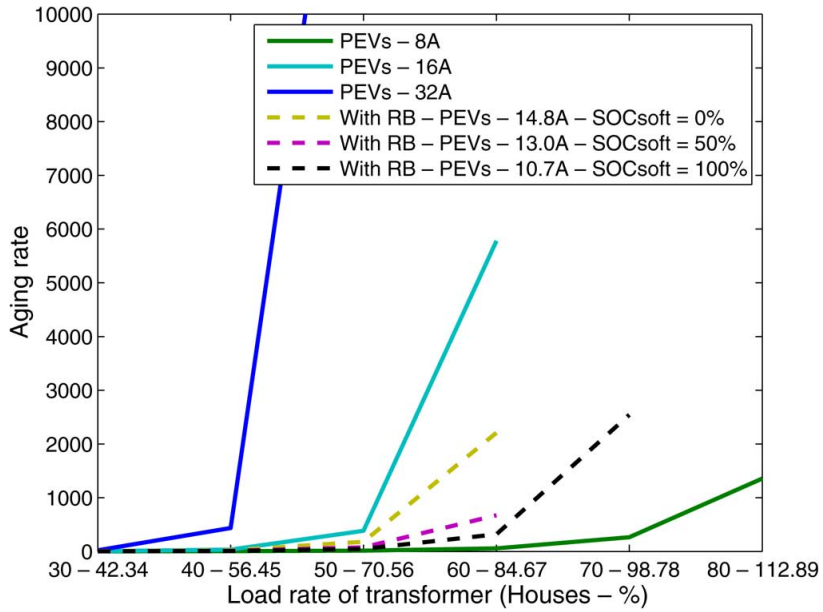

Figure 4.12: Aging rate of the transformer with the application of the rule-based algorithm of Sect.3.1.1.

variables x_k^i of each EV, at each time step, as the difference of two positive valued variables w_k^i and s_k^i. These auxiliary vectors lie within sets W^i and S^i, defined by certain boundaries, besides the positivity constraints.

Chargers are assumed to be able to handle bidirectional power flow. Moreover, they have limited rates of power consumption/injection that must be taken into account in the load scheduling problem. For each EV, power consumption/injection is limited by,

$$-\overline{p}^i \leq x_k^i \leq \overline{p}^i, \quad \forall k = \{1, 2, \cdots, K^i\}, \quad \forall i = \{1, 2, \cdots, J\}, \tag{3.15}$$

where $\overline{p}^i$ is the nominal power of the charger. If x_k^i is expressed as the difference of two positive variables $x_k^i = w_k^i - s_k^i$ then constraint (3.15) can be separated in the following two constraints,

$$0 \leq w_k^i \leq \overline{p}^i, \quad 0 \leq s_k^i \leq \overline{p}^i, \quad \forall k = \{1, 2, \cdots, K^i\}, \quad \forall i = \{1, 2, \cdots, J\}, \tag{3.16}$$

which are valid for all the connection time of each EV. The reached state of charge of EV battery at the end of time step k, is given by,

$$soc_k^i = soc_0^i + \tau \sum_{\kappa=1}^{k} (w_\kappa^i - s_\kappa^i), \quad \forall k = \{1, 2, \cdots, K^i\}, \quad \forall i = \{1, 2, \cdots, J\}. \tag{3.17}$$

In order to avoid aging issues on batteries due to deep cycles, partial states of charge must be constrained between certain boundaries,

$$\begin{aligned} \underline{soc}^i \leq & soc_k^i \leq \overline{soc}^i, \quad \forall k = \{1, 2, \cdots, K^i\}, \quad \forall i = \{1, 2, \cdots, J\}, \\ \underline{soc}^i \leq & soc_0^i + \tau \sum_{\kappa=1}^{k} (w_\kappa^i - s_\kappa^i) \leq \overline{soc}^i. \end{aligned} \tag{3.18}$$

Here, $\overline{soc}^i$ and $\underline{soc}^i$ are the upper and lower constraints, respectively, imposed to all partial states of charge. On the other hand, the final state of charge has a more restrictive constraint. It has to be equal to a desired state of charge soc_d^i imposed by the EV owner. This constraint can be expressed as,

$$soc_0^i + \tau \sum_{k=1}^{K^i} (w_k^i - s_k^i) = soc_d^i, \quad \forall i = \{1, 2, \cdots, J\}, \tag{3.19}$$

As it can be observed, states of charges are linear functions of the decision variables of the problem, i.e. the power consumption/injection variables $x_k^i = w_k^i - s_k^i$. In order to include the effect of instantaneous power consumption/injection of EVs over voltage levels, let us consider the following constraints,

$$v_{min} \leq v_k^n \leq v_{max}, \quad \forall k = \{1, 2, \cdots, K\}, \quad \forall n = \{1, 2, \cdots, N\}. \tag{3.20}$$

Here, v_k^n represents the voltage at the node n of a grid with N nodes, at time step k. This voltage is limited to be between a lower limit v_{min} and an upper limit v_{max}.

The proposed linear EV load scheduling strategy is illustrated on Fig.4.13. This scheme centralizes the optimization of schedules in order to minimize costs of energy consumption. At a given time step k, a central controller (CC) is in charge of gathering all the information from recently arrived EVs. This information includes initial and desired states of charge, nominal power of the charger, node of the grid where the EV is connected, and estimated or desired time of departure. The CC is also in charge of collecting the information of load forecast at each of the nodes of the grid where residential load is served. Once it has collected all the information, the CC runs the linear optimization procedure and sends the power consumption/injection schedules for each of the served EVs. In the next step of time k it is likely to have new recently arrived EVs, so the procedure is repeated only with the newly arrived ones.

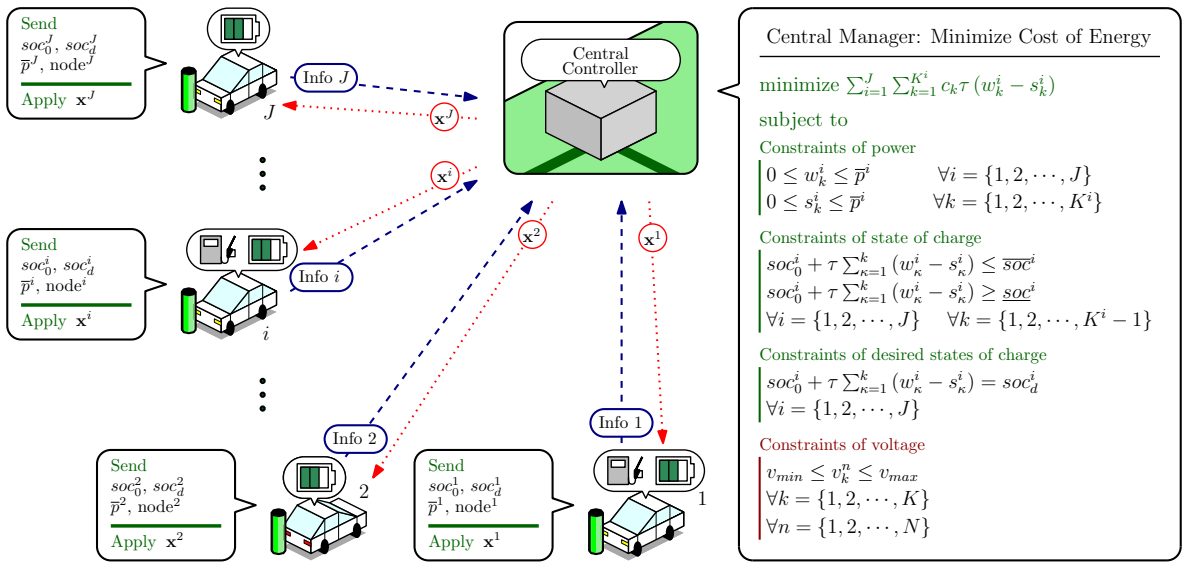

Figure 4.13: Illustration of the interactions, and flow of information, in the proposed centralized linear approach for EV load management.

a. Illustrative Example with 8-node Grid Topology

To test the centralized linear programming approach of Sect. 3.1.2, a test residential grid has been used. This residential grid has eight nodes, each one serving a residence. Three EVs are assumed to be connected to the grid during a charging period. They are connected on the nodes highlighted with a red circle of Fig.4.14. The linear programming strategy is applied

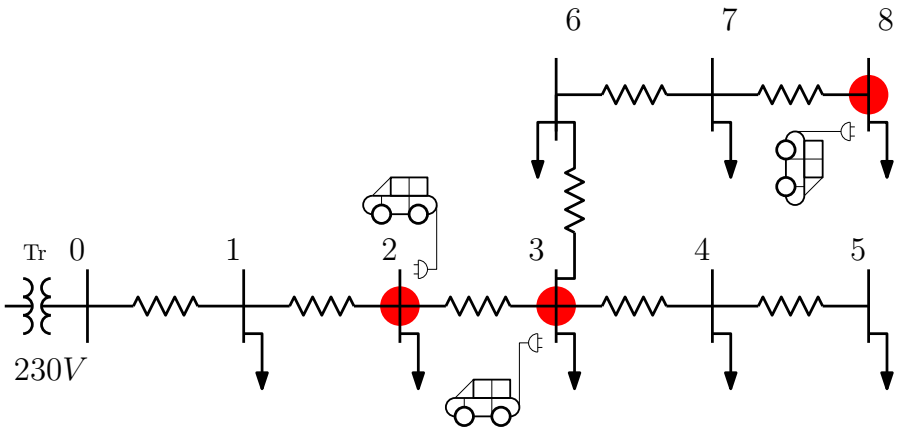

Figure 4.14: Radial Grid proposed in order to test the linear programming strategy.

several case studies. The results of a case study with two tariffs scenario (high tariff during 18h-22h, and a lower one during 22h-06h) will be presented. The power consumption profiles are shown on Fig. 4.15(a). Power consumption is redistributed during the whole charging period. However, EVs try to sell as much of their initial SOC as possible during the high tariff hours, in order to reduce the cost of recharging their batteries. It is possible to confirm this in the SOC profiles of Fig.4.15(b). Although the first and second EVs charge their batteries at the beginning of the charging period, at the end of the high tariff hours the three EVs are fully discharged. They sell their initial energy and during the lower tariff hours, they fully recharge their batteries. As it is required, the voltage profiles corresponding to every node are kept within the desired limits, even during peak demand hours, as it is shown on Fig.4.15(c).

3.1.3 Dynamic Programming Strategy

A dynamic programming technique has been employed for the problem of EV charging. The state of charge at the end of time step k can be chosen as the state variable of the system:

$$soc_k^i = soc_{k-1}^i + \tau x_k^i,$$

where the soc_k^i is the state of charge of vehicle i at the end of time step k, and x_k^i is the power consumption rate during the time step. As it can be inferred, the control variable here is the power consumption rate x_k^i, and the set of possible control decisions is defined by,

$$-\overline{p}^i \leq x_k^i \leq \overline{p}^i, \quad \forall k \in \left\{0, \cdots, K^i - 1\right\}.$$

The set of possible states of the state variable (for EV i at time k) is defined, in this case, depending on the limits that must be imposed to the state of charge at each time step k. In principle, the boundaries are defined by the lower and upper constraints, $\underline{soc}^i$ and $\overline{soc}^i$.

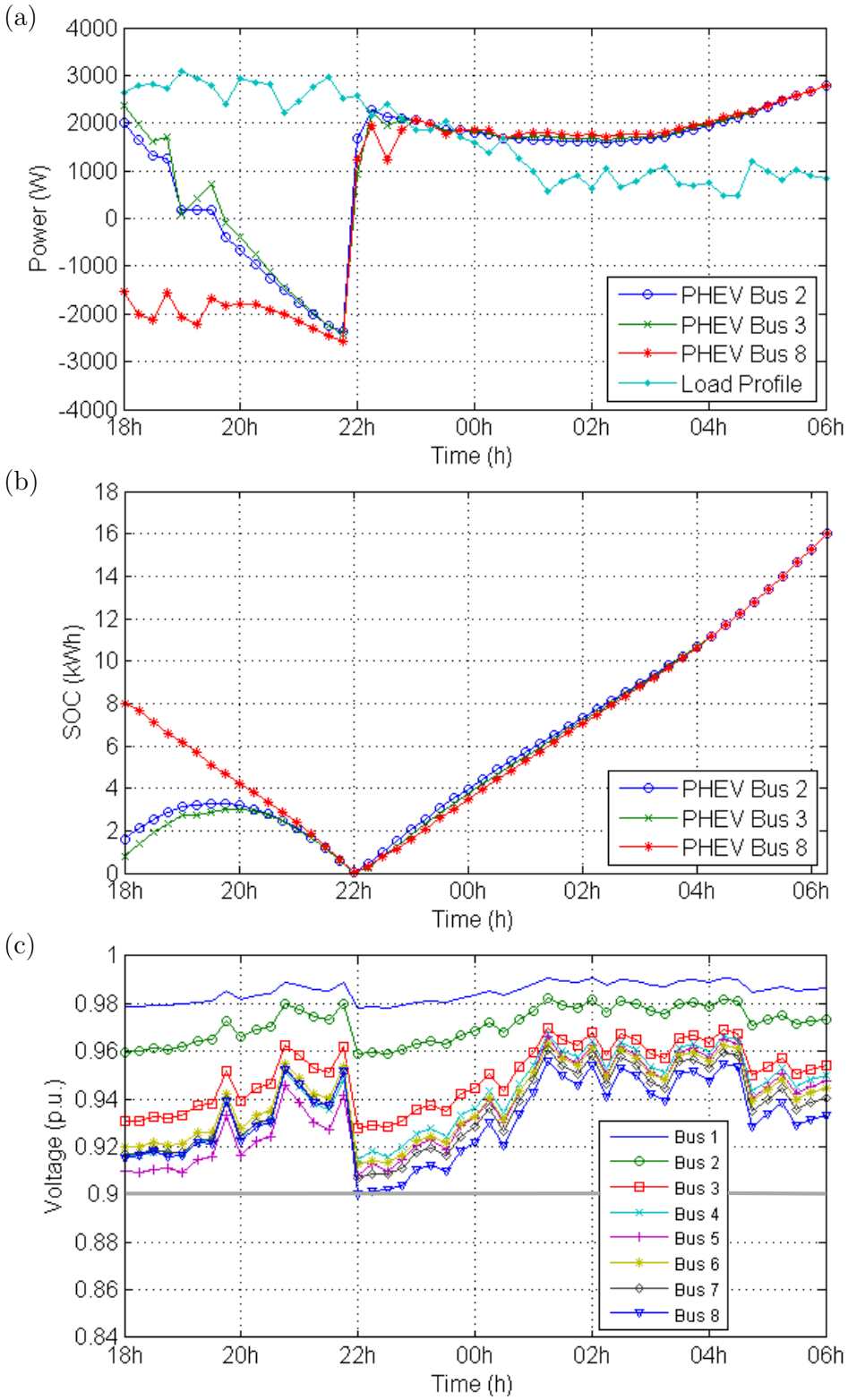

Figure 4.15: Power consumption of EVs, state of charge of batteries, and voltage profiles in the case of two-tariff scenario.

producing future states of charge over the limit, i.e. $soc_{k+1} > \overline{soc}^i$. In this sense, and for the purpose of the forward DP algorithm adaptation, knowing the arrival state of charge soc_k^i, the feasible root states in $k-1$ leading to soc_k^i by applying feasible control decisions, are defined by,

$$\underline{soc}_{k-1}^i \leq soc_{k-1}^i \leq \overline{soc}_{k-1}^i$$

where $\underline{soc}_{k-1}^i$ and $\overline{soc}_{k-1}^i$ are functions similar to eqs. (3.21) and (3.22), but depending on soc_k^i as follows,

$$\underline{soc}_{k-1}^i = \max\left\{ \ \underline{soc}^i, \ soc_0^i - (\tau\overline{p}^i)(k-1), \ soc_k^i - \tau\overline{p}^i \ \right\}$$

$$\overline{soc}_{k-1}^i = \min\left\{ \ \overline{soc}^i, \ soc_0^i + (\tau\overline{p}^i)(k-1), \ soc_k^i + \tau\overline{p}^i \ \right\}.$$

These limits are better illustrated on Fig. 4.16. Based on these inequalities, the subset $U_k^i(soc_k^i)$ is defined by,

$$\frac{soc_k^i - \overline{soc}_{k-1}^i}{\tau} \leq x_k^i \leq \frac{soc_k^i - \underline{soc}_{k-1}^i}{\tau}$$

Fig. 4.17 allows to have a wider view on the evolution of the FDP algorithm for one EV. In this figure, the whole procedure is illustrated, from the discretization of the state space, until obtaining the final optimal trajectory of the state variable. Once the state space has been discretized both in terms of time and energy, the constraints are considered, as it was explained with Fig.4.16. The set of feasible trajectories of the state of charge variable are then defined, and the algorithm can start the construction of the *optimal cost function*. Forward DP algorithm starts at k=2, and explores all the possible paths from the initial state of charge soc_0^i, to all the possible states of charge at time step k =2 . The algorithm stores all the optimal paths for this stage, and their associated costs. Thus, once the algorithm starts the same procedure with all the possible states at k=3, the optimal paths for states in the preceding time step (k=2) will be already stored on memory. The algorithm continues with this procedure until the end of the horizon time k=K when the final optimal path is obtained. The main drawback of this strategy is that memory demand increases as the algorithm advances through the time horizon. In addition, if discretization steps (on both time and energy) are refined, then both computational time and memory demands will increase. Including more than one EV in the DP algorithm will exponentially increase the quantity of admissible states to visit at each step of time. For all these reasons, a Game Theory approach is considered in order to decentralize the optimization procedures, reduce the memory and computational time requirements, and avoid flexibility issues of fully centralized optimization approaches.

3.2 Decentralized Approach

In a decentralized scheme, decisions and flow of information are achieved in the decentralized manner at the level of EV. The advantage of such an approach is that the authority of control stays with the vehicle owner and not with another entity such as the aggregator. Results of [69] show that separation in local sub-problems partially reduces the limitations of the centralized approach in terms of the dependence on collecting information for executing optimization routines. However, when the number of sub-controllers is increased, the performance is affected. Authors of [101] explore the advantages and disadvantages of a grid model based centralized approach compared to a decentralized linear approach where constraints on voltage and EV load effects are considered. The proposed objectives seek to maximize the EVs charging rates, but leaving full final states of charge unguaranteed.

An interesting decentralized approach is proposed based on a communication channel analogy [100]. In this approach, each EV divides its charging requirements in several packets of short duration at the maximal charging rate considering the owner's projected time of connection. Permissions are asked for each packet to an aggregator, which grants permits or not, depending on the availability of consumption capacity. This approach has the important advantage of fairly providing EVs with access to the available power resources, while fulfilling grid constraints. Authors of [75] propose a decentralized scheduling method, where EVs provide a regulation service by absorbing the uncertainties of generation and load, and smooth the power imbalance fluctuations. The proposed distributed algorithms are based on the gradient projection method to solve the optimization problems locally. A non-cooperative potential game has been presented in [88]. In this scenario, EVs are represented as players, and strategies they choose are represented by their power consumption profiles. Given fixed strategies from all the players, the profit of each one given its chosen strategy, and strategies from others, is defined by a function common to all the players. In [82], an interesting non-cooperative game approach where an economic cost function is "crafted" such that Nash equilibrium is achieved when strategies from players achieve valley filling. This cost function is defined based on the assumption that the amount of EVs tends to infinity and even in that case their demand is not as big as the base load demand. In the following section, a decentralized approach to manage the charging operation of multiple EVs. An N-person non-cooperative game approach is formulated.

3.2.1 Game Theory Approach [92]

In this approach, a number J of players is considered, where each EV is considered as a player. Each player is labeled with $i = \{1, 2, \cdots, i, \cdots, J\}$, and the set of possible strategies for player i is defined as the set of all possible charging profiles $\mathbf{x}^i = [x_1^i, x_2^i, \cdots, x_k^i, \cdots, x_{K^i}^i]$. On the other hand, for player i, the strategies chosen by the $J-1$ players left are grouped in the following expression,

$$\mathbf{x}^{-i} = [\mathbf{x}^1, \mathbf{x}^2, \cdots, \mathbf{x}^{i-1}, \mathbf{x}^{i+1}, \cdots, \mathbf{x}^J]$$

The payoff function for player i, depends on the strategy it chooses, and the strategies chosen by other players. This payoff functions is defined as the negative of the squared euclidean distance between the total load at each step of time and the average load,

$$G_i(\mathbf{x}^i, \mathbf{x}^{-i}) = -\sum_{k=1}^{K} \left(\left(x_k^i + \sum_{j=1, j\neq i}^{N} x_k^j + l_k \right) - l_{avg} \right)^2, \tag{3.23}$$

where, l_k is the forecast of the grid's load (without EVs) at the transformer, and l_{avg} is the average load during the whole charging period including grid's base load and EVs load. The best reply (BR) strategy $\mathbf{x}^{i*}$ for player i is given by,

$$\mathbf{x}^{i*} \in \arg \max_{\mathbf{x}^i \in \Theta^i} G_i(\mathbf{x}^i, \mathbf{x}^{-i}). \tag{3.24}$$

where Θ^i is a set defined by the constraints. This game is a best response potential game [123, 49], with potential function $G_i(\mathbf{x}^i, \mathbf{x}^{-i})$ given by (3.23). Given the strict concavity of utility functions for each player and the fact that sets Θ^i are convex, closed and bounded, the game is a strictly concave N-person game where the Nash equilibrium exists and it is unique

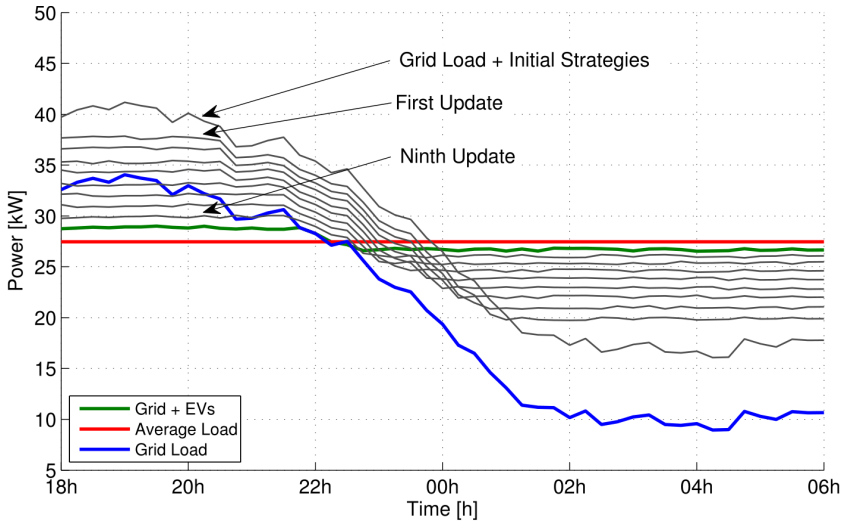

Figure 4.19: Evolution of the game with 10 EVs.

If players update their BR strategies in an asynchronous fashion, their payoffs will either increase or remain the same. Since the distance to the average load is bounded below (in the best case it could be zero), then the algorithm will converge to the desired point or the Nash equilibrium [89].

a. Illustrative Example

In order to evaluate the performance of the charging management approach of this chapter, a test case is proposed with 10 EVs having the following characteristics. All of them have battery capacities of 20kWh, and their state of charge profiles are constrained to be between 30% and 80% of the capacity (6kWh to 16kWh). Chargers are considered to be bidirectional with charging rates of going from -3.2kW to $+3.2$kW ($\overline{p}^i = 3.2$kW). The period of charge is chosen between 18h in the evening and 06h in the morning. The initial states of charge for each EV are chosen randomly with a uniform probability distribution between 30% and 40%.

Given these initial strategies, the initial load curve including grid and EVs is shown on Fig. 4.19. As it can be observed, this initial profiles has the same shape of the grid's load forecast, with an offset that corresponds to the EVs load. The subsequent updates of each EV are also shown on this figure. It is important to notice that once the last EV updates its strategy, the final load curve does not change much since the Nash equilibrium is almost reached. Also, it is important to notice how the total load curve becomes flatter with the progress of the game. This occurs because the utility of each player is higher if the total load at each step of the changing period becomes closer to the average load. Equilibrium strategies (i.e. the final optimal power consumption schedules) are shown on Fig.4.20. On the other hand, state of charge profiles are shown on Fig.4.21. It is important to notice how each player respects the constraints of minimum state of charge (30%), final desired state of charge (80%), and power limits (± 3.2kW).

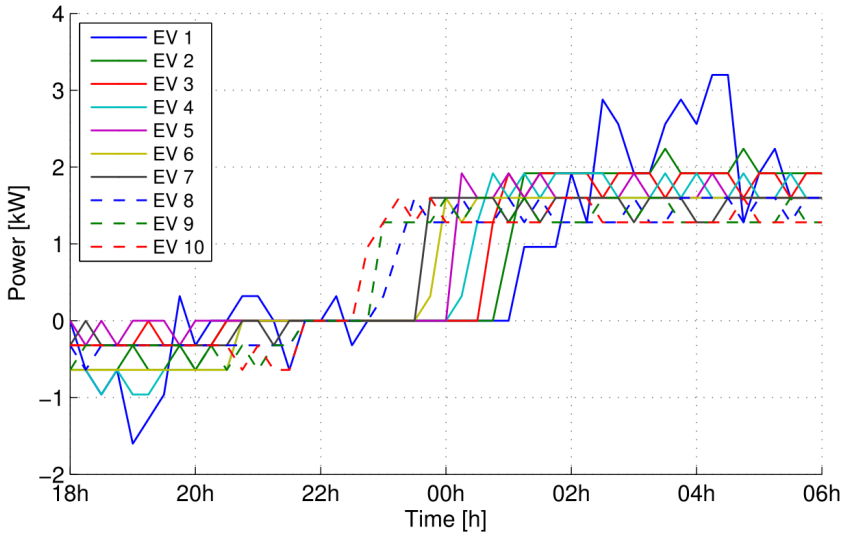

Figure 4.20: Optimal power consumption profiles, final strategies in the Nash equilibrium.

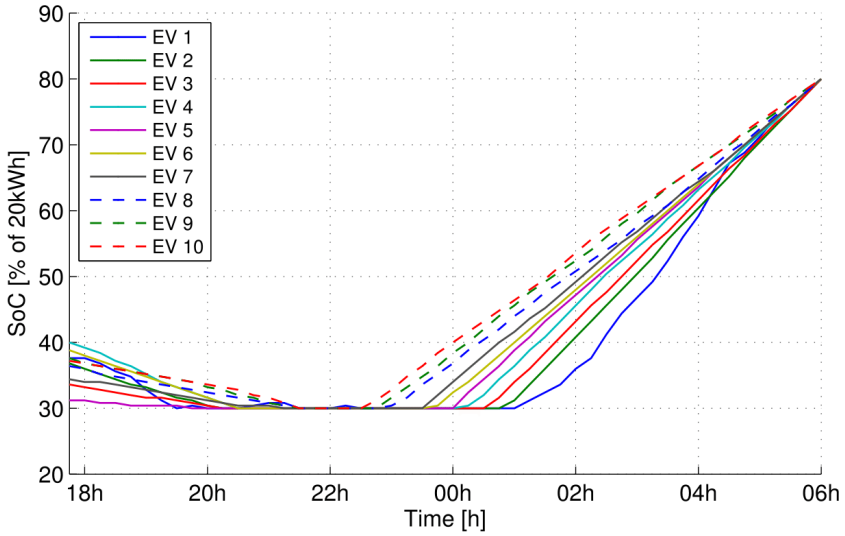

Figure 4.21: Optimal charging schedules, states of charges for each player.

4 Conclusions

This chapter provides control strategies to compute optimal charging schedules of multiple EVs in a centralized and decentralized manner. Additionally, the proposed strategies employ the energy storage capacity of EVs in order to provide a service of load flattening. The proposed schemes are evaluated under multiple cases in order to test their capabilities. EV impact on the voltage plan and the aging rate of a low voltage transformer has been also addressed.

Chapter 5

Prespectives

1 Introduction

Different approaches have been followed in the modeling and control AWE systems. These control strategies have been validated numerically and experimentally on indoor lab demonstrators. The integration of AWE systems to the grid has been tested in HIL experiments (see Chapter 3). For EV integration to the grid, different load management methodologies has been proposed aiming to minimize the impacts on the grid of this integration while respecting the owners objectives (see Chapter 4).

In this chapter, I will give some guidelines that can be followed in future research to address the new challenging problems in the AWE field, EV integration and load management in general, and the control of energetic systems. This can be considered my research project for the next five years.

2 Perspectives on Airborne Wind Energy Systems

Modeling and control of AWE are now relatively well-understood in the scientific community with several theoretical and experimental results that have been reported in the literature. However, there are several challenges to be addressed. The first challenge is **taking-off and landing** of these systems which is not completely addressed. One answer to this open question is to use Magnus effect-based AWE system (see Sect.3.2). These lighter than air systems can simplify the take-off and landing procedures. A complementary promising solution is to use rotors as done recently by Twingteg [8]. A preliminary simulation study where a simplified model of Magnus effect-based cylinder combined to a X4MaG shows a reduction of 60% of the thrust once the quadrirotors stabilized its circular path. A first prototype is also built in order to understand the technical difficulties related to this problem (Fig.5.1). The second challenge is to increase power performance of Magnus effect-based AWE systems. In the frame of equilibrium motion theory, the power that can be generated with a tethered airfoil in crosswind conditions has been set by [78] and refined in [33] to take into consideration the β losses:

$$P_{prod} = \frac{1}{2}\rho\frac{4}{27}S_{cyl}(v_w\cos(\beta))^3 C_L\left(\frac{C_L}{C_D}\right)^2 \tag{2.1}$$

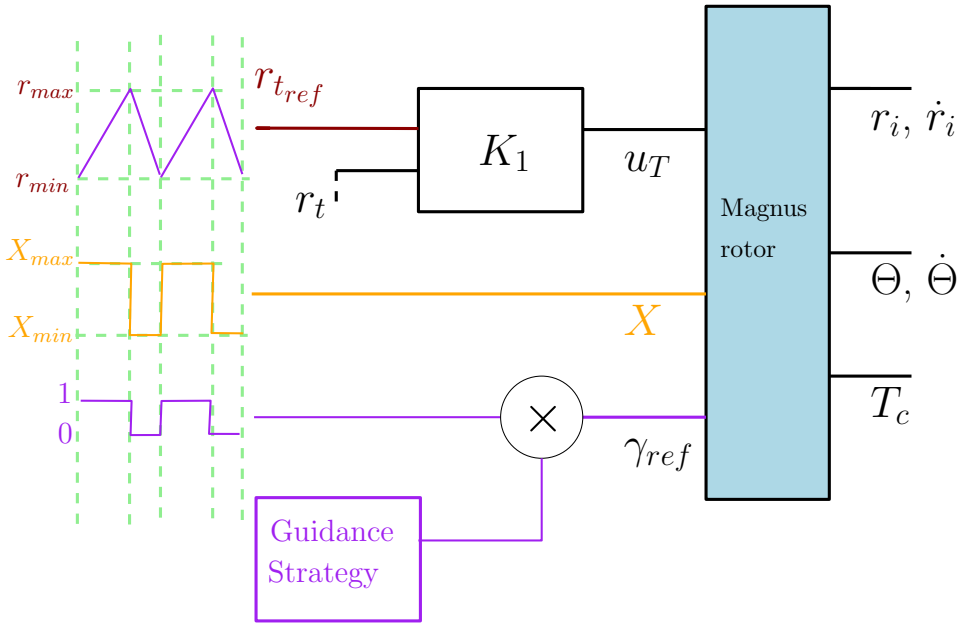

Figure 5.2: An overview of a possible control strategy to increase the perfronce of a Magnus effect-baesd AWE system.

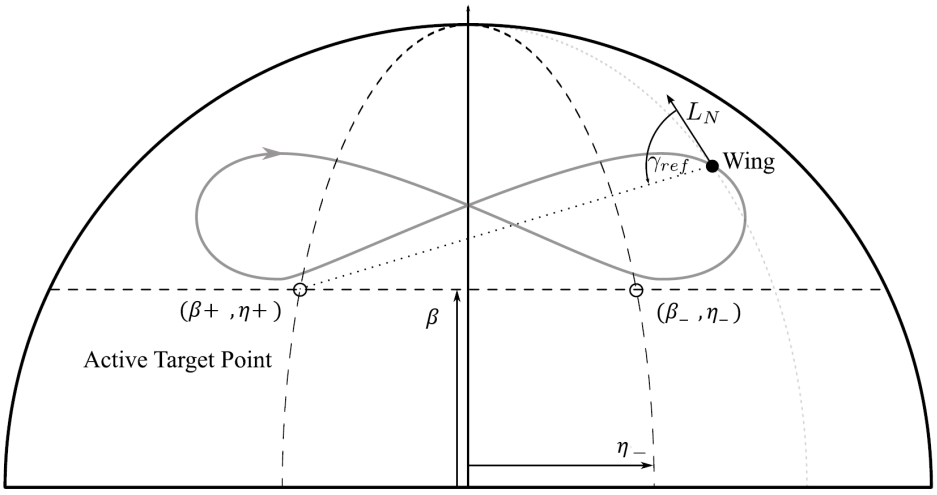

Figure 5.3: Sketch of a guidance strategy borrowed from [51].

of figure-eight trajectory that keeps the covered area constant all over the production phase. In Fig.5.5 the main variables of the system are presented. Evolution of speed of rotation shows that the system can follow the variations of apparent wind speed by adapting ω in order to keep spin ratio $X = X_{max}$. Finally, evolution of yaw variables gives also an idea of what type of control performance is needed in order to perform figure-eight trajectories with Magnus effect-based AWE system. In Fig.5.6, evolution of output power is shown. The minimum value

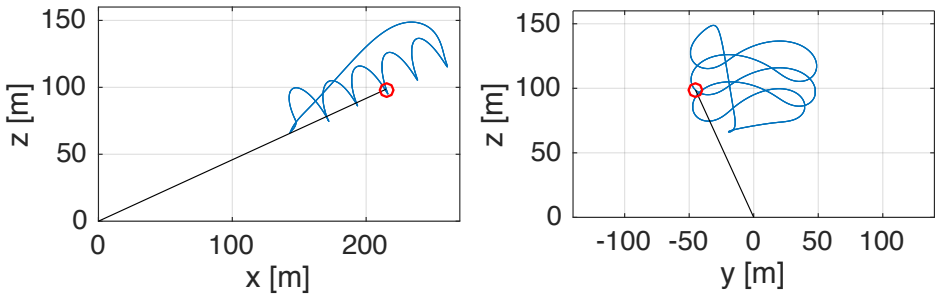

Figure 5.4: Trajectories of the Magnus rotor in xz and yz planes for the 3 cycles.

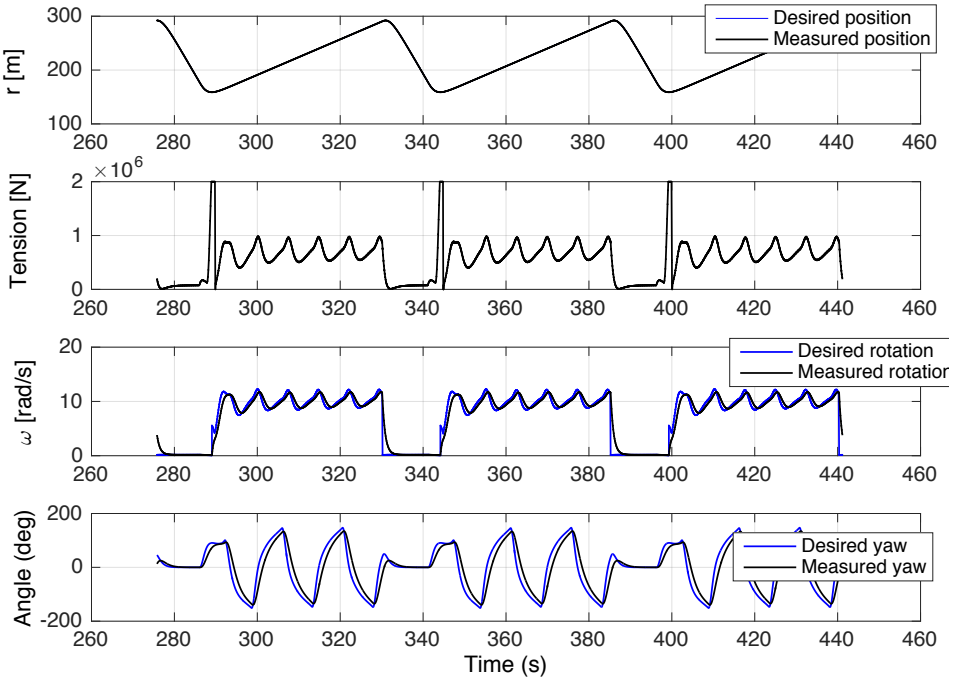

Figure 5.5: Reference and state variable for tether length (r, r_{ref}), tether tension, angular speed of the Magnus rotor (ω, ω_{ref}) , and yaw angle (γ, γ_{ref}), as function of time for the 3 cycles.

is -1.9MW and maximum is 3.9MW. This results in a mean power of the full cycle of 1.47MW. Note that embedded motor consumption to rotate the Magnus cylinder has to be subtracted from this value in order to have the total net power produced. This has to be done a in future work. Simplified model under static assumptions is also shown and is close to the mean of P_g dynamically simulated. The total mean power for simplified model $P_{cycle} = 1.67$MW, which is only 14% more. One can note that in order to produce around 1.5 MW of nominal power for $10m/s$ wind and this set of parameters, the generator has to be able to produce $4e6$ Nm torque and 6.6rad/s of rotation speed. This leads to a $26.6MW$ generator. A trade-off has then probably to be found in order to use a reasonable size of generator for the on-ground

station. As these 2 extreme values are not needed in the same time, a gear box can also be considered. A 3.9 MW generator is then needed instead. Finally, the maximum torque can also be more limited, but a degradation of tether length control will occur.

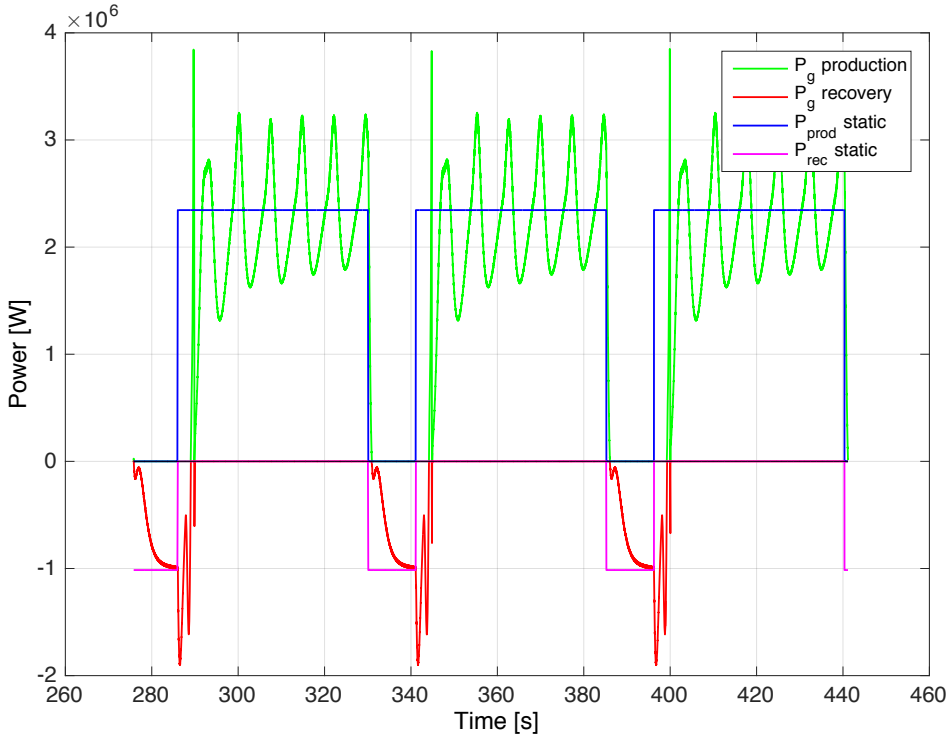

Figure 5.6: The output power simulated P_g during production and recovery phases for the 3 cycles with a comparison with simplified model under static assumption. The mean output power is 1469 kW for dynamic simulation and 1674 kW for the simplified model.

After this discussion, my main objective is to develop, construct and operate a fully autonomous airborne wind energy system that can be used and installed in urban areas. A new system shown on Fig.5.7 can be used. For this new mobile airborne wind energy system, one can advance the following applications:

1. With 100 % autonomous system, we can imagine a parachute drop in conflict or disaster zones followed then by automatic deployment.

   To try to compare with conventional solutions currently operational, one can advance the following numbers, which will be confirmed and clarified throughout the project:

   - ◇ Since the proposed system aims to produce a power of 3kW, it can be contained in a volume of about 1 m^3 with a weight around 100kg, excluding batteries.
   - ◇ A wind turbine of equivalent power, weighs substantially more, would have a diameter of 3m and require the construction of a mast of at least 6m high. Being much closer to the ground, it would also produce less power and would be sensitive to the reliefs within a radius of at least 100 m.

Appendices

A selection of scientific papers representing my research

1. Guerrero-Castellanos, Fermi; Marchand, Nicolas; Hably, Ahmad; Lesecq, Suzanne; Delamare, Jérôme, **"*Bounded attitude control of rigid bodies: Real-time experimentation to a quadrotor mini-helicopter*"**, *Control Engineering Practice* (2011) **19**, **8**, 790-797.
   In the list of the most cited articles in Control Engineering Practice Journal (Elsevier) since 2011.

2. Turker, Harun; Bacha, Seddik; Hably, Ahmad, **"*Rule-Based charging of plug-in electric vehicles (PEVs): Impacts on the aging rate of low-voltage transformer*"**, *IEEE Transactions on Power Delivery* (2014) **29**, **3**, 1012-1019.

3. Ovalle, Andres; Fernandez, Julian; Bacha, Seddik; Hably, Ahmad, **"*Mixed strategist dynamics and Entropy maximization: Electric vehicle distributed load scheduling*"**, *IEEE Transactions on Industrial Electronics* (2016) **63**, **5**, 3060-3071.

4. Hably, Ahmad; Dumon, Jonathan; Smith, Garrett, **"*Control of an airborne wind energy system with a Magnus effect*"**, ACC 2016 - USA.

Control Engineering Practice 19 (2011) 790–797

Contents lists available at ScienceDirect

Control Engineering Practice

journal homepage: www.elsevier.com/locate/conengprac

Bounded attitude control of rigid bodies: Real-time experimentation to a quadrotor mini-helicopter

J.F. Guerrero-Castellanos [a], N. Marchand [b], A. Hably [b,*], S. Lesecq [c], J. Delamare [d]

[a] Autonomous University of Puebla (BUAP), Faculty of Electronics Av. San Claudio y 18 Sur, Ciudad Universitaria 72570, Puebla, Mexico
[b] GIPSA-lab, Control Systems Department, ENSE3 bat B - BP 46, Domaine Universitaire, 38400 Saint Martin d'Heres, France
[c] CEA DRT/LETI/DCIS/PILSI, 17 rue des martyrs, 38054 Grenoble, France
[d] G2Elab, ENSE3 bat D - BP 46, Domaine Universitaire, 38400 St Martin d'Heres Cedex, France

ARTICLE INFO

Article history:
Received 25 September 2009
Accepted 10 April 2011
Available online 7 May 2011

Keywords:
Nonlinear control
Attitude stabilization
Embedded control
Quadrotor helicopter

ABSTRACT

A quaternion-based feedback is developed for the attitude stabilization of rigid bodies. The control design takes into account a priori input bounds and is based on nested saturation approach. It results in a very simple controller suitable for an embedded use with low computational resources available. The proposed method is generic not restricted to symmetric rigid bodies and does not require the knowledge of the inertia matrix of the body. The control law can be tuned to force closed-loop trajectories to enter in some a priori fixed neighborhood of the origin in a finite time and remain thereafter. The global stability is guaranteed in the case where angular velocity sensors have limited measurement range. The control law is experimentally applied to the attitude stabilization of a quadrotor mini-helicopter.

1. Introduction

The problem of attitude control of a rigid body has attracted considerable amount of interest since the 1950s within the scientific communities of aeronautics, aerospace, control and robotics. Indeed many systems such as spacecrafts, satellites, helicopters, tactical missiles, coordinated robot manipulators, underwater vehicles, aerial vehicles and others can enter within the framework of rigid bodies with a need for attitude control. Several approaches were applied such as feedback linearizing control law (Fjellstad & Fossen, 1994; Wie, Weiss, & Arapostathis, 1989), feedback proportional-derivative control law (Egeland & Godhavn, 1994; Joshi, Kelkar, & Wen, 1995; Tsiotras, 1994; Wen & Kreutz-Delgado, 1991), predictive control (applied to a spacecraft in Wen, Seereeram, & Bayard, 1997 and a to micro-satellite in Hegrenas, Gravdahl, & Tondel, 2005), backstepping (quaternion based in Kristiansen & Nicklasson, 2005 and nonlinear adaptive in Singh & Yim, 2002), robust control applied to tactical missiles (Song, Kim, Kim, & Nam, 2005). Adaptive control technique is applied on a flexible launch vehicle (Oh, Bang, & Park, 2008). This list is of course far from being exhaustive. Within these mentioned approaches, a feedback linearization coupled with a proportional-derivative control is probably the most widely used method to solve the attitude control problem. This ensures stabilization with a simple implementation of the control law. Sometimes, the linearization step is even not applied. The major criticism of this approach is that for large attitude or angular velocity errors, a large control effort is required. Furthermore, the linearization step requires a relatively accurate model of the system.

In practice, the limitations on available energy impose bounded input signal. Moreover, it is common that the output of the system are bounded due to sensors limitation. Actually, the above cited attitude control approaches do not consider the problem which takes the input and/or output constraints into account. Few publications have dealt with this problem. In Tsiotras and Luo (2000), the stabilization of an underactuated rigid spacecraft subject to input constraints is studied. Although this approach uses an innovative attitude representation that allows the decomposition of general motion into two rotations, the proposed control law and its analysis are restricted only to the kinematic level. In Belta (2004), a control law that drives a rigid underwater vehicle between arbitrary initial and final region of the state space while satisfying bounds on control and state is proposed. The approach is based in a control of multi-affine systems. The authors in Boskovic, Li, and Mehra (1999) have studied the robust sliding mode stabilization of the spacecraft attitude dynamics in the presence of control input saturation based on the variable structure control (VSC) approach. Unfortunately, the stabilizing bounded control laws applied in these works are nonsmooth and this fact renders difficult their practical implementation. The application of optimal control of a rigid body's attitude has been the interest of many researches (see Scrivener & Thompson, 1994 and references therein). However, when the problem is subject to control constraints a difficulty

* Corresponding author. Fax: +33 4 76 82 63 88.
E-mail address: ahmad.hably@gipsa-lab.grenoble-inp.fr (A. Hably).

0967-0661/$ - see front matter © 2011 Elsevier Ltd. All rights reserved.
doi:10.1016/j.conengprac.2011.04.004

Rule-Based Charging of Plug-in Electric Vehicles (PEVs): Impacts on the Aging Rate of Low-Voltage Transformers

Harun Turker, Seddik Bacha, *Member, IEEE*, and Ahmad Hably

***Abstract*—Massive deployment of plug-in electric vehicles (PEVs) in the coming years will create more challenges for the power system including the aging rate of transformers. It will be an essential requirement to propose solutions to minimize the impacts related to the integration of PEVs. Special attention must be given to the residential electric grid where charging will mostly take place. In this paper, first we propose a rule-based (RB) algorithm which determines the minimum charging power levels of home-charged PEVs with/without a charging ban during peak hours. Second, we evaluate the consequences of supplying an RB algorithm on life duration of a low-voltage transformer supplying a residential area.**

***Index Terms*—Aging rate, life duration, low-voltage (LV) transformer, plug-in electric vehicle, residential electric grid, rule-based algorithm.**

I. Introduction

SEVERAL papers have evaluated the plug-in electric vehicles' (PEVs) impact, both electric vehicles (EVs) and plug-in hybrid electric vehicles (PHEVs), on residential electric grids [1], [2] and on distribution power grids [3]–[7]. Many studies quantify the life duration losses of high- and low-voltage transformers [8]–[13] caused by the recharging of PEVs. We can consider that the impacts associated with the integration of PEVs are known. Currently, significant research work is carried out to minimize such impacts [14]–[22].

In parallel, "active" algorithms have been developed for smart charging of PEVs mainly in the residential areas. To this end, [23] proposes a "local" algorithm of energy management for housing with one PEV and photovoltaic installations to minimize CO2 emissions. Voltage profile control and loss minimization algorithms using PEVs are proposed in [24] and [25]. In [26], the authors have proposed an algorithm to smooth the load curve using vehicles and minimizing the user's energy bill. Although peak shaving enables preserving, on one hand, the operation of the electric grid (voltage plan, losses, etc.) and, on the other hand, life duration of grid elements (transformers and cables), this research topic is uncommon in the literature. This is enhanced in [27]–[30], where the authors have proposed algorithms that determine the available energy for charging PEVs connected to the electric grid while minimizing the transformer's aging.

Generally, these "active" algorithms proposed in the literature relate the integration of PEVs to technoeconomic aspects [31]–[37]. Few studies evaluate the impact of these algorithms on the life duration of grid elements.

In this paper, a different approach is proposed in order to solve the integration of PEVs into the electric grid. The focus of the current study is to develop an RB algorithm that is applied to one house equipped with a single PEV. The study is conducted with the assumption that the PEV leaves and arrives at home once a day. The idea is to define a minimal constant-charging power level while allowing recharging PEVs at any time and strictly prohibiting charging during peak hours. In this way, it is guaranteed that the vehicle's battery reaches a desired state of charge (SOC) at the departure time. The RB algorithm is applied on 10 000 real case studies using daily loads profiles (DLPs) of houses and PEVs. Databases have resulted from real electricity consumption of domestic electrical devices, corroborated with the distribution of the vehicle's arrival and departure times, categories, and battery SOC. These distributions are obtained by applying a probabilistic algorithm of the PEV's connections.

Thus, for PEVs charged at home, we determine the charging power levels of 2460 W and 3400 W, respectively, when allowing recharging vehicles at any time and prohibiting charging during peak hours. These charging levels ensure statistically that 99% of the batteries of PEVs have an SOC equal to 100% for the next use.

After applying the charging power levels obtained from the RB algorithm, we show that the aging rate is minimized for an LV transformer that feeds a residential power grid where the number of houses is variable without any charging restriction of PEVs during peak hours. In general, this analysis answers the pragmatic requirement to prohibit charging during peak hours for home-charged PEVs.

The proposed methodology has a strong feature because it is not linked with any deployments related to smart grids. Indeed, the recommendation is applicable now for existing power grids without additional infrastructure.

Manuscript received February 24, 2012; revised June 06, 2012, September 13, 2012, January 10, 2013, and June 09, 2013; accepted November 05, 2013. Date of publication February 19, 2014; date of current version May 20, 2014. Paper no. TPWRD-00193-2012.

H. Turker and S. Bacha are with the Grenoble Electrical Engineering Laboratory, Grenoble 38402, France (e-mail: harun.turker.mhp@gmail.com; seddik.bacha@g2elab.grenoble-inp.fr).

A. Hably is with the Grenoble Image Parole Signal Automatique Laboratory, Grenoble 38402, France (e-mail: ahmad.hably@grenoble-inp.fr).

Color versions of one or more of the figures in this paper are available online at http://ieeexplore.ieee.org.

Digital Object Identifier 10.1109/TPWRD.2013.2292066

An Electric Vehicle Load Management Application of the Mixed Strategist Dynamics and the Maximum Entropy Principle

Andres Ovalle, *Student Member, IEEE*, Julian Fernandez, *Student Member, IEEE*, Ahmad Hably, *Member, IEEE*, and Seddik Bacha, *Member, IEEE*

***Abstract*—An application of an evolutionary game dynamics called mixed strategist dynamics (MSD), for the decentralized load scheduling of plug-in electric vehicles (PEVs), is proposed in this paper. Following an analogy with the maximum entropy principle (MEP) for tuning parameters of discrete probability distributions, entropy of the total load distribution and the local load distributions are considered as objectives of the scheduling approach, and a tradeoff among them is defined by the electric vehicle owners' convenience. While entropy maximization for the local load distributions contributes to preserve the batteries' states of health, entropy maximization for the total load distribution reduces the undesirable peak effects over the transformer loading. The problem is formulated such that final states of charge are assured depending on time constraints defined by the owners. Furthermore, mixed strategies in the MSD are defined such that they represent the vertices of the convex set of feasible load profiles which results from the constraints imposed by owners and chargers. The synergy of several PEVs is modeled as an application of the MSD in a multipopulation scenario, where the interaction among populations follows another evolutionary game dynamics called best reply (BR) dynamics. The performance of the proposed approach is tested on real data measured on a distribution transformer from the SOREA utility grid company in the region of Savoie, France.**

***Index Terms*—Distributed optimization, entropy maximization, evolutionary game theory, mixed strategist dynamics (MSD), plug-in electric vehicles (PEVs), smart charging.**

Manuscript received June 5, 2015; revised September 17, 2015; accepted November 15, 2015. Date of publication January 12, 2016; date of current version April 8, 2016. This work was supported in part by the ARC Energies Région Rhône-Alpes, in part by the ANR PARADISE Project, in part by the Grenoble Electrical Engineering Laboratory, and in part by the Grenoble Image Parole Signal Automatique Laboratory, France.

A. Ovalle and S. Bacha are with the Grenoble Electrical Engineering Laboratory, Université de Grenoble Alpes, 38402 Grenoble, France (e-mail: andres.ovalle-villamil@g2elab.grenoble-inp.fr; seddik.bacha@g2elab.grenoble-inp.fr).

J. Fernandez is with the Universidad Sergio Arboleda, Bogotá 1111, Colombia (e-mail: fernandjul@gmail.com).

A. Hably is with Grenoble Image Parole Signal Automatique Laboratory, Université de Grenoble Alpes, 38402 Grenoble, France (e-mail: ahmad.hably@gipsa-lab.grenoble-inp.fr).

Color versions of one or more of the figures in this paper are available online at http://ieeexplore.ieee.org.

Digital Object Identifier 10.1109/TIE.2016.2516975

I. Introduction

PLUG-IN electric vehicles (PEVs) represent part of the future of transportation systems, and even more, environmental, technical, and economic opportunities for future electricity grids [1]–[5]. PEV's energy storage potential availability for grid support represents several benefits for the electric distribution systems in terms of: intermittency reduction of nonconventional energy sources, power quality enhancement, energy transportation, etc. [1]–[7]. Nevertheless without the existence of dedicated charging infrastructure, a high PEVs penetration rate may have a negative impact on voltage levels, load balancing, stability issues, etc. [7]–[10]. In order to overcome these issues and take advantage of the potential benefits of PEVs, optimal management schemes for energy fluxes become a key element. In particular, given the importance of vehicle owner's autonomy, decentralized management schemes become desirable [11], [12].

Several approaches concerning this issue have been published during the last years. Centralized approaches generally aim to find optimal schedules for power consumption of PEVs, based on the forecasting of the inelastic base demand and a model of the grid. Some centralized approaches define linear economic costs of energy as objectives, given fixed tariffs, and apply linear programming tools [3], [13]. Some of these approaches use grid modeling in order to fix constraints aiming to reduce the impact of PEVs, on voltage levels for instance [14]. Other centralized approaches propose nonlinear cost functions. Authors of [15] propose power losses on the grid as a quadratic objective function to minimize. In [16], authors propose as objective function, a third degree polynomial representing the economic cost of energy where the price is defined by the ratio of demanded power and available power. Even if centralized approaches are able to use modeling or power flow techniques to get interesting results on variables like voltage or power limits, the communication infrastructure and the amount of information required to execute those approaches make them impractical and inflexible [11], [12], [17].

More flexible solutions can be provided by decentralized approaches. Authors of [17] compare a model-based centralized approach with a decentralized linear approach where constraints of voltage and loading effects of PEVs are considered. These constraints are based on off-line computed sensitivities

2016 American Control Conference (ACC)
Boston Marriott Copley Place
July 6-8, 2016. Boston, MA, USA

Control of an airborne wind energy system with a Magnus effect

Ahmad Hably*, Jonathan Dumon
Univ. Grenoble Alpes, GIPSA-Lab,
F-38000 Grenoble, France.
{ahmad.hably, jonathan.dumon}@gipsa-lab.fr

Garrett Smith
Wind Fisher S.A.S., 2 allee du Vivarais,
31770 Colomiers, France.
garrett.smith@wind-fisher.com

***Abstract*—The control of an airborne wind energy system with a Magnus effect device has been studied. The proposed strategy aims to control the amount of the output energy produced for a given cycle. The control scheme has been applied numerically and experimentally on a small scale indoor setup of Gipsa-lab, and validated numerically for Omnidea's experimental platform. Results have shown the good performance of the proposed control strategy.**

I. INTRODUCTION

Airborne wind energy systems have attracted a lot of interest in the last few years. Due to the quality of higher altitude wind which is stronger and more persistent they are considered as a promising alternative to traditional wind turbines with limitations related to weight and size, and therefore the investment cost when the targeted power increases. There are many ways to capture the wind energy using aerodynamic surfaces with moving center of mass and orientation. The existing prototypes can be divided into two main classes:

- On-ground production using the lift mode as noted in [1]. A traction phase, in which the airfoil is pulled by the wind, unrolling the cable which turns a ground-based electrical machine; and a recovery phase, that begins when the cable reaches its predefined maximum length, and hence needs to be reeled-in, an operation that consumes energy. These systems are studied by [2], Kitegen [3], and Ampyx Power [4].
- On-board production using the drag mode. The generator is embedded and electric energy is produced in the sky and sent to the ground using conducting cables. This type of system is investigated for example by Makani Power [5].

Most of the aforementioned systems use either flexible kites or rigid wings. However, Omnidea Lda has proposed to use the Magnus effect in its HAWE project [7]. The operation principle of their platform is based on the rotation of a buoyant cylinder attached to the ground by cables. The Magnus effect generates an aerodynamic lift force which depends on the apparent wind speed with relation to the cylinder and the cylinder rotational speed itself. Electrical energy is produced using the pumping mode. The Magnus cylinder is almost static and therefore the apparent wind speed remains close to the real wind speed [8]. This type of system using the Magnus effect must be explored. In addition, a key difference compared to the AWE systems using kites or wings whose lift and drag coefficients depend on the angle of attack, is that Magnus effect systems are independent of angle of attack. The control of the angle of attack is sometimes critical and depends on some parameters which are difficult to measure.

The paper is organized as follows. Section II introduces the system modeling. The control strategy is presented in Sect.III. This control strategy is applied to the experimental platform described in Sect.IV. Both simulation and experimental results are shown in Sect.V. A numerical application of the proposed control strategy for Omnidea' s experimental platform is presented in Sect.VI. Section VII provides some conclusions and perspectives.

II. THE SYSTEM MODELING

The airborne wind energy system under study is composed of a ground-based motor that will supply a traction force to a tether connected to a light-weight rotating Magnus cylinder. In this study the movement of the Magnus cylinder is limited to the vertical plane. The system's dynamical model can be given by:

$$\ddot{\theta} = \frac{1}{r}\Big[-2\dot{\theta}\dot{r} + \frac{F_T}{M_{Mag}}\Big] \quad (1)$$

$$\ddot{r} = \frac{1}{M_{Mag}+M_D}\Big[r\dot{\theta}^2 M_{Mag} + F_R - T\Big] \quad (2)$$

$$\dot{T} = \beta_T\Big(u_T - T\Big) \quad (3)$$

where r is the tether length from the Magnus cylinder to the motor on the ground, θ is the angle that the tether makes with respect to the horizon, $M_D = \frac{I}{R_d^2}$ with I the inertia of the ground-based motor and R_d its radius, T is the traction on the tether. The Magnus cylinder mass M_{Mag} is the sum of cylinder mass M, the mass of the gas used to fill it, and M_l:

$$M_{\text{Mag}} = M + V_o\rho_{\text{gas}} + M_l r \quad (4)$$

with ρ_{gas} is the gas density and M_l denotes the mass per tether length and V_o is the volume of the Magnus cylinder. Equation 3 represents the first order dynamic response of the actuator used in the experimental platform to control the traction force in the tether. F_R and F_T are respectively the radial and tangential forces acting on the Magnus cylinder due to lift force L, drag force D, the weight of the Magnus cylinder P, and the buoyant force B. Denoting $s_i := \sin(\theta - \alpha_w)$ and $c_i := \cos(\theta - \alpha_w)$, these forces can be expressed as follows:

$$F_R = -T + Ls_i + Dc_i - P\sin\theta + B\sin\theta \quad (5)$$

$$F_T = Lc_i - Ds_i - P\cos\theta + B\cos\theta \quad (6)$$

978-1-4673-8682-1/$31.00 ©2016 AACC

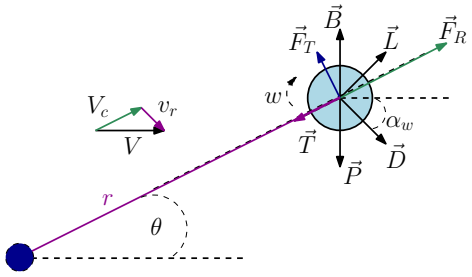

Fig. 1. The forces acting on the Magnus cylinder airborne wind energy system.

with α_w is the wind angle defined later in equation (11). Lift and drag forces can be expressed by:

$$L = 0.5\rho S v_r^2 C_L, \quad D = 0.5\rho S v_r^2 C_D \tag{7}$$

where ρ is the air density, S is the Magnus cylinder projected surface area, v_r as we will see later is the norm of the apparent wind velocity vector (equation 12). The buoyancy force can be calculated from the Archmiedes's principle:

$$B = \rho V_o g \tag{8}$$

Vertical relative airspeed v_v and horizontal relative airspeed v_h depend on the motion of the rotating Magnus cylinder. One has:

$$v_h = V + r\dot{\theta}\sin\theta - \dot{r}\cos\theta \tag{9}$$

$$v_v = -(r\dot{\theta}\cos\theta + \dot{r}\sin\theta) \tag{10}$$

with V is the airspeed with respect to the ground. Using these equations, one obtains, v_r, the norm of the apparent wind velocity vector and the angle of this vector with respect to the ground α_w.

$$\alpha_w = \arctan\frac{-(r\dot{\theta}\cos\theta + \dot{r}\sin\theta)}{V + r\dot{\theta}\sin\theta - \dot{r}\cos\theta} \tag{11}$$

$$v_r = \sqrt{(r\dot{\theta}\cos\theta + \dot{r}\sin\theta)^2 + (V + r\dot{\theta}\sin\theta - \dot{r}\cos\theta)^2} \tag{12}$$

For lifting devices using the Magnus effect, aerodynamic lift coefficient C_L and drag coefficient C_D are functions of the spin ratio X and not of the angle of attack as for airfoil wings. The Magnus cylinder spin ratio is given by the following equation [8]:

$$X = \frac{wR}{v_r} \tag{13}$$

with w is the Magnus cylinder rotational velocity and R is its radius.

III. THE CONTROL STRATEGY

The control strategy to be applied on the Magnus-based system aims to control the amount of energy produced by forcing some variables, namely the tether traction force T and its length r, to track some "optimized" profile related to desired power. This system has two phases: a generation (traction) phase where the tether is pulled by the Magnus cylinder using the aerodynamic forces and then a consumption (recovery) phase where the Magnus cylinder is pulled by the tether to return to its initial departure point in order to start a new cycle. For simplicity, desired power P_{ref} will be assumed constant, but the control strategy can be adapted to varying P_{ref} as we will see in the results section. During the cycle, the Magnus cylinder moves from minimum position r_{min} to a maximum position r_{max} at a speed $\dot{r}_{prod}$ and $\dot{r}_{rec}$ respectively during production and recovery phases. The proposed algorithm is based on the following rules. A given cycle is defined by the beginning of the recovery phase (t_0) until the end of the production phase (t_1).

- The consumed energy is measured from t_0 to time t

$$E_{rec}(t) = \int_{t_0}^{t} P_{mes}dt \tag{14}$$

P_{mes} is the measured power defined by:

$$P_{mes} = P_{gen} + P_{Mag} \tag{15}$$

with P_{gen} is the measured power produced or consumed by the generator on the ground and P_{Mag} is the power consumed by the Magnus actuator.

- At the end of the recovery cycle, the remaining energy to be produced E_{prod} has to satisfy $E(t_1) = P_{ref} \times (t_1 - t_0) = E_{ref}$.

$$E_{prod}(t) = E_{ref} - E_{rec}(t) \tag{16}$$

- The traction force has to satisfy

$$T_{ref} = \frac{1}{\dot{r}_{prod}}\frac{E_{ref} - E_{rec}(t)}{(t_1 - t)} \tag{17}$$

Three controllers have been used to implement this control strategy (2). Controller K_3 is used to find the desired tension T_{ref} as a function of the desired power P_{ref} (Eq. 17). This desired tension is controlled in its turn by a controller, denoted by K_2, to get the Magnus cylinder spin ration X. The tether length is controlled by K_1 in order to obtain the traction controlu_T. During the cycle, the Magnus cylinder moves from r_{min} to r_{max} at a speed $\dot{r}_{prod}$ and $\dot{r}_{rec}$ respectively during production and recovery phases. The parameters K_1 and K_2

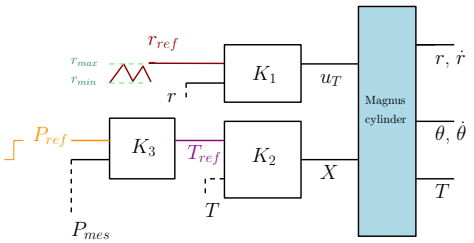

Fig. 2. An overview of the proposed control system.

are tuned empirically to separate the dynamics of the inner

and outer loop and in order to have a fast response time to obtain maximum power for a given wind speed as we will see later in the results section.

IV. PLATFORM DESCRIPTION

In order to validate the proposed system and the control strategy, the Gipsa-lab experimental test bench is used. This experimental setup was built for our work using rigid wings [9], the same algorithm was also used in [10]. This indoor experimental setup gives us some flexibility and allows us to test our prototypes and the proposed control strategies sheltered from outside weather conditions. It is composed of a wind tunnel, the Magnus cylinder, and the ground station.

A. Wind Tunnel

The wind tunnel is composed of 9 brushless motors with 2-blade fans of 0.355m diameter. These motors, 800W each, are distributed on a surface of 1.85 m^2. Turbulent air flow is produced at speeds up to 9 m/s. A hot wire wind speed sensor (1 measurement per second with a serial interface) is used to measure the airspeed. Controllers are implemented on the experimental setup using the xPC target real-time toolbox of Matlab (Fig. 3).

Fig. 3. The development and target computers for real-time experiments using Matlab/Simulink xPC target real-time toolbox.

B. The Magnus Cylinder

The Magnus cylinder used in our platform is a light-weight cylinder built with carbon rods, polystyrene and transparent plastic (Fig. 4). The rotation of the Magnus cylinder is provided by one mini DC motor mounted at one extremity of the Magnus cylinder. Its current control and speed sensing is done using a homemade driver. The parameters of the Magnus cylinder are given in Table I.

C. The Ground Station

The ground station is composed of dynamo-motor system Maxon 2260L DC 100W driven by a 4 quadrants amplifier Maxon ADS 50/10. Two incremental encoders provide measurement of the angle θ and the tether length r. Control references of DC motors are sent to drivers with a DAC PCI DA S1200 from Measurement Computing and a torque sensor provides an accurate measurement of tether tension.

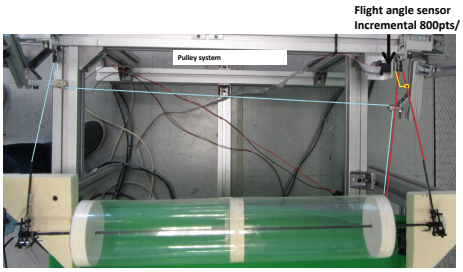

Fig. 4. The Magnus cyinder.

TABLE I
PARAMETERS OF THE MAGNUS CYLINDER

Symbol	Name	Value
M_{Mag}	Magnus cylinder mass	0.11 Kg
M_l	Mass per tether length	0 Kg/m (neglected)
R	Magnus cylinder radius	0.047 m
L_m	Magnus cylinder length	0.45 m
M_{IM}	Rotor mass	0.0481 Kg
ρ	Air density	1.225 Kg/m^3

V. RESULTS

Before applying the control strategy presented previously, an important phase of characterizing the different elements of the experimental setup was needed.

A. Characterization

Firstly, the response time of the DC motor used to rotate the Magnus cylinder is characterized and its energy consumption is quantified for different wind speeds. The second step is to identify the lift and drag coefficients as a function of the spin ratio. The results are very near to the theoretical results [11] used in [12] where the drag and lift aerodynamic coefficients are calculated as a function of speed ratio X.

$$C_D = 0.73X^2 - 1.2X + 1.2131$$
$$C_L = 0.0126X^4 - 0.2004X^3 + 0.7482X^2 + 1.3447X - 0.2$$

The last step in the characterization phase is to find the limits of our platform. We have noticed that friction in the pulleys is significant. We have measured the tension in the tether as a function of the tether length r for different rotational speed w of the Magnus cylinder and the tether speed $\dot{r}$ and we have found our platform can provide a limited difference of traction force that can be used to produce energy. This is shown in the difference between the upper and lower zones of Fig. 6

B. Simulation Results

In this section, the proposed control strategy is tested numerically. Our objective is to validate the control strategy and to have cycle with a positive production result. For this, the controller block K_3 is not active in these tests because of

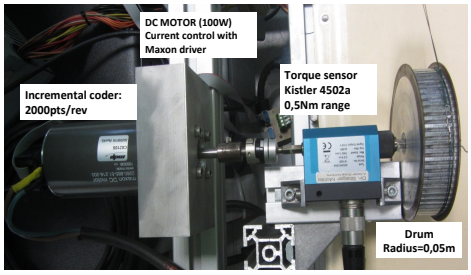

Fig. 5. The ground station.

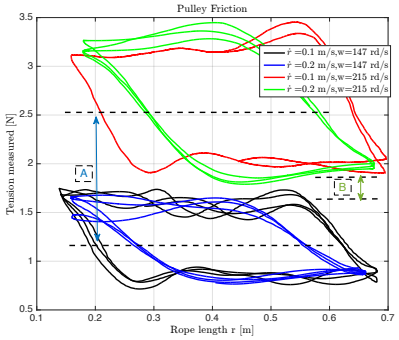

Fig. 6. The measured tension as a function of tether speed $\dot{r}$ (rp in the figure) and the Magnus cylinder rotaltional speed w. The zone **A** is the possible force difference that can be used to produce energy. This zone is reduced to zone **B** due to the pulleys' friction.

the identified friction in the setup. The following conditions are used.

- The minimum tether length $r_{min} = 0.1$ m and its maximum is $r_{max} = 0.7$ m. These limits are imposed by the wind window of the wind tunnel.
- The tether speed in the traction phase $\dot{r}_{prod} = 0.1$ m/s and in the recovery one $\dot{r}_{rec} = -0.1$ m/s.
- The response time of the actuators used to turn the Magnus cylinder is too long in order to maintain a constant value of X. In addition, one has fast variations of the relative wind speed related to oscillation on θ. For this and in order to validate our control strategy, we have chosen to control only w which gives a mean X value. A constant rotational Magnus cylinder speed is used in the traction phase $w_{prod} = 200$ rd/s and and in the recovery phase $w_{rec} = 140$ rd/s. This corresponds by approximating $v_r \approx V$ to have a spin ratio in the traction phase $X_{prod} = 1.5161$ and $X_{rec} = 1.0613$ in the recovery phase.
- The wind speed is 6.2 m/s. Reynolds number is 4×10^4.

The tether length follows perfectly the desired position as shown on Fig. 7. As expected, the traction force increases as the rotational Magnus cylinder' speed increases. The application of this control strategy enables us to produce a positive result as shown on Fig. 8.

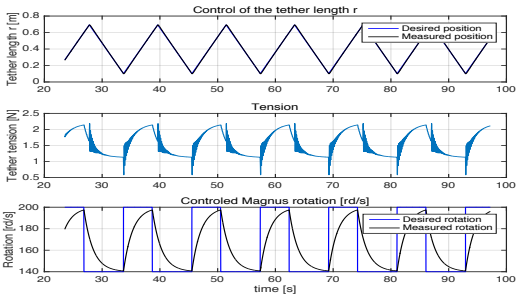

Fig. 7. Tether length, tether tension and the Magnus rotational speed as function of time in the simulation of small scale system. The oscillation in the tether tension is due to the choice of controller parameters.

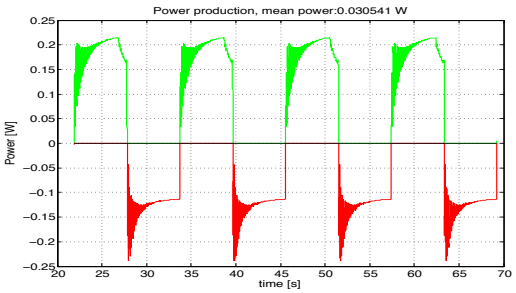

Fig. 8. The power produced in the simulation.

C. Experimental Results

The same control strategy has been experimentally applied to the setup using the same conditions used in the previous section. Similar results have been obtained as shown in the Figs. 9-11. A movie that shows the experimental results can be found on our website [13].

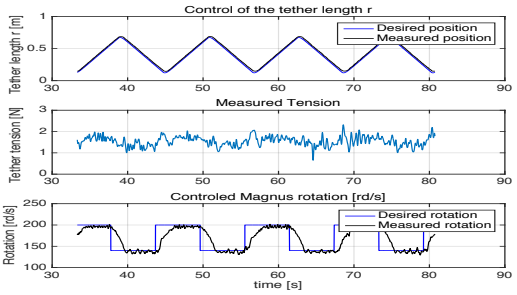

Fig. 9. Tether length, tether tension and the Magnus rotational speed as function of time in the experimentation on Gipsa-lab platform.

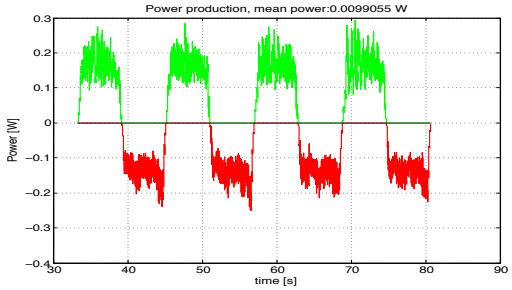

Fig. 10. The power produced in the experimentation on Gipsa-lab platform.

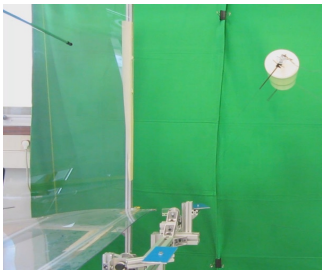

Fig. 11. The Magnus cylinder airborne.

VI. NUMERICAL APPLICATION TO OMNIDEA SYSTEM

The complete control strategy has been numerically applied for Omnidea's platform. We have taken the dimensions of the Magnus cylinder currently in service. Its parameters are listed in Table II. The Magnus lift and drag coefficients used for

TABLE II
PARAMETERS OF OMNIDEA MAGNUS CYLINDER

Symbol	Name	Value
M_{Mag}	Magnus cylinder mass	91.22 Kg
R	Magnus cylinder radius	1.25 m
L_m	Magnus cylinder length	16 m
ρ_{He}	Helium density	0.1427 Kg/m^3
ρ_{air}	Air density	1.225 Kg/m^3
M_l	Mass per tether length	0.2 Kg/m
M_D	Ground station rotor mass	2000 Kg

Reynolds number $R_e = 3.8 \times 10^4$:

$$\begin{aligned} C_D &= -0.0211X^3 + 0.1837X^2 + 0.1183X + 0.5 \\ C_L &= 0.0126X^4 - 0.2004X^3 + 0.7482X^2 + 1.3447X \end{aligned}$$

We want to have an optimal production cycle with vertical trajectories similar to those suggested in [12]. We have determined the feasibility regions for $r_{min} = 200$ m and $r_{max} = 300$ m. For a wind speed $V = 10$m/s, the tether speed in the traction phase $\dot{r}_{prod}$ and in the recovery one $\dot{r}_{rec}$ are found numerically offline. One gets $\dot{r}_{prod} = 0.33 \times V$ and $\dot{r}_{rec} = -0.52 \times V$. The choice of the spin ratio value of Omnidea's Magnus cylinder depends on the following objectives: 1) To maximize the lift-to-drag ratio $\frac{L}{D}$, one has to take $X = 2.4$, and 2) To maximize the aerodynamic forces, i.e $\sqrt{C_L^2 + C_D^2}$, the spin ratio must be equal to $X = 5.4$. For a vertical trajectory, the spin ratio will take a value between $X = 5.4$, which maximizes power without taking part of the relative wind, and $X = 3.6$, which maximizes the crosswind power if one reaches the theoretical relative speed $vr = \frac{L}{D}V$. By simulating this system at a wind speed $V = 10$ m/s (see next section for details), we get the mean power produced during a full cycle as a function of X (Fig. 12). Note that we do not consider here the motor consumption that actuates the Magnus cylinder. The maximum power is $P_{moy} = 59.23$ KW for $X = 4.3$ which is between 3.6 and 5.4 as expected. For this set of parameters, the energetic performance is 1.48 kW/m^2 which is consistent with 1.25 kW/m^2 found in [12].

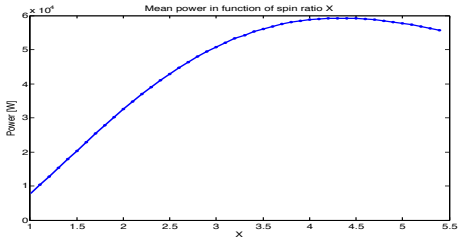

Fig. 12. Omnidea results: The variation of the mean power as a function of the spin ratio X.

A. Nominal production cycle

In this section, the results of the production cycle are presented. In order to have a smooth movement of the Magnus cylinder, the reference tether length r_{ref} is filtered by $\frac{1}{(\tau_R s+1)^2}$ with $\tau_R = 2$s. The PID controller K_1 parameters are $K_p = 8250$ N/m, $K_i = 1.32$ N/(m.s), $K_d = 45 \times 10^3$ N.s/m. We find that the relative wind speed increases thanks to the evolution of flight angle θ which produces the vertical shape of the cycle (Fig. 13). with a maximum of $v_r = 14.26$ m/s in the production phase and $v_r = -14.79$ m/s in the recovery phase. On Fig. 14, we show the evolution of the control. One can find the maximum tension in the tether is $T_{max} = 42.4$ kN, the maximum rotational speed $w_{max} = 49.02$ rd/s. The production speed is 3.3 m/s with an overshoot measured at 8 m/s, the traction speed is set to -5.2 m/s, without any observed overshoot. Omnidea' current system cannot completely meet these values since the announced maximum force is 5 kN with a maximum rotational speed of 9.42 rd/s.

B. Energy control

A production cycle using the complete control strategy has been tested. To find the control parameters of the controller K_2 (PD controller), we have chosen the increasing line

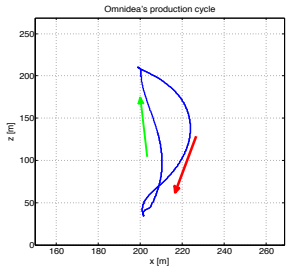

Fig. 13. The production cycles of Omnidea's platform. The direction of the arrows indicates the movment of the Magnus cylinder: Green for the traction phase and red for the recovery one.

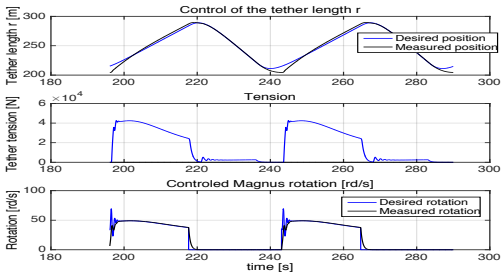

Fig. 14. Tether length, tether tension and the Magnus rotational speed as function of time for Omnidea's platform.

slope of Fig. 12 between $X = 1$ and $X = 4.3$. The control parameters are then $K_p = 6.4 \times 10^{-3}\ N^{-1}$ and $K_d = 6.4 \times 10^{-3}$ s/N. One can clearly see the performance of the proposed control strategy (Fig. 15). The measure produced power will follow the desired one even in the presence of noise on the wind speed. The control variables are shown on Fig. 16. It is worth noting that if the output of PD is saturated, one can simply apply a very large reference to achieve the maximum power, with X = 4.3 throughout the production phase

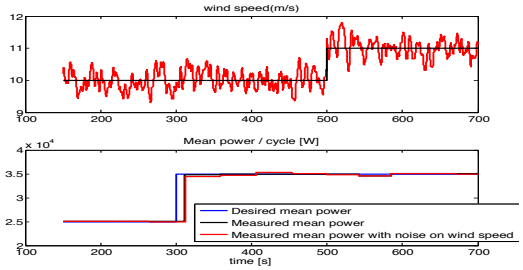

Fig. 15. The mean power produced as function of the desired power and change in wind speed for Omnidea's platform. Noise is added to the wind speed to test the performance of the control strategy.

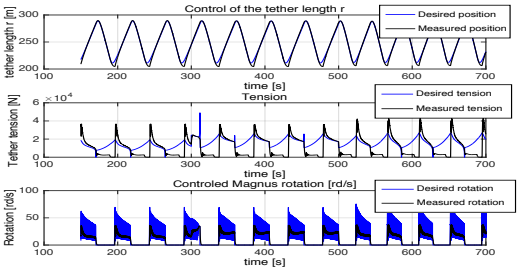

Fig. 16. The evolution of the control variables in absence of noise for Omnidea's platform.

VII. CONCLUSIONS AND PERSPECTIVES

In this paper, we have presented the control of airborne wind energy system based on a Magnus cylinder. The indoor small-scale experiments have enabled us to master different aspects of the system and to validate part of our approach. The Magnus model was validated for a spin ratio ranging from 1 to approximately 2.3. Our goal for future work is experiment with models capable of spin ratio greater than 5.5. The small size of our wind tunnel does not allow us to reach tethers speeds that would achieve the simulated performance 1.48 kW/m^2, but faster dynamics of the actuators rotating the Magnus cylinder would allows us to achieve more vertical cycles thus experiencing the dynamic exploitation of the relative wind due to the increase of the flight angle θ.

VIII. ACKNOWLEDGMENT

The authors of this paper would like to thank the technical staff of Gipsa-lab and the trainees Azzam Alwann, Alexandre Kajiyama and Pierre Estadieu.

REFERENCES

[1] M. Loyd, "Crosswind kite power," *J. ENERGY*, vol. 4(3), 1980.
[2] L. Fagiano, M. Milanese, and D. Piga, "High-altitude wind power generation," *Energy Conversion, IEEE Transactions on*, vol. 25, no. 1, pp. 168–180, 2010.
[3] M. Canale, L.Fagiano, and M.Milanese, "Kitegen: A revolution in wind energy generation," *Energy*, vol. 34, pp. 355–361, 2009.
[4] "http://www.ampyxpower.com."
[5] http://www.makanipower.com/.
[6] "http://www.altaerosenergies.com."
[7] "http://www.omnidea.net/hawe/."
[8] J. Seifert, "A review of the magnus effect in aeronautics," *Progress in Aerospace Sciences*, vol. 55, pp. 17–45, 2012.
[9] A. Hably, R. Lozano, Alamir, and J. M. Dumon, "Observer-based control of a tethered wing wind power system : indoor real-time experiment," in *The 2013 American Control Conference, (ACC2013).*, 2013.
[10] R. Lozano, J. Dumon, A. Hably, and M. Alamir, "Energy production control of an experimental kite system in presence of wind gusts," in *Intelligent Robots and Systems (IROS), 2013 IEEE/RSJ International Conference on*. IEEE, 2013, pp. 2452–2459.
[11] F. White, *Fluid mechanics*. McGraw-Hill Higher Education, 2015.
[12] M. Milutinović, M. Čorić, and J. Deur, "Operating cycle optimization for a magnus effect-based airborne wind energy system," *Energy conversion and management*, vol. 90, pp. 154–165, 2015.
[13] "http://www.gipsa-lab.grenoble-inp.fr/recherche/plates-formes.php?id_plateforme=70."
[14] "http://omnidea.net/site/index.php."

Bibliography

[1] http://www.gipsa-lab.grenoble-inp.fr/recherche/plates-formes.php?id_plateforme=70.

[2] http://chinahummer.en.alibaba.com.

[3] http://edition.cnn.com/interactive/2014/06/tech/cnn10-inventions/.

[4] http://fee.asso.fr/politique-de-leolien/eolien-en-mer/.

[5] http://homes.esat.kuleuven.be.

[6] https://www.x-wind.de/en/.

[7] http://technologyreview.me/en/energy/how-smart-microgrids-could-ease-lebanons-electricity-woes/.

[8] http://twingtec.ch),.

[9] http://www.altaerosenergies.com.

[10] http://www.ampyxpower.com.

[11] http://www.awec2015.com),.

[12] http://www.ccomptes.fr/Publications/Publications/Les-couts-de-la-filiere-electro-nucleaire.

[13] http://www.e-kite.com.

[14] http://www.enerkite.de/en/.

[15] http://www.gipsa-lab.fr/projet/PARADISE/accueil.html),.

[16] http://www.kitenergy.net.

[17] http://www.magenn.com/.

[18] http://www.omnidea.net/hawe/.

[19] http://www.skysails.info.

[20] http://www.soitec.com.

[21] http://www.swisskitepower.ch.

[22] *Airborne Wind Energy*. Springer, 2013.

[23] Mariam Ahmed, Ahmad Hably et Seddik Bacha : High altitude wind power systems: A survey on flexible power kites. *In Electrical Machines (ICEM), 2012 XXth International Conference on*, pages 2085–2091. IEEE, 2012.

[24] Mariam Ahmed, Ahmad Hably et Seddik Bacha : Kite generator system periodic motion planning via virtual constraints. *In 39th Annual Conference of the IEEE Industrial Electronics Society (IECON 2013)*, pages 1–6, 2013.

[25] Mariam Ahmed, Ahmad Hably, Seddik Bacha et Andres Ovalle : Kite generator system: Grid integration and validation. *In Industrial Electronics Society, IECON 2014-40th Annual Conference of the IEEE*, pages 2139–2145. IEEE, 2014.

[26] Mohammed Sh Ahmed, Ahmad Hably et Seddik Bacha : Kite generator system modeling and grid integration. *Sustainable Energy, IEEE Transactions on*, 4(4):968–976, 2013.

[27] M.S. Ahmed, A. Hably et S. Bacha : Grid-connected kite generator system: Electrical variables control with MPPT. *Industrial Engineering Conference, Melbourne, Australia*, November 2011.

[28] M.S. Ahmed, A. Hably et S. Bacha : Power maximization of a closed-orbit kite generator system. *In 50th Conference on Decision and Control Conference (IEEE CDC), Orlando, USA*, 2011.

[29] Changsun Ahn, Chiao-Ting Li et Huei Peng : Optimal decentralized charging control algorithm for electrified vehicles connected to smart grid. *Journal of Power Sources*, 196(23):10369–10379, 2011.

[30] Mazen Alamir, Ahmad Hably, Haiyang Ding et France Saint Martin d'Heres : A novel distributed nmpc control structure for partially cooperative systems under limited information sharing. *In Proceedings of the 18th IFAC World Congress*, 2011.

[31] N.P.I. Aneke, D.A Lizarraga et H. Nijmeijer : Homogeneous stabilization of the extended chained form system. *In IFAC 15th Triennial World Congress, Barcelona, Spain*, 2002.

[32] Cristina L Archer : An introduction to meteorology for airborne wind energy. *In Airborne Wind Energy*, pages 81–94. Springer Berlin Heidelberg, 2013.

[33] I. Argatov, P. Rautakorpi et R. Silvennoinen : Estimation of the mechanical energy output of the kite wind generator. *Renewable Energy*, 34:1525–1532, 2009.

[34] I. Argatov, P. Rautakorpi et R. Silvennoinen : Estimation of the mechanical energy output of the kite wind generator. *Renewable Energy*, 34:1525–1532, 2009.

[35] I. Argatov et R. Silvennoinen : Energy conversion efficiency of the pumping kite wind generator. *Renewable Energy*, 35(5):1052–1060, 2010.

[36] I. Argatov et R. Silvennoinen : Structural optimization of the pumping kite wind generator. *Structural and Multidisciplinary Optimization*, 40(1):585–595, 2010.

[37] Kaustav Basu, Ahmad Hably, Vincent Debusschere, Seddik Bacha et Andres Ovalle : A comparative study of low sampling non intrusive load dis-aggregation. *In (IECON 2016)*, Florence, Italy, 2016.

[38] Kaustav Basu, Lamis Hawarah, Nicoleta Arghira, Hussein Joumaa et Stephane Ploix : A prediction system for home appliance usage. *Energy and Buildings*, 67(0):668 – 679, 2013. ISSN 0378-7788.

[39] Kaustav Basu, Andres Ovalle, Baoling Guo, Ahmad Hably, Seddik Bacha et Khaled Hajar : Online forecasting of electrical load for distributed management of plug-in electric vehicles. *In International Conference on Renewable Energies for Developing countries (REDEC 2016)*, Zouk Mosbeh, Lebanon, juillet 2016. URL https://hal.archives-ouvertes.fr/hal-01323253.

[40] R.W. Brockett : *Differential Geometric Control Theory*, chapitre Asymptotic stability and feedback stabilization, pages 181–191. University of Michigan Press, Ann Arbor, Michigan, 1983.

[41] M. Canale, L. Fagiano, M. Ippolito et M. Milanese : Control of tethered airfoils for a new class of wind energy generator. *In Proceedings of the 45th IEEE Conference on Decision and Control*, 2006.

[42] M. Canale, L. Fagiano et M. Milanese : High altitude wind energy generation using controlled power kites. *IEEE Transactions On Control Systems Technology*, 18(2):279 – 293, 2010.

[43] M. Canale, L.Fagiano et M.Milanese : Kitegen: A revolution in wind energy generation. *Energy*, 34:355–361, 2009.

[44] Fermi Guerrero Castellanos, Ahmad Hably et Nicolas Marchand : Bounded attitude stabilization: Application on four-rotor helicopter. *In 2007 IEEE International Conference on Robotics and Automation, ICRA'07*. IEEE, 2007.

[45] K. Clement-Nyns, E. Haesen et J. Driesen : The impact of vehicle-to-grid on the distribution grid. *Electric Power Systems Research*, 81(1):185 – 192, 2011. ISSN 0378-7796.

[46] M. Diehl : *Real time optimization for Large Scale Nonlinear Processes*. Thèse de doctorat, University of Heidelburg, 2001.

[47] Haiyang Ding, Mazen Alamir, Francois Bonne, Ahmad Hably et Patrick Bonnay : Distributed cooperative control framework of a cryogenic system. *In ICIT 2015*, Séville, Spain, mars 2015. URL https://hal.archives-ouvertes.fr/hal-01134613.

[48] Haiyang Ding, Mazen Alamir et Ahmad Hably : A distributed cooperative control scheme with optimal priority assignment and stability assessment. *In The 19th World Congress of the International Federation of Automatic Control, IFAC 2014*, pages 1–8, 2014.

[49] Davide Dragone, Luca Lambertini et Arsen Palestini : A class of best-response potential games. *Working Paper DSE 635, Department of Economics, University of Bologna*, 6 2008. URL AvailableatSSRN:http://ssrn.com/abstract=1148690.

[50] L. Fagiano : *Control of Tethered Airfoils for High Altitude Wind Energy Generation*. Thèse de doctorat, Politechnico di Torino - Doctoral School, 2009. URL: http://lorenzofagiano.altervista.org/.

[51] L. Fagiano, A. U. Zgraggen, M. Morari et M. Khammash : Automatic crosswind flight of tethered wings for airborne wind energy:modeling, control design and experimental results. *IEEE Transactions on Control System Technology*, 22(4):1433–1447, July 2014. ISSN 1063-6536.

[52] Julian Alberto FERNANDEZ, Seddik Bacha, Delphine Riu et Ahmad Hably : Plug-in electric vehicle collaborative charging for current unbalance minimization: Ant system optimization application. *In ICIT 2015*.

[53] Julian Alberto FERNANDEZ, Ahmad Hably et Antoneta Iuliana Bratcu : Assessing the economic profit of a vehicle-to-grid strategy for current unbalance minimization. *In 2015 IEEE International Conference on Industrial Technology-ICIT 2015*, 2015.

[54] Julian Alberto Fernandez, Delphine Riu, Seddik Bacha, Marc Paupert et Ahmad Hably : Real-time plug-in electric vehicle charging strategies for current and voltage unbalance minimization. *Journal Européen des Systèmes Automatisés (JESA)*, 49(3):271–298, 2016.

[55] F. Grognard, R. Sepulchre et G. Bastin : Improved performance of low-gain designs for bounded control of linear systems. 38 (10):1777–1782, 2002.

[56] JF Guerrero-Castellanos, Nicolas Marchand, Ahmad Hably, Suzanne Lesecq et Jérôme Delamare : Bounded attitude control of rigid bodies: Real-time experimentation to a quadrotor mini-helicopter. *Control Engineering Practice*, 19(8):790–797, 2011.

[57] A. Hably, R. Lozano, Alamir et J. M. Dumon : Observer-based control of a tethered wing wind power system : indoor real-time experiment. *In The 2013 American Control Conference, (ACC2013).*, 2013.

[58] Ahmad Hably et Jonathan Dumon : Eoliennes volantes: Airborne wind energy activities at the gipsa-lab. *In* Roland Schmehl, éditeur : *Book of Abstracts of the International Airborne Wind Energy Conference 2015*, page 41, Delft, The Netherlands, 2015. Delft University of Technology. ISBN 978-94-6186-486-4.

[59] Ahmad Hably, Jonathan Dumon et Garrett Smith : Control of an airborne wind energy system with a magnus effect. *In The 2016 American Control Conference*, 2016.

[60] Ahmad Hably, Farid Kendoul, Nicolas Marchand et Pedro Castillo : Further results on global stabilization of the pvtol aircraft. *Positive Systems*, pages 303–310, 2006.

[61] Ahmad Hably et Nicolas Marchand : Bounded control of a general extended chained form systems. *In 53rd IEEE Conference on Decision and Control*, pages 6–p, 2014.

[62] Ahmad Hably, Nicolas Marchand et Mazen Alamir : Constrained minimum-time-oriented stabilization of extended chained form systems. *In IEEE CONFERENCE ON DECISION AND CONTROL*, volume 44, page 6158. IEEE; 1998, 2005.

[63] Khaled Hajar, Ahmad Hably, Seddik Bacha, Ahmad Rafhi et Ziad Obeid : An application of a centralized model predictive control on microgrids. *In (EPEC 2016)*, Ottawa, Canada, 2016.

[64] Khaled Hajar, Ahmad Hably, Seddik Bacha, Ahmad Rafhi et Ziad Obeid : Optimal centralized control application on microgrids. *In International Conference on Renewable Energies for Developing countries (REDEC 2016)*, Zouk Mosbeh, Lebanon, juillet 2016. URL https://hal.archives-ouvertes.fr/hal-01323250.

[65] Khaled Hajar, Ahmad Hably, Ahmad Elrafhi, Ziad Obeid et Seddik Bacha : Optimization of a microgrid with renewable energy and distributed generation: a case study. *In The 9th International Conference on System Theory, Control and Computing*. IEEE, 2015.

[66] Salam Hajjar, Antoneta Iuliana Bratcu et Ahmad Hably : A day-ahead centralized unit commitment algorithm for a multi-agent smart grid. *In The Federated Conference on Computer Science and Information Systems*, FedCSIS 2015.

[67] Turker Harun, Ahmad Hably et Seddik Bacha : Housing peak shaving algorithm (hpsa) with plug-in hybrid electric vehicles (phevs): Vehicle-to-home (v2h) and vehicle-to-grid (v2g) concepts. *In 4th International Conference on Power Engineering, Energy and Electrical Drives (IEEE PowerENG 2013)*, pages 1–7, 2013.

[68] J. Hauser, S. Sastry et Meyer G. : Non linear control design for slightly nonminimum phase systems: Application to v/stol aircraft. *Automatica*, 28:665–679, 1992.

[69] Yifeng He, Bala Venkatesh et Ling Guan : Optimal scheduling for charging and discharging of electric vehicles. *IEEE transactions on smart grid*, 3(3):1095–1105, 2012.

[70] J. Hofbauer et K. Sigmund : *The Theory of Evolution and Dynamical systems*. Cambridge University Press, 1988.

[71] B. Houska et M. Diehl : Optimal control of towing kites. *In 45th IEEE Conference on Decision and Control, pages 2693-2697*, San Diego, CA, USA 2006.

[72] M. Ippolito : Vertical axis wind turbine with control system steering kites, février 27 2008. EP Patent 1,672,214.

[73] Chenrui Jin, Jian Tang et P. Ghosh : Optimizing electric vehicle charging: A customer's perspective. *IEEE Trans. Vehicular Tech.*, 62(7):2919–2927, Sept 2013.

[74] B. Lansdorp, B. Remes et W.J. Ockels : Design and testing of a remotely controlled surfkite for the laddermill. *In World Wind Energy Conference, Melbourne, Australia*, 2005.

[75] Junhao Lin, Ka-Cheong Leung et Victor OK Li : Optimal scheduling with vehicle-to-grid regulation service. *IEEE Internet of Things Journal*, 1(6):556–569, 2014.

[76] Z. Lin et A. Saberi : Semiglobal exponential stabilisation of linear systems subject to input saturation via linear feedbacks. 21 (3):225–239, 1993.

[77] Chunhua Liu, KT Chau, Diyun Wu et Shuang Gao : Opportunities and challenges of vehicle-to-home, vehicle-to-vehicle, and vehicle-to-grid technologies. *Proceedings of the IEEE*, 101(11):2409–2427, 2013.

[78] M.L. Loyd : Crosswind kite power. *J. ENERGY*, 4(3), 1980.

[79] R Lozano, Jonathan Dumon et Ahmad Hably : Reverse pumping: theory and experimental validation on a multi-kites system. *In System Theory, Control and Computing (ICSTCC), 2013 17th International Conference*, pages 311–318. IEEE, 2013.

[80] Rogelio Lozano, Jonathan Dumon, Ahmad Hably et Mazen Alamir : Energy production control of an experimental kite system in presence of wind gusts. *In Intelligent Robots and Systems (IROS), 2013 IEEE/RSJ International Conference on*, pages 2452–2459. IEEE, 2013.

[81] R. Lozano Jr, M. Alamir, J. Dumon, A. Hably *et al.* : Control of a wind power system based on a tethered wing. *Proceedings of second EGNCA 2012*, 2012.

[82] Zhongjing Ma, Duncan S Callaway et Ian A Hiskens : Decentralized charging control of large populations of plug-in electric vehicles. *IEEE Transactions on Control Systems Technology*, 21(1):67–78, 2013.

[83] Nicolas Marchand et Ahmad Hably : Global stabilization of multiple integrators with bounded controls. *Automatica*, 41(12):2147–2152, 2005.

[84] Nicolas Marchand, Ahmad Hably et Ahmed Chemori : Global stabilization with low computational cost of the discrete-time chain of integrators by means of bounded controls. *Automatic Control, IEEE Transactions on*, 52(5):948–952, 2007.

[85] A. Megretski : L_2 BIBO output feedback stabilization with saturated control. *In Proc. 13th IFAC World Congress*, volume D, pages 435–440, 1996.

[86] Milan Milutinović, Mirko Čorić et Joško Deur : Operating cycle optimization for a magnus effect-based airborne wind energy system. *Energy Conversion and Management*, 90:154–165, Jan 2015. ISSN 0196-8904.

[87] R.M. Murray et S. Sastry : Nonholonomic motion planning: Steering using sinusoids. *IEEE Transactions on Automatic Control*, 38,:700–716, 1993.

[88] Hung Khanh Nguyen et Ju Bin Song : Optimal charging and discharging for multiple phevs with demand side management in vehicle-to-building. *Journal of Communications and Networks*, 14(6):662–671, 2012.

[89] Hung Khanh Nguyen et Ju Bin Song : Optimal charging and discharging for multiple phevs with demand side management in vehicle-to-building. *Journal Communications and Networks*, 14(6):662–671, Dec 2012.

[90] Van Linh Nguyen, Tuan Tran Quoc, Seddik Bacha et Ngoc An Luu : Charging strategies to minimize the energy cost for an electric vehicle fleet. *In IEEE PES ISGT Istambul*, Oct 2014.

[91] A. Ovalle, J. Fernandez, A. Hably et S. Bacha : An electric vehicle load management application of the mixed strategist dynamics and the maximum entropy principle. *IEEE Trans. Ind. Electron.*, 63(5):3060–3071, 5 2016. ISSN 0278-0046.

[92] A. Ovalle, A. Hably et S. Bacha : Optimal management and integration of electric vehicles to the grid: Dynamic programming and game theory approach. *In ICIT 2015 - International Conference on Industrial Technology*, March 2015.

[93] Andres Ovalle, Seddik Bacha, Ahmad Hably et Kaustav Basu : On the most convenient Mixed Strategies in a Mixed Strategist Dynamics Approach for Load Management of Electric Vehicle Fleets. *In (IECON 2016)*, Florence, Italy, 2016.

[94] Andres Ovalle, Ahmad Hably et Seddik Bacha : Optimal management and integration of electric vehicles to the grid: Dynamic programming and game theory approach. *In Industrial Technology (ICIT), 2015 IEEE International Conference on*, pages 2673–2679. IEEE, 2015.

[95] Andres Ovalle, Ahmad Hably, Seddik Bacha et Mariam Ahmed : Voltage support by optimal integration of plug-in hybrid electric vehicles to a residential grid. *In Industrial Electronics Society, IECON 2014-40th Annual Conference of the IEEE*, pages 4430–4436. IEEE, 2014.

[96] Andres Ovalle, Ahmad Hably, Seddik Bacha et Mariani Ahmed : Mixed strategist dynamics: Electrical vehicle distributed load scheduling. *In Industrial Electronics Society, IECON 2014-41st Annual Conference of the IEEE*, pages 4430–4436, 2015.

[97] Andres Ovalle, Gustavo Ramos, Seddik Bacha, Ahmad Hably et Axel Rumeau : Decentralized control of voltage source converters in microgrids based on the application of instantaneous power theory. *Industrial Electronics, IEEE Transactions on*, 62(2):1152–1162, 2015.

[98] E. Paparoditis et T. Sapatinas : Short-term load forecasting: The similar shape functional time-series predictor. *Power Systems, IEEE Transactions on*, 28(4):3818–3825, Nov 2013. ISSN 0885-8950.

[99] Luka Perković, Pedro Silva, Marko Ban, Nenad Kranjčević et Neven Duić : Harvesting high altitude wind energy for power production: The concept based on magnus' effect. *Applied Energy*, 101:151–160, 2013.

[100] Pooya Rezaei, Jeff Frolik et Paul DH Hines : Packetized plug-in electric vehicle charge management. *IEEE Transactions on Smart Grid*, 5(2):642–650, 2014.

[101] Peter Richardson, Damian Flynn et Andrew Keane : Local versus centralized charging strategies for electric vehicles in low voltage distribution systems. *IEEE Transactions on Smart Grid*, 3(2):1020–1028, 2012.

[102] Bryan W Roberts, David H Shepard, Ken Caldeira, M Elizabeth Cannon, David G Eccles, Albert J Grenier et Jonathan F Freidin : Harnessing high-altitude wind power. *Energy Conversion, IEEE Transactions on*, 22(1):136–144, 2007.

[103] J. B. Rosen : Existence and uniqueness of equilibrium points for concave N-Person games. *Econometrica*, 33(3):520–534, 1965.

[104] A. Saberi, Z. Lin et A. R. Teel : Control of linear systems with saturating actuators. 41(3):368–378, 1996.

[105] S. Sarabi, A. Bouallaga, A. Davigny, B. Robyns, V. Courtecuisse, Y. Riffonneau et M. Regner : The feasibility of the ancillary services for vehicle-to-grid technology. *In European Energy Market (EEM), 2014 11th International Conference on the*, pages 1–5, May 2014.

[106] Jost Seifert : A review of the magnus effect in aeronautics. *Progress in Aerospace Sciences*, 55:17–45, 2012.

[107] Jost Seifert : A review of the magnus effect in aeronautics. *Progress in Aerospace Sciences*, 55:17–45, 2012.

[108] Wencong Su, Habiballah Eichi, Wente Zeng et Mo-Yuen Chow : A survey on the electrification of transportation in a smart grid environment. *IEEE Transactions on Industrial Informatics*, 8(1):1–10, 2012.

[109] H. J. Sussmann, E. D. Sontag et Y. Yang : A general result on the stabilization of linear systems using bounded controls. 39 (12):2411–2425, december 1994.

[110] H. J. Sussmann et Y. Yang : On the stabilizability of multiple integrators by means of bounded feedback controls. pages 70–73, Dec. 1991.

[111] A. R. Teel : Semi-global stabilizability of linear null controllable systems with input nonlinearities. 40(1):96–100, 1995.

[112] R. Thresher, M. Robinson et P. Veers : To capture the wind. *IEEE power & energy magazine*, pages 34–46, 2007.

[113] H. Turker, S. Bacha, D. Chatroux et A. Hably : Low-voltage transformer loss-of-life assessments for a high penetration of plug-in hybrid electric vehicles (phevs). *IEEE Transactions on Power Delivery*, 27(3):1323–1331, July 2012.

[114] H. Turker, A Hably, S. Bacha et D. Chatroux : Rule based algorithm for plug-in hybrid electric vehicles (phevs) integration in residential electric grid areas. *In Innovative Smart Grid Technologies (ISGT), 2012 IEEE PES*, pages 1–7, Jan 2012.

[115] Harun Turker, Seddik Bacha, Daniel Chatroux et Ahmad Hably : Aging rate of low voltage transformer for a high penetration of plug-in hybrid electric vehicles (phevs). *In Innovative Smart Grid Technologies (ISGT), 2012 IEEE PES*, pages 1–8. IEEE, 2012.

[116] Harun Turker, Seddik Bacha, Daniel Chatroux et Ahmad Hably : Modelling of system components for vehicle-to-grid (v2g) and vehicle-to-home (v2h) applications with plug-in hybrid electric vehicles phevs. *In ISGT*, pages 1–8, 2012.

[117] Harun Turker, Seddik Bacha et Ahmad Hably : Rule-based charging of plug-in electric vehicles (pevs): Impacts on the aging rate of low-voltage transformers. *Power Delivery, IEEE Transactions on*, 29(3):1012–1019, 2014.

[118] Harun Turker, Ahmad Hably et Seddik Bacha : Dynamic programming for optimal integration of plug-in hybrid electric vehicles (phevs) in residential electric grid areas. *In IECON 2012-38th Annual Conference on IEEE Industrial Electronics Society*, pages 2942–2948. IEEE, 2012.

[119] Harun Turker, Ahmad Hably et Seddik Bacha : Smart charging of plug-in hybrid electric vehicles (phevs) on the residential electric grid regarding the voltage plan. *In Electric Vehicle Conference (IEVC), 2013 IEEE International*, pages 1–6. IEEE, 2013.

[120] Harun Turker, Matthieu Hauck, Ahmad Hably et Seddik Bacha : A tool of vehicle-to-grid (v2g) concept for voltage plan control of residential electric grid areas with plug-in hybrid electric vehicles (phevs). *In IECON 2012-38th Annual Conference on IEEE Industrial Electronics Society*, pages 2883–2888. IEEE, 2012.

[121] http://www.jobyenergy.com/.

[122] http://www.makanipower.com/.

[123] Mark Voorneveld : Best-response potential games. *Economics Letters*, 66(3):289 – 295, 2000. ISSN 0165-1765. URL http://www.sciencedirect.com/science/article/pii/S0165176599001962.

[124] J.N. Webb : *Game Theory: Decisions, Interaction and Evolution*. Springer Undergraduate Mathematics Series. Springer, 2007.

[125] Chenye Wu, H. Mohsenian-Rad, Jianwei Huang et A.Y. Wang : Demand side management for wind power integration in microgrid using dynamic potential game theory. *In 2011 IEEE GLOBECOM Workshops (GC Wkshps)*, pages 1199–1204, Dec 2011.

[126] Murat Yilmaz et Philip T Krein : Review of the impact of vehicle-to-grid technologies on distribution systems and utility interfaces. *IEEE Transactions on Power Electronics*, 28(12):5673–5689, 2013.